Assessment of U-238, Th-232, and K-40 in Commonly Consumed Bangladeshi Fruits and Age-dependent Annual Effective Dose in Dhaka City, Bangladesh

By

Shuzosh Rahman
19211001
Mehedat Amin Siddique
19111002

A thesis submitted to the Department of Mathematics and Natural Sciences in partial fulfillment of the requirements for the degree of
Physics

Department of Mathematics and Natural Science (MNS)
BRAC University
August 2025

Declaration

It is hereby declared that

1. The thesis submitted is our own original work while completing our degree at BRAC University.

2. The thesis does not contain material previously published or written by a third party, except where this is appropriately cited through full and accurate referencing.

3. The thesis does not contain material which has been accepted, or submitted, for any other degree or diploma at a university or other institution.

4. We have acknowledged all main sources of help.

Student's Full Name & Signature:

Shuzosh Rahman	**Mehedat Amin Siddique**
19211001	19111002

Approval

The thesis/project titled "Assessment of U-238, Th-232, and K-40 in Commonly Consumed Bangladeshi Fruits and Age-dependent Annual Effective Dose in Dhaka City, Bangladesh" submitted by

1. Shuzosh Rahman (19211001)

2. Mehedat Amin Siddique (19111002)

of Summer, 2025 has been accepted as satisfactory in partial fulfillment of the requirement for the degree of Physics on August 09, 2025.

Examining Committee:

Supervisor:
(Member)

____
Dr. Munima Haque
Associate Professor, Department of Mathematics and Natural Sciences
Brac University

Program Coordinator:
(Member)

____
Muhammad Lutfor Rahman
Assistant Professor, Department of Mathematics and Natural Sciences
BRAC University

Departmental Head:
(Chair)

____
Dr. Md. Firoze H. Haque
Chairperson and Associate Professor, Department of Mathematics and Natural Sciences
BRAC University

Abstract

Radionuclides in consumed food pose potential health risks via internal exposure. Fruits may accumulate radioactive isotopes via root uptake or atmospheric deposition. Previous Bangladeshi fruit studies are scarce and lack age-dependent annual ingestion dose data. This study assesses radionuclide concentrations in common Bangladeshi fruits and estimates age-dependent annual ingestion doses in Dhaka City. Thirteen fruit samples from Dhaka markets were analyzed using High-Purity Germanium (HPGe) gamma spectrometry. Using secondary data, we estimated age-stratified average fruit consumption and annual ingestion doses for infants (0-5 years), children (6-15 years), and adults (16-70 years). Activities of U-238, Th-238, and K-40 ranged from 1.23 ± 0.63 Bq/kg to 8.28 ± 0.65 Bq/kg, BDL to 6.01 ± 0.66 Bq/kg, and 30.62 ± 1.88 Bq/kg to 227.7 ± 11.14 Bq/kg, respectively. Mean concentrations were 3.62 ± 0.67 Bq/kg, 2.33 ± 0.48 Bq/kg, and 80.98 ± 18.26 Bq/kg for U-238, Th-238, and K-40, respectively. The annual effective dose from fruit ingestion was 0.0502 mSv/y, 0.0569 mSv/y, and 0.0673 mSv/y for adults, children, and infants, respectively. All values were below the international safety limit. This study provides reassurance regarding the radiological safety of fruits in Bangladesh. However, continuous monitoring is essential to ensure safety and prevent future contamination risks. Further studies and up-to-date data, like age-dependent fruit consumption, are necessary for more accurate findings.

Keywords: Radionuclide concentrations, Radioactivity levels, Fruits Safety, Bangladeshi fruits

Acknowledgments

This thesis could not have been completed without the support of many individuals to whom I owe my deepest gratitude. I am forever indebted to my parents, brother and sister-in-law for their constant support, patience, and belief in me, even at times when I could not extend the same to myself. A core part of me, and everything that I will become, will forever be thanks to them.

I am profoundly thankful to our supervisor, Dr. Munima Haque, for her guidance, generosity, and patience throughout this research. Her support shaped both the direction and the integrity of this work.

I also extend my sincere thanks to the Chairperson of the Department of MNS, Dr. Md. Firoze Haque for guiding and assisting me with any academic issues. I am equally grateful to Dr. Tibra Ali sir whose words and teachings had given me the courage to pick myself up at my lowest. I would like to also thank the thesis committee and faculty members have contributed meaningfully to my academic development.

To my thesis partner and friend, Mehedat Amin Siddique—thank you for your efforts, even through periods of personal and academic difficulty. Special thanks are due to our lab's Research Assistant and friend, Atiar Md. Suja Sami, whose kind helpful nature, and solidarity made an invaluable difference in this work. To my friends who accidentally ended up getting entangled in this thesis but gave me immense strength—Chandrima Saha, Afroza Khanam, and Fabiha Saiyara.

To my dearest friends—Muhammad Abdullah, Saif Ar Rasul, Umme Fatema Fiza, Mashaekh Hassan, and others unmentioned but not forgotten—who had been with me since the start and helped shape me into who I am today.

To the many workers without whom the world would cease to function—the lab floor staff, the bus drivers and conductors, the rickshaw pullers, etc.—the contributions of these invisible heroes can not be understated.

Lastly, to the person who has made it this far: All good things take time.

— Shuzosh Rahman

I am profoundly grateful to my family for their unwavering support, patience, and encouragement throughout this journey, especially during moments when I doubted myself. My deepest thanks go to my supervisor, Dr. Munima Haque, whose insightful guidance, generosity, and patience were invaluable in shaping both the direction and quality of this research. I also sincerely appreciate the Chairperson of the Department of Mathematics and Natural Sciences, Dr. Md. Firoze Haque, for his guidance and support, as well as all the faculty members whose teaching and advice have contributed significantly to my academic growth.

I am truly thankful to my thesis partner and friend, Shuzosh Rahman, whose dedication and perseverance made completing this work together possible. Special appreciation goes to our Research Assistant and friend, Atiar Md. Shuja Sami, whose kindness, technical expertise, and solidarity greatly enriched this project. Finally, I want to express my gratitude to my friends and colleagues for their encouragement and to the laboratory staff for their helpful support throughout this work.

— Mehedat Amin Siddique

Table of Contents

Declaration **2**
Approval **3**
Abstract **4**
Acknowledgments **5**
Table of Contents **7**
List of Tables **12**
List of Figures **13**
Blank Page **15**
Chapter 1: Introduction **1**
1.1 Background Radiation 1
1.1.1 NORM 1
1.2 TENORM 2
1.3 Exposure Pathways of Radionuclides 3
Figure 1.1: Terrestrial pathways of transfer of radionuclides and dose to humans. (UNSCEAR, 2000, p. 24) 3
1.4.1 External Exposure 3
1.4.2 Internal Exposure 5
Inhalation 5
Ingestion 5
Figure 1.2: Detailed Exposure Pathways (IAEA, 2005, p. 23) 6
1.4 Bangladesh's Climatic and Agricultural Context 6
1.5 NORM in Fruits 7
1.6 Problem Statement 8
1.7 Aim and Objectives 9
Chapter 2: Theoretical Background and Literature Review **10**
2.1 Radioactive Decay 10
Figure 2.1: A list of some decay constants (Groch, 1998, p. 1249) 11
Figure 2.2: Decay Curve for Uranium-239 (Burton & Kebler, 1960) 12
2.1.1 Half-life 12
2.1.2 Radiation Types and Decay Processes 13
Figure 2.3: Possible decay paths in the Segrè Chart for a parent radionuclide (N, Z) to reach a stable configuration. The parent (solid black circle), and the daughter (open circles) (Podgorsak, 2016, p. 519) 14
Alpha (α) Decay 14
Beta (β) Decay 15
Gamma (γ) Decay 16
Spontaneous Fission (SF) 17
Proton Emission (PE) Decay 17
Neutron Emission (NE) Decay 18

2.1.3 Decay Chains 18
Figure 2.4: U-238 (right)and Th-232 (left) Decay Series (Cowart & Burnett, 1994, p. 652) 19
Figure 2.5: Decay Scheme of K-40 (Leutz et al., 1965, p. 151) 19
2.2 Gamma–Matter Interaction 20
2.3.1 Photoelectric Effect 21
Figure 2.6: Schematic Diagram of Photoelectrice Effect (Podgorsak, 2016, p. 336) 21
2.3.2 Compton Scattering 22
Figure 2.7: (a) A schematic diagram of Compton scattering. (b) a vector representation of Compton Scattering(Podgorsak, 2016, p. 297) 23
2.3.3 Pair Production 23
Figure 2.8: Schematic Diagram of (a) Nuclear Pair Production (b) Electron Pair Production (Podgorsak, 2016, p. 358) 24
2.3 Radioactive Equilibrium 25
2.5.1 Secular Equilibrium 25
2.4 Gamma Spectrometry and HPGe Detector 26
2.4.1 Principles of Gamma Spectrometry 26
Energy Calibration 27
Efficiency Calibration 27
2.4.2 High Purity Germanium (HPGe) Detector 28
2.4.3 System Components 29
Figure 2.9: Block Diagram of HPGe Detector System (Mustakim et al., 2018) 30
Liquid Nitrogen Dewar 30
Cryostat 30
Preamplifier 31
Power Supply 32
Multi-Channel Analyser (MCA) 32
Shielding Arrangement 33
2.4.4 Efficiency Metrics 33
Intrinsic photo-peak Efficiency 34
Absolute Efficiency 34
Relative Efficiency 34
2.5 Biological Effects of Radiation 36
2.5.1 Deterministic Effects (Harmful Tissue Reactions) 36
2.5.2 Stochastic Effects 37
Risk of Cancer 37
Risk of Hereditary Effects 38
Genetic Susceptibility to Cancer 38
2.6 Radiation Dose Assessment 38
2.6.1 The Representative Person 39

2.6.2 Absorbed Dose 40
2.6.3 Equivalent Dose 40
Figure 2.10: Weighing Factors (ICRP, 2012, p. 11) 41
2.6.4 Effective Dose 41
2.6.5 Dose Coefficients 41
Figure 2.11: Tissue Weighing Factors (ICRP, 2012, p. 12) 42
2.6.6 Annual Ingestion Dose and Annual Effective Dose 42
2.6.7 Public Exposure Limits 42
Recommended Limits for Effective Dose 43
2.7 Previous Studies on Radionuclide Analysis 43
2.8.1 Limitations 51
Chapter 3: Methodology 53
3.1 Sample Collection 53
3.1.1 Rationale for Sampling Dhaka Markets 53
3.2 Sample Processing 54
Figure 3.1: Example of fruit slices. Dragon fruits (Left) and Orange (right). 55
Figure 3.2: Dried fruit slices stored in zip-lock bag and measured in weighing machine. 56
Figure 3.3: Final dried fruit powder samples put in air-tight plastic containers, labeled, and stored for at least 30 days 57
Table 3.1: Fruit sample data 58
3.2.1 Dry-to-wet mass ratio 59
3.3 Gamma Spectrometry with HPGe Detector 59
3.3.1 Instrumentation 59
Figure 3.4: Energy vs Effiency curve (Mustakim et al., 2018) 60
3.3.2 Radioactivity Measurement 60
Figure 3.5: Typical gamma spectrometry system for fruit samples (Mustakim et al., 2018) 62
Activity Concentration Calculation 62
3.4 Tools for Statistical Analysis: Google Sheets and SPSS 63
Data Processing and Visualisation with Google Sheets 63
Statistical Analysis with SPSS 63
3.5 Annual Dose Calculation 64
Table 3.2: Age-dependent Dose Coefficients of U-238, Th-232, and K-40 65
Table 3.3: Population sizes 67
Table 3.4: Population of Urban Dhaka categorised by age range 68
Table 3.5: Population of Bangladesh categorised by age range 68
Chapter 4: Results 69
4.1 Activity Concentrations 69
Table 4.1: Activity Concentrations in Bq/kg 70
Table 4.2: Some Descriptive Statistics of the Results 71
Figure 4.1: Mean U-238 and Th-232 concentrations of the present study 72

Figure 4.2: Mean K-40 concentrations of the present study 72
4.1.1 Comparison with previous studies 73
Table 4.4: Mean activity concentrations of the studies in Bq/kg 73
Figure 4.3: Mean U-238 and Th-232 concentrations of selected studies 74
Figure 4.4: Mean K-40 concentrations of selected studies 74
Bananas 75
Table 4.5: Concentrations of Bananas 75
Figure 4.5: Banana activity concentrations for U-238 and Th-232 76
Figure 4.6: Banana activity concentrations for K-40 76
Mangoes 77
Table 4.6: Concentrations of Mango 77
Figure 4.7: Mango activity concentrations for U-238 and Th-232 77
Figure 4.8: Mango activity concentrations for K-40 78
Pineapples 78
Table 4.7: Concentrations of Pineapple 78
Figure 4.9: Pineapples activity concentrations for U-238 and Th-232 79
Figure 4.10: Pineapple activity concentrations for K-40 79
Oranges 80
Table 4.8: Concentrations of Orange 80
Figure 4.11: Orange activity concentrations for U-238 and Th-232 80
Figure 4.12: Orange activity concentrations for K-40 81
Guava 81
Table 4.9: Concentrations of Guava 81
Figure 4.13: Guava activity concentrations for U-238 and Th-232 82
Figure 4.14: Guava activity concentrations for K-40 82
Jujube 82
Figure 4.15: Jujube activity concentrations for U-238 and Th-232 83
Figure 4.16: Jujube activity concentrations for K-40 83
Table 4.10: Concentrations of Jujube 84
Starfruit 84
Figure 4.17: Starfruit activity concentrations for U-238 and Th-232 84
Table 4.11: Concentrations of Star fruit 85
Figure 4.18: Starfruit activity concentrations for K-40 85
Papaya 85
Table 4.12: Concentrations of Papaya 86
Figure 4.19: Papaya activity concentrations for U-238 and Th-232 86
Figure 4.20: Papaya activity concentrations for K-40 87
4.2 Estimated Age-dependent Fruit Consumption Rate 87
Table 4.13: Age-dependent Fruit Consumption Rates (Dhaka City) 88
Table 4.14: Age-dependent Fruit Consumption Rates (Bangladesh) 88
4.3 Annual Effective Dose (AED) 88

Table 4.15: Age-dependent Annual Effective Dose from Fruit Ingestion in Dhaka City 89
Table 4.16: Age-dependent Annual Effective Dose from Fruit Ingestion in Bangladesh 90
4.3.1 AED comparison with other studies 90
Table 4.17: Annual Ingestion Dose from Studies 91
4.3.2 Threshold for Fruit Consumption 92
Table 4.18: Age-dependent Fruit Consumption Rates Threshold in Dhaka City 92
Chapter 5: Discussions **93**
5.1 Differences and Similarities Within Study 93
5.1.1 Activity consentrations 93
5.1.2 Age-dependent Annual Effective Dose 94
5.2 Differences and Similarities With Previous studies 95
5.2.1 Activity Concentrations 95
5.2.2 Annual Effective Dose 96
5.3 Implications 97
5.4 Study Limitations 97
5.4 Future Study Possibilities and Recommendations 98
Chapter 6: Conclusions **100**
Bibliography **101**

List of Tables

Table 3.1: Fruit sample data 58
Table 3.2: Age-dependent Dose Coefficients of U-238, Th-232, and K-40 64
Table 3.3: Population sizes 66
Table 3.4: Population of Urban Dhaka categorized by age range 67
Table 3.5: Population of Bangladesh categorized by age range 68
Table 4.1: Activity Concentrations in Bq/kg 70
Table 4.2: Some Descriptive Statistics of the Results 71
Table 4.4: Mean activity concentrations of the studies in Bq/kg 73
Table 4.5: Concentrations of Bananas 75
Table 4.6: Concentrations of Mango 77
Table 4.7: Concentrations of Pineapple 78
Table 4.8: Concentrations of Orange 80
Table 4.9: Concentrations of Guava 81
Table 4.10: Concentrations of Jujube 84
Table 4.11: Concentrations of Star fruit 85
Table 4.12: Concentrations of Papaya 86
Table 4.13: Age-dependent Fruit Consumption Rates (Dhaka City) 88
Table 4.14: Age-dependent Fruit Consumption Rates (Bangladesh) 88
Table 4.15: Age-dependent Annual Effective Dose from Fruit Ingestion in Dhaka City 89
Table 4.16: Age-dependent Annual Effective Dose from Fruit Ingestion in Bangladesh 90
Table 4.17: Annual Ingestion Dose from Studies 91
Table 4.18: Age-dependent Fruit Consumption Rates Threshold in Dhaka City 92

List of Figures

Figure 1.1: Terrestrial pathways of transfer of radionuclides and dose to humans. (UNSCEAR, 2000, p. 24) 3

Figure 1.2: Detailed Exposure Pathways (IAEA, 2005, p. 23) 6

Figure 2.1: A list of some decay constants (Groch, 1998, p. 1249) 11

Figure 2.2: Decay Curve for Uranium-239 (Burton & Kebler, 1960) 12

Figure 2.3: Possible decay paths in the Segrè Chart for a parent radionuclide (N, Z) to reach a stable configuration. The parent (solid black circle), and the daughter (open circles) (Podgorsak, 2016, p. 519) 14

Figure 2.4: U-238 (right)and Th-232 (left) Decay Series (Cowart & Burnett, 1994, p. 652) 19

Figure 2.5: Decay Scheme of K-40 (Leutz et al., 1965, p. 151) 19

Figure 2.6: Schematic Diagram of Photoelectric Effect (Podgorsak, 2016, p. 336) 21

Figure 2.7: (a) A schematic diagram of Compton scattering. (b) a vector representation of Compton Scattering(Podgorsak, 2016, p. 297) 23

Figure 2.8: Schematic Diagram of (a) Nuclear Pair Production (b) Electron Pair Production (Podgorsak, 2016, p. 358) 24

Figure 2.9: Block Diagram of HPGe Detector System (Mustakim et al., 2018) 30

Figure 2.10: Weighing Factors (ICRP, 2012, p. 11) 41

Figure 2.11: Tissue Weighing Factors (ICRP, 2012, p. 12) 42

Figure 3.1: Example of fruit slices. Dragon fruits (Left) and Orange (right). 55

Figure 3.2: Dried fruit slices stored in a zip-lock bag and measured in a weighing machine. 56

Figure 3.3: Final dried fruit powder samples put in air-tight plastic containers, labeled, and stored for at least 30 days 57

Figure 3.4: Energy vs Efficiency curve (Mustakim et al., 2018) 60

Figure 3.5: Typical gamma spectrometry system for fruit samples (Mustakim et al., 2018) 62

Figure 4.1: Mean U-238 and Th-232 concentrations of the present study 72

Figure 4.2: Mean K-40 concentrations of the present study 72

Figure 4.3: Mean U-238 and Th-232 concentrations of selected studies 74

Figure 4.4: Mean K-40 concentrations of selected studies 74

Figure 4.5: Banana activity concentrations for U-238 and Th-232 76

Figure 4.6: Banana activity concentrations for K-40 76

Figure 4.7: Mango activity concentrations for U-238 and Th-232 77

Figure 4.8: Mango activity concentrations for K-40 78

Figure 4.9: Pineapples activity concentrations for U-238 and Th-232 79

Figure 4.10: Pineapple activity concentrations for K-40 79

Figure 4.11: Orange activity concentrations for U-238 and Th-232 80

Figure 4.12: Orange activity concentrations for K-40 81
Figure 4.13: Guava activity concentrations for U-238 and Th-232 82
Figure 4.14: Guava activity concentrations for K-40 82
Figure 4.15: Jujube activity concentrations for U-238 and Th-232 83
Figure 4.16: Jujube activity concentrations for K-40 83
Figure 4.17: Starfruit activity concentrations for U-238 and Th-232 84
Figure 4.18: Starfruit activity concentrations for K-40 85
Figure 4.19: Papaya activity concentrations for U-238 and Th-232 86
Figure 4.20: Papaya activity concentrations for K-40 87

Blank Page

Chapter 1: Introduction

1.1 Background Radiation

All living organisms are constantly exposed to ionizing radiation from both natural and human-made sources. Natural background radiation arises from cosmic rays and radioactive materials in the Earth's crust, while man-made sources include medical procedures and fallout. The vast majority of the radiation received by an average person comes from natural sources; roughly about 82 % of the annual radiation can be attributed to natural radiation, including cosmic rays, terrestrial radionuclides in soil and rocks, and radionuclides in food and water (Egidi, 1997, p. 3). Only 18 % comes from artificial sources such as medical imaging, industrial activities, nuclear power, and consumer products.

Cosmic radiation refers to both the primary energetic particles in space hitting Earth's atmosphere and also the secondary particles caused by the interaction of those particles with the atmosphere. Cosmogenic radionuclides come about from the collision of highly energetic cosmic rays with stable elements of the atmosphere and ground (Egidi, 1997, p. 5). While the amount of radiation varies with time and location, the overall dose from this, however, is minimal.

1.1.1 NORM

The term "Naturally Occurring Radioactive Material" (NORM) refers to radioactive substances that originate in nature. NORM includes the radionuclides originally present in rocks, soils, water, plants, and other natural media that contribute to the overall background dose. We also call the radiation from NORM "Terrestrial radiation", which originates from long-lived radionuclides that occur in minerals and soils. NORM is omnipresent at low levels. The primordial radionuclides are generally of two categories: Non-series and Series decay. Series decay primordial, such as the Uranium series (U-238) and Thorium series (Th-323), are those that decay or break down via emission of alpha, beta, or gamma particles (see section 2.1.2) to more stable isotopes of lead through a chain of radionuclides of varying half-lives (Egidi, 1997, p. 6). By contrast, non-series primordial, such as Potassium-40 (K-40), are those that decay directly to a stable nuclide. Among the most relevant NORM isotopes are the ^{238}U, ^{232}Th and ^{40}K, as they are the principal primordials in terms of doses (United Nations Scientific Committee on the Effects of Atomic Radiation [UNSCEAR], 2000, p. 28). They are ever-present in the Earth's crust, with half-lives of 4.47×10^9, 14.05×10^9 and 1.277×10^9 years respectively, have likely been present since before Earth's formation (Podgorsak, 2016, pp. 525-526).

1.2 TENORM

Technologically Enhanced Naturally Occurring Radioactive Materials (TENORM) refer to naturally occurring radioactive isotopes (NORM) whose concentration or potential for human exposure has been significantly increased due to human technological activities (Vearrier et al., 2009). Industrial processes like mining, ore processing (particularly phosphate rock), fossil fuel extraction and combustion, fertilizer production, and even commercial aviation can concentrate these radionuclides or redistribute them into the environment in forms more accessible to humans and ecosystems, creating TENORM (Vearrier et al., 2009; UNSCEAR, 2000).

The primary mechanism by which TENORM affects plant-based foodstuffs would be through the contamination of agricultural soil and irrigation water. Radionuclides released or leached from industrial waste sites such as phosphate stacks, oil/gas scale disposal areas, and coal ash deposits can enter the soil-water system and plants then absorb these radionuclides through their roots (see section 1.3). The extent of uptake depends on the specific radionuclide, soil chemistry, plant species, and agricultural practices (UNSCEAR, 2000). When crops, including fruits, are cultivated on land contaminated by such industrial residues, they may accumulate higher concentrations of radionuclides.

1.3 Exposure Pathways of Radionuclides

Humans can be exposed to radiation externally, from sources outside the body, or internally, from radioactive substances that have entered the body. External exposure comes from cosmic rays and gamma radiation from nearby rocks or atmosphere. Internal exposure occurs when radionuclides enter the body by inhalation or ingestion (UNSCEAR, 2000, p. 24). In Figure 1.1, we see a simplified diagram of pathways by which humans can be exposed to radiation. From International Atomic Energy Agency [IAEA] (2005), we get a detailed version of the pathways, as shown in Figure 1.2.

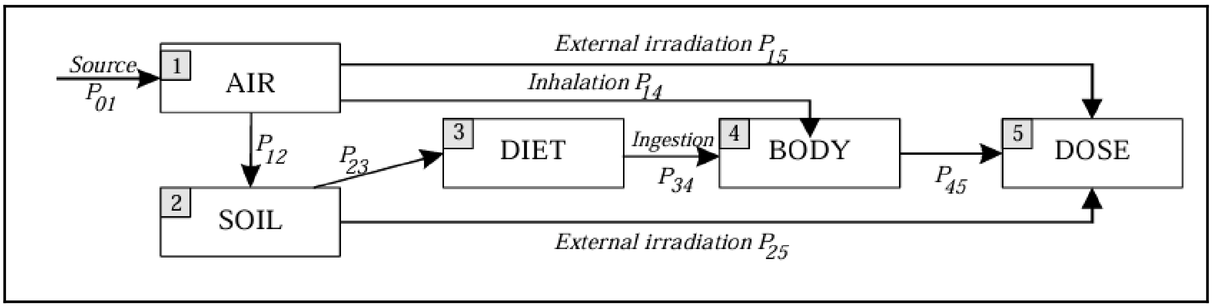

Figure 1.1: Terrestrial pathways of transfer of radionuclides and dose to humans. (UNSCEAR, 2000, p. 24)

1.4.1 External Exposure

Gamma rays emitted by natural radionuclides in soil or building materials can penetrate the body from outside. For reference, the UNSCEAR (2000) report shows that the worldwide average of annual dose from external terrestrial radiation comes out to be 0.48 mSv, with cosmogenic exposure of 0.39 mSv (p. 140). From Figure 1.1, we can get a general idea of what pathways external radiation might look like. Generally, a person may receive irradiation dose from the air or atmosphere, and soil. The Safety Guide by IAEA (2005) states the main pathways for external exposure (p. 21):

(a) *Source of radiation → human*

- Humans can receive direct irradiation exposure from a source of ionizing radiation, such as a power plant. This is the most direct form of radiation exposure that workers are generally exposed to.

(b) *Source of radionuclides → atmosphere or water body → human*

- Radionuclides from sources may get discharged, which end up as a plume of radionuclides in the atmosphere or 'cloud shine', or water. This, of course, emits radiation that reaches humans.

(c) *Source of radionuclides → atmosphere or water body → human skin*

- Similar to the previous case, this time the human skin may come in contact with radionuclides, resulting in radiation dosage.

(d) *Source of radionuclides → atmosphere or water body → soil or sediment or building surface or vegetation → human*

- The longest pathway in the external exposure route is where the radionuclides are deposited on the ground or sediments—on the shores of rivers, lakes, or the sea—or building surfaces such as walls, roofs, and floors, or vegetation. These sources emit radiation that reaches humans.

1.4.2 Internal Exposure

We understand that internal exposure can be of two main types: ingestion and inhalation. In both cases, rather than being exposed to radiation, per se, humans take in radionuclides, which then expose our tissues and organs to their radiation. Worldwide, annual exposure from internal exposure is out at roughly 1.55 mSv, which is significantly more than that of external exposure (UNSCEAR, 2000, p. 140).

Inhalation

Even within internal exposures, inhalation seems to be the greatest risk to the public, with an average annual dose to the public of 1.26 mSv. Breathing air containing radioactive particles or gases such as radon is a major pathway. Radon gas seeps from soil and rock into buildings and radiates into the breathable air. Radionuclide-laden dust can also be inhaled. The pathways for this are as follows (IAEA, 2005, p. 22):

1. *Source of radionuclides → atmosphere → human*
   - The radionuclide discharge from sources reaches the atmosphere, where humans inhale it in the plume, resulting in internal exposure radiation from within the lungs.
2. *Soil or sediment → human*
   - The radionuclides that are present in the soil or sediments can be resuspended, which are then inhaled by humans.

Ingestion

Out of the pathways, the ingestion pathway is the longest and generally the least deadly. Consuming food and drink contaminated with radionuclides can lead to their deposition inside the body. Terrestrial radionuclides are deposited from sources to the atmosphere or water body via rain and disposal, which then reach the soil and sediment. These radionuclides then travel to plants, vegetables, trees (via uptake), water, and other food sources—and finally, are consumed by humans. For example, potassium-40 is naturally present in many foods, especially those rich in potassium, such as bananas. Ingested radionuclides then irradiate internal organs as they decay. The pathway is as follows:

Source of radionuclides → atmosphere or water body → (soil or sediment) → vegetation and/or meat, milk, eggs, or marine food → human.

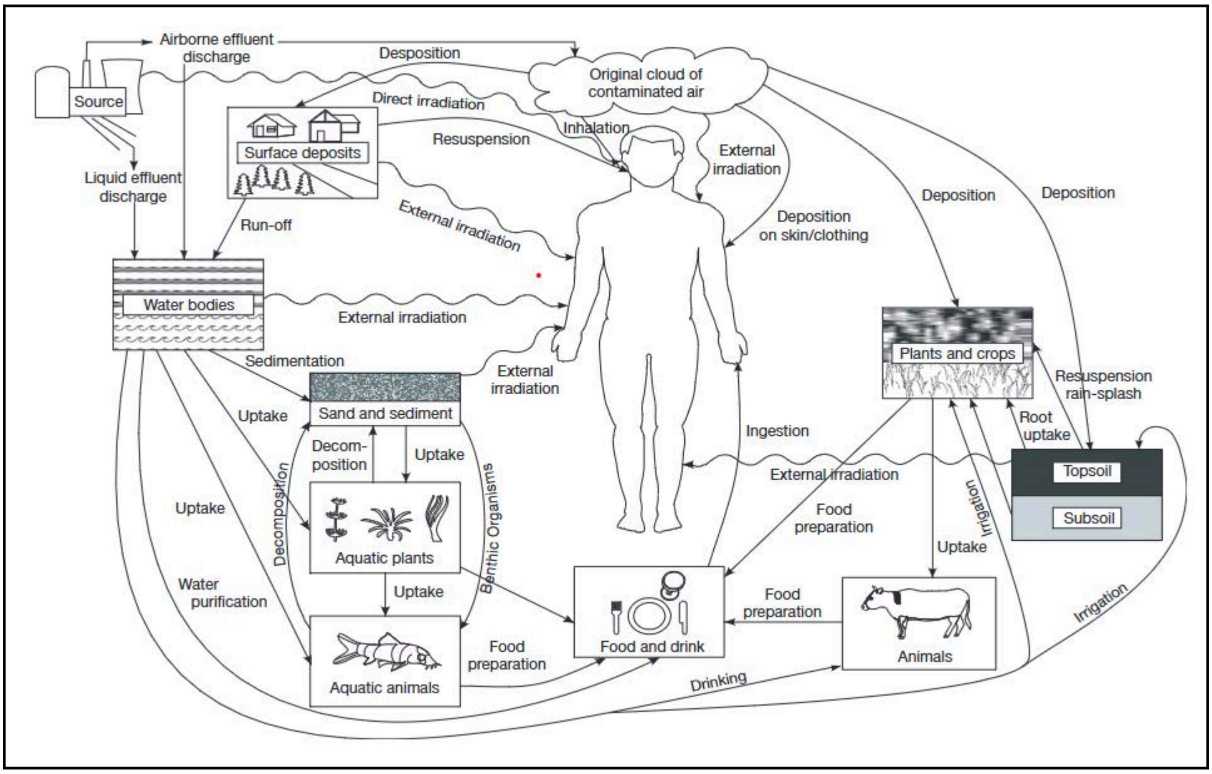

Figure 1.2: Detailed Exposure Pathways (IAEA, 2005, p. 23)

1.4 Bangladesh’s Climatic and Agricultural Context

Bangladesh lies in the lower Ganges–Brahmaputra river delta and has rich alluvial soils. Over two-thirds of the country’s land is on fertile floodplains, and the soil is known to contain abundant minerals and nutrients favorable to agriculture. In terms of the climate situation, Bangladesh has a humid subtropical to tropical monsoon climate. The combination of high humidity, warm temperatures, and heavy seasonal rains supports diverse crop production. Given the climate, Bangladesh is very well known for its high fruit production. According to the Bangladesh Bureau of Statistics [BBS] (2025), Bangladesh produced 5.94 million metric tons of fruits in 2024. Common fruits include mangoes, bananas, jackfruits, pineapples, guavas, and citrus fruits. The prevailing environmental conditions in Bangladesh also affect radionuclide behavior. For instance, monsoon floods can redistribute soil and NORM throughout the plains (Guagliardi et al., 2016). Irrigation and fertilizer use in fruit orchards may also influence the uptake of radionuclides from soil to plants (Nursapina et al., 2022). Additionally, after rice and vegetables, fruits are the most highly consumed foodstuff in Bangladesh, making up about 8% to 9.2% of daily consumption in grams (BBS, 2023, p. 48). This makes fruits an important source for potential radionuclide contamination.

1.5 NORM in Fruits

Among foods, fruits are of special interest for several reasons. First, fruits are widely consumed and often contain essential elements, such as potassium (^{40}K), the radioactive isotope of potassium, is naturally present in fruits—especially fruits such as bananas. Thus, fruits contribute to internal radiation exposure when eaten. Second, following Figure 1.2. we see the fruit consumption pathway, which is of great interest to us. Fruits may collect radionuclides from root uptake from the soil where they grow. They may also receive radionuclide from the atmosphere: direct deposition and absorption from plume through plant roots and leaves, or resuspension by rain-splash. Consequently, many fruits contain measurable levels of ^{238}U, ^{232}Th and ^{40}K. In this way, consumption of fruits becomes a direct ingestion pathway for NORM to enter the human body. Because fruits are a direct dietary item, assessing their radioactivity is important for estimating radiation dose from diet. In other words, understanding NORM levels in fruits helps quantify the internal exposure of consumers. While most fruits contain only low concentrations of radioactivity, routine monitoring provides reassurance of safety and helps identify any unusually high exposures.

1.6 Problem Statement

Naturally occurring radioactive materials (NORM), including U-238, Th-232, and K-40, are present in the environment and can be introduced into the food chain through human and natural processes. While these radionuclides originate from geological sources, human activities such as industrial waste disposal, fertilizer application, and the use of phosphate-based agrochemicals may elevate their concentrations in agricultural soil. In particular, phosphate fertilizers, which are commonly used in fruit cultivation, often contain elevated levels of radionuclides due to their derivation from phosphate rock. These inputs can lead to the accumulation of NORM in plants, including fruits, through uptake from the soil during nutrient absorption, which then end up in our bodies through ingestion.

Fruits, as a regular part of the Bangladeshi diet, may thus act as contributors for internal radiation exposure. Ingesting contaminated fruits could lead to the gradual buildup of radionuclides within human organs, increasing the long-term radiological risk. Although several studies have investigated natural radioactivity in soils and selected food items, there remains a notable lack of data concerning the levels of U-238, Th-232, and K-40 in seasonal fruits consumed in urban regions such as Dhaka City. Given the widespread use of agricultural inputs and regional differences in environmental conditions, a focused assessment of NORM in fruits from local markets in Dhaka is needed to provide baseline radiological data and estimate potential exposure risks. Without such data, it is difficult to assess the actual ingestion dose and health implications for the population.

1.7 Aim and Objectives

The overall aim of this study is to assess the activity concentrations of naturally occurring radionuclides U-238, Th-232, and K-40 in seasonal fruits from local markets of Dhaka, Bangladesh, and to evaluate the associated radiological dose to consumers. To accomplish this aim, the specific objectives are to:

A. Collect representative samples of major seasonal fruits from local markets in Dhaka City.
B. Prepare and analyze the fruit samples using a high-purity gamma spectrometry detector to quantify the activity concentrations of U-238, Th-232, and K-40.
C. Identify an estimated annual fruit consumption rate stratified by age groups in urban regions.
D. Calculate the age-dependent annual effective dose for consumers based on the measured radionuclide concentrations.
E. Compare the results with relevant international safety guidelines and with published data from other regions.

These objectives will be addressed through a structured experimental and analytical approach described in subsequent chapters. By achieving these goals, the study will provide new data on dietary radiation exposure in Bangladesh and contribute to the formulation of appropriate safety standards for natural radioactivity in foods.

Chapter 2: Theoretical Background and Literature Review

This section covers the theoretical background of this study as well as a literature review and analysis of the previous studies. The section first covers the foundation of decay, how gamma radiation interacts with matter, and its effects on the human body. Afterwards, we look into studies relevant to our topic, their limitations and gaps, and how this study attempts to fill those gaps.

2.1 Radioactive Decay

Radioactive decay is the process by which a parent nuclide breaks down and transforms into its daughter nuclides, accompanied by the emission of radiation. These unstable nuclides emit particles and radiation such as Alpha (α) particles, Beta (β) particles, and Gamma (γ) rays, until a stable nucleus is formed. Each unstable nucleus has a constant probability per unit time of decaying, following the radioactive decay law. In a radioactive material, the radioactive decay per unit time is directly proportional to the total number of radioactive materials in the sample. The time when a particular radioisotope will undergo nuclear decay cannot be predicted, as this decay process is random and all the atoms are identical. However, in the case when a radioactive sample contains a very large number of atoms, the behavior of the ensemble can be predicted with high accuracy (Groch, 1998, p. 1247).

Activity, or the rate of decay, is equal to the rate of change of the number of atoms. N_t , as expressed in equation 2.1.

$$A_t = -\frac{dN_t}{dt} \tag{2.1}$$

The t refers to the time when the activity and number of atoms are sampled. This formulation implies that the rate of decay depends on the number of radioatoms undergoing transition, where the minus sign points to a decrease in activity over time. The unit of activity is decays per second, s^{-1}, with the SI unit being the becquerel (Bq). Our activity from equation 2.1 can also be written as

$$A_t = \lambda \times N_t \tag{2.2}$$

Where λ is the decay constant. Decay constant can be said to be the probability that probability per unit time—typically in seconds (s)—that an individual radionuclide will decay. These decay constants are also unique to each radionuclide, being invariant to change in temperature, pressure, and other physical properties that govern chemical reaction (Groch, 1998, p. 1249). Some examples of decay constants are provided below:

Isotope	Symbol	Decay Constant	Half-life
Uranium-238	U-238	4.9×10^{-18}/sec	4.5×10^{9} y
Radium-226	Ra-226	1.3×10^{-11}/sec	1,640 y
Iodine-131	I-131	1.0×10^{-6}/sec	8.05 d
Thallium-201	Tl-201	2.6×10^{-6}/sec	73 h
Technetium-99m	Tc-99m	3.2×10^{-5}/sec	6 h
Fluorine-18	F-18	1.1×10^{-4}/sec	1.8 h
Nitrogen-13	N-13	1.2×10^{-3}/sec	9.97 min
Oxygen-15	0-15	5.6×10^{-3}/sec	122 sec

Figure 2.1: A list of some decay constants (Groch, 1998, p. 1249)

Combining equations 2.1 and 2.2, we can derive an exponential decay formulation, as shown below.

$$A_t = -\frac{\mathrm{d}N_t}{\mathrm{d}t} = \lambda \times N_t \tag{2.3}$$

$$\implies \int_{N_0}^{N_t} \mathrm{d}N_t = -\lambda \int_{t=0}^{t} \mathrm{d}t \tag{2.4}$$

$$\implies \ln(N_t) - \ln(N_0) = -\lambda \times t \tag{2.5}$$

$$\implies \ln\left(\frac{N_t}{N_0}\right) = -\lambda t \tag{2.6}$$

$$\implies \frac{N_t}{N_0} = e^{-\lambda t} \tag{2.7}$$

$$A_t = A_0 e^{-\lambda t} \tag{2.8}$$

From this, we get the idea that the activity is exponentially decreasing, similar to the figure below:

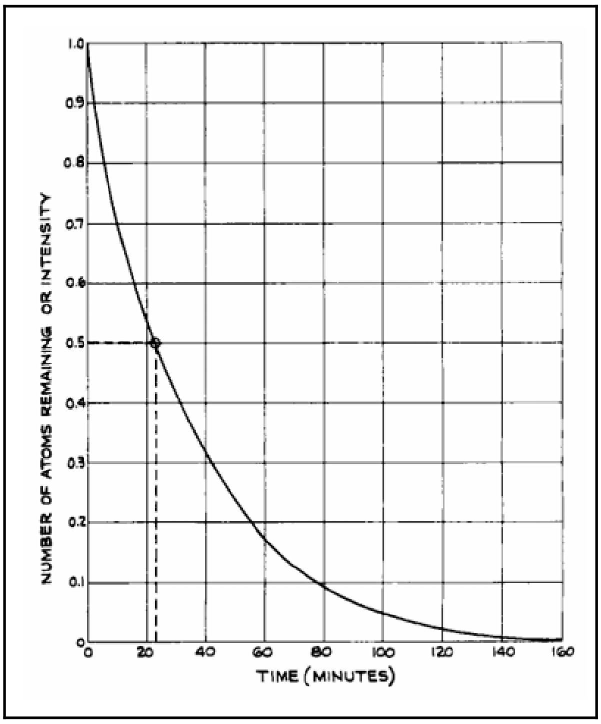

Figure 2.2: Decay Curve for Uranium-239 (Burton & Kebler, 1960)

2.1.1 Half-life

Half-life is defined as the time needed for one-half of a given sample of radioactive atoms to decay. In other words, time $t = T_{1/2}$, the activity $A_{T_{1/2}}$ remaining is 50% or half of the initial activity A_0 (Groch, 1998, p. 1252). Each isotope has a fixed half-life, which can range from fractions of a second to billions of years. For example, I-131 has a half-life of about 8 days, whereas U-238 has a half-life of about 4.5×10^9 years (International Atomic Energy Agency [IAEA], n.d.). Using the previous exponential decay equation, we can derive a relation with the decay constant.

$$A_{T_{1/2}} = \frac{A_0}{2} = A_0 e^{-\lambda T_{1/2}} \tag{2.9}$$

$$\implies e^{-\lambda T_{1/2}} = \frac{1}{2} \tag{2.10}$$

$$\implies e^{\lambda T_{1/2}} = 2 \tag{2.11}$$

$$\implies \lambda T_{1/2} = \ln(2) \tag{2.12}$$

$$\implies T_{1/2} = \frac{\ln(2)}{\lambda} \tag{2.13}$$

2.1.2 Radiation Types and Decay Processes

We see that there exist six primary modes of radioactive decay: *Alpha (α) decay*, *Beta (β) decay*, *Gamma (γ) decay*, *Spontaneous Fission (SF)*, *Photon Emission (PE)*, and *Neutron Emission (NE)* (Podgorsak, 2016, p. 476). And upon further inspection, these categories can be divided into sub-categories, which we will look into in a short while. Additionally, during nuclear transformations such as decay processes, some important quantities are conserved, which are:

1. Total energy
2. Momentum
3. Charge
4. Atomic number, Z
5. Atomic mass number (number of nucleons) A.

A diagram of the possible decay paths can be seen in figure showing the changes in A and Z with each decay.

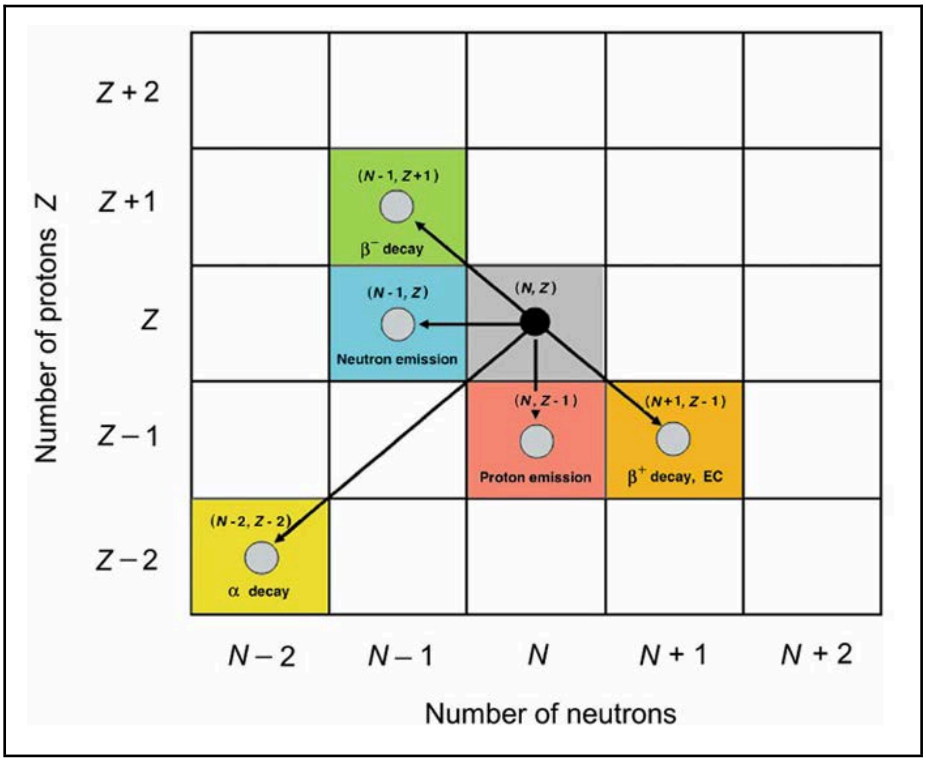

Figure 2.3: Possible decay paths in the Segrè Chart for a parent radionuclide (N, Z) to reach a stable configuration. The parent (solid black circle) and the daughter (open circles) (Podgorsak, 2016, p. 519)

Alpha (α) Decay

Alpha decay involves the emission of a helium-4 nucleus $\left({}_{2}^{4}\mathrm{He}\right)$ from an unstable parent nucleus, forming a more stable daughter nucleus (Podgorsak, 2016, p. 478). After emission, the daughter atom sheds two orbital electrons to achieve neutrality, while the α-particle captures electrons to form a neutral helium atom. This decay mode is common in naturally occurring radionuclides like uranium and radium. The alpha particle also has a very stable configuration with a binding energy of 7 MeV/nucleon. The number of protons and neutrons is conserved:

$$ {}_{\mathrm{Z}}^{\mathrm{A}}\mathrm{P} \rightarrow {}_{\mathrm{Z}-2}^{\mathrm{A}-4}\mathrm{D} + {}_{2}^{4}\mathrm{He} = {}_{\mathrm{Z}-2}^{\mathrm{A}-4}\mathrm{D} + \alpha \tag{2.14} $$

This process reduces the parent's atomic number Z by 2 and atomic mass number A by 4. From the naturally occurring radionuclides, the α released are of energies between 4 MeV and 9 MeV, corresponding to a range in air of roughly 1 cm to 10 cm, and tissue of about 10^{-3} cm and 10^{-2} cm, respectively. The decay occurs predominantly in heavy nuclei $(\mathrm{Z}>83)$, as a mechanism to reduce Coulomb repulsion. The emitted α-particle must overcome a Coulomb barrier via quantum tunneling.

Beta (β) Decay

Beta decay encompasses three processes where Z changes by ±1 while A remains constant (Podgorsak, 2016, p. 483). Thus, both the number of nucleons and the total charge are conserved in the β decay processes. The daughter D can be referred to as an isobar of the parent P.

Out of three categories, *Beta minus (β^-) decay* is when a neutron-rich radioactive nucleus transforms a neutron into a proton, emitting an electron e^- and an electron antineutrino $\overline{\nu}_e$ (Podgorsak, 2016, p. 487). This increases Z by 1 ($\mathrm{Z} \rightarrow \mathrm{Z}+1$):

$$n \rightarrow p + e^- + \overline{\nu}_e \qquad {}^{\mathrm{A}}_{\mathrm{Z}}\mathrm{P} \rightarrow {}^{\mathrm{A}}_{\mathrm{Z+1}}\mathrm{D} + e^- + \overline{\nu}_e \tag{2.15}$$

Next, *Beta plus (β^+) decay* is when a proton-rich nucleus converts a proton into a neutron, emitting a positron (e^+) and an electron neutrino ν_e, decreasing Z by 1 ($\mathrm{Z} \rightarrow \mathrm{Z} - 1$) (Podgorsak, 2016, p. 492).

$$p \rightarrow n + e^+ + \nu_e \qquad {}^{\mathrm{A}}_{\mathrm{Z}}\mathrm{P} \rightarrow {}^{\mathrm{A}}_{\mathrm{Z-1}}\mathrm{D} + e^+ + \nu_e \tag{2.16}$$

Finally, *Electron capture (EC)* is when a proton-rich nucleus captures an orbital electron (typically from the K-shell), converting a proton into a neutron and emitting a neutrino, reducing Z by 1 (Podgorsak, 2016, p. 496).

$$\mathrm{p} + \mathrm{e}^- = \mathrm{n} + \nu_e \qquad {}^{\mathrm{A}}_{\mathrm{Z}}\mathrm{P} + e^- = {}^{\mathrm{A}}_{\mathrm{Z-1}}\mathrm{D} + \nu_e \tag{2.17}$$

In many cases, the ground state of the daughter nucleus cannot directly be reached via beta decay of the parent nucleus, and instead, we get an unstable or metastable excited state of the daughter. We will see in the following that the excited state de-excites through emission of γ-rays or emission of internal conversion electrons

Gamma (γ) Decay

α and β decay processes, when producing a daughter nucleus from the parent, may not expend the full energy available, leaving behind an excited state (Podgorsak, 2016, p. 500). So, to reach ground state, the daughter may go through one of the two following ways:

1. *Gamma* (γ) *decay*: Emission of energy in the form of a γ photon.
2. *Internal Conversion (IC)*: Transferring the energy to one of its associated atomic orbital electrons.

In γ decays, though this photon is released from the excited daughter nucleus, we consider the emission to be from the parent nucleus as α and β decays occurs instantaneously. In addition, for certain decays, the de-excitation can be delayed. In such cases, the daughter is referred to as a *metastable state*, with a specified half-life $t_{1/2}$. The de-excitation process is called an *isomeric transition.* This process can be represented by the following:

$${}^{\mathrm{A}}_{\mathrm{Z}}\mathrm{X}^* \rightarrow {}^{\mathrm{A}}_{\mathrm{Z}}\mathrm{X} + \gamma + Q_\gamma \tag{2.18}$$

Where,

${}^{\mathrm{A}}_{\mathrm{Z}}\mathrm{X}^*$ is the excited state of ${}^{\mathrm{A}}_{\mathrm{Z}}\mathrm{X}$

Q_γ is the γ-decay energy.

An alternative to γ emission is *internal conversion (IC)*, where energy is transferred parent nucleus to an orbital electron of the same atom almost fully and is represented as follows (Podgorsak, 2016, p. 503):

$$ {}^{\mathrm{A}}_{\mathrm{Z}}\mathrm{X}^* \rightarrow {}^{\mathrm{A}}_{\mathrm{Z}}\mathrm{X}^+ + e^- + Q_{\mathrm{IC}} \rightarrow {}^{\mathrm{A}}_{\mathrm{Z}}\,\mathrm{X} \quad (2.19) $$

Where,

${}^{\mathrm{A}}_{\mathrm{Z}}\mathrm{X}^+$ is the ionized state of atom ${}^{\mathrm{A}}_{\mathrm{Z}}\mathrm{X}$ following internal conversion decay

Q_{IC} is the decay energy for internal conversion.

Spontaneous Fission (SF)

Spontaneous fission occurs in very heavy nuclei, only energetically feasible for nuclides with atomic masses above 230u, which split into two fission fragments of comparable mass while emitting 2–4 neutrons (Podgorsak, 2016, p. 505). SF is not self-sustaining (unlike neutron-induced fission) and has a half-life inversely correlated with atomic mass. This is a competing process to α decay, becoming more prominent as A increases above uranium-238 (${}^{238}U$). For the heaviest nuclei, Spontaneous fission (SF) becomes the primary mode of decay.

Proton Emission (PE) Decay

A competing process to β^+ and α decays is Proton Emission (PE), which occurs in the extreme case of a proton-excess nuclei, where one or two protons may be ejected directly to reach stability (Podgorsak, 2016, p. 506). The atomic number Z and atomic mass A goes down by 1:

$$ {}^{\mathrm{A}}_{\mathrm{Z}}\mathrm{P} \rightarrow {}^{\mathrm{A-1}}_{\mathrm{Z-1}}\mathrm{D} + p \quad (2.20) $$

As a proton gets ejected, the parent P sheds an electron from its outermost shell and becomes a neutral daughter atom. The ejected proton, then, captures an electron to become a hydrogen atom when moving through the absorber medium. Proton Emission decay preserves the neutron number N, making parent and daughter *isotones*.

Neutron Emission (NE) Decay

A different competing decay process to β^- decay is Neutron Emission (NE) decay. This is extremely rare compared to β^-, and is not observed from, naturally occurring radionuclides. This process involves the ejection of a neutron from a neutron-rich nucleus, decreasing A by 1 while Z remains unchanged. As such, the daughter and the parent are isotopes of the same species. Its representation is as follows (Podgorsak, 2016, pp. 509-510):

$$^{\mathrm{A}}_{\mathrm{Z}}\mathrm{X} \rightarrow {}^{\mathrm{A-1}}_{\mathrm{Z}}\mathrm{X} + n \tag{2.21}$$

2.1.3 Decay Chains

Many heavy radionuclides decay through a series of successive transformations called a decay series or chain. Each series begins with a long-lived parent and proceeds through a chain of radioactive daughters until a stable nuclide is reached. For example, Uranium-238 (U-238) undergoes a series of consecutive α or β decays before the chain ends at stable Polonium-208 (Po-208) element, as shown in Figure 2.4. Similarly, Thorium-232 (Th-232) also reaches Po-208, taking a slightly different path.

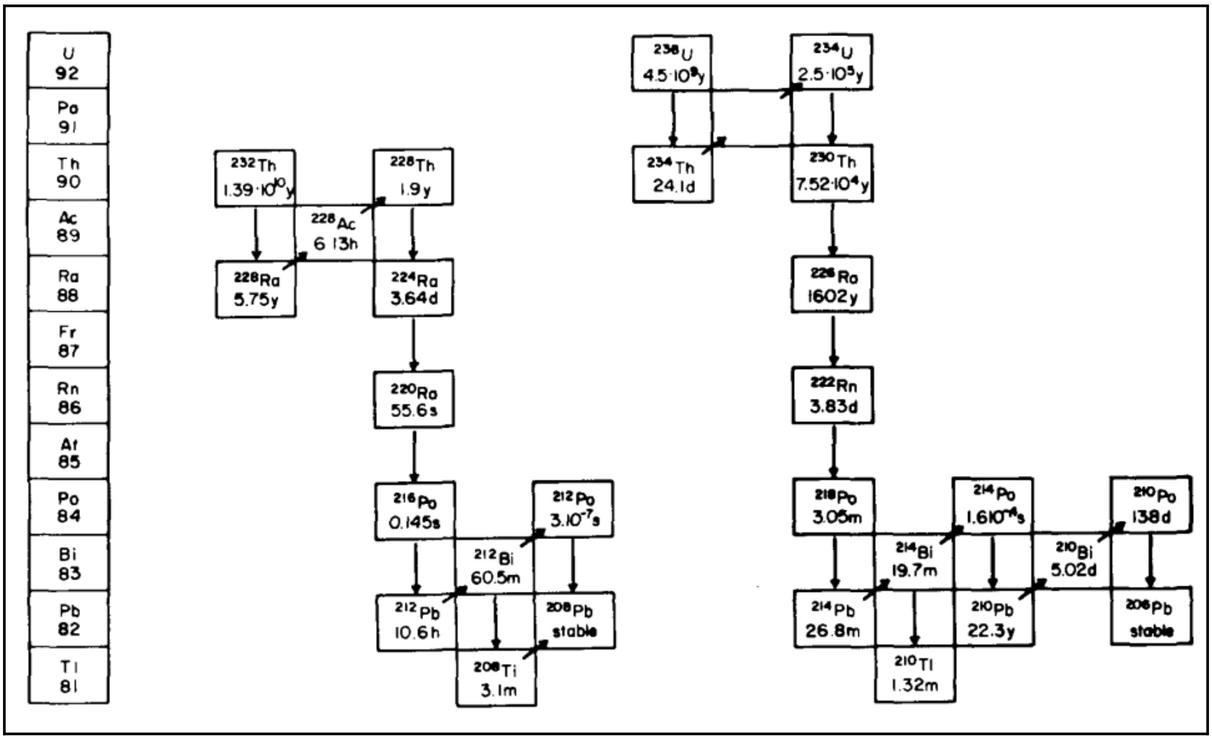

Figure 2.4: U-238 (right)and Th-232 (left) Decay Series (Cowart & Burnett, 1994, p. 652)

Potassium-40 (K-40), while a non-series decay radionuclide, decays in the following manner:

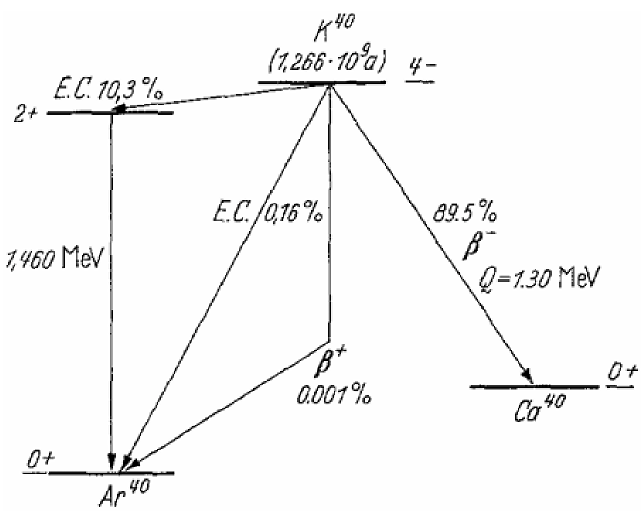

Figure 2.5: Decay Scheme of K-40 (Leutz et al., 1965, p. 151)

2.2 Gamma–Matter Interaction

Given that our study concerns gamma rays or photons and their consequences for humans, we ought to have some understanding of their interactions with matter. Categorized as two broader parts, photons may experience various interactions with atoms of the absorbing medium. The categories are as follows (Podgorsak, 2016, p. 278):

1. *Photon-nuclei interactions*: this interaction may be direct photon-nucleus or between the photon and the electrostatic field of the nucleus.
2. *Photon-orbital electron interactions*: interactions between the photon and either a loosely bound electron or a tightly bound electron.

A *loosely bound electron* is considered to be a "free" electron in the context of interaction with a photon. Its binding energy E_B is small relative to the photon energy $h\nu$. In comparison, the binding energy of *tightly bound electrons* is similar to that of the photon energy, if not larger or slightly smaller. Such interaction is considered to be between a photon and the atom as a whole.

After the interaction, the photon's fate can be one of the following:

1. The *photon disappears,* and some of its energy gets transferred to electrons and positions.
2. *The photon gets scattered* with two possibilities:
    a. *No electrons or positrons are released as no change in energy between the incident and resultant photon is observed.*
    b. *Excess energy is transferred to an electron as the resultant photon's energy is less than the incident photon.*

These interactions where light charged particles (electrons and positrons) are released or produced are of special consideration because they will then either deposit their energy to the medium through Coulomb interactions with orbital electrons of the absorbing medium—or, radiate the energy in the form of photon through coulomb interactions with the nuclei of the absorbing medium (Podgorsak, 2016, p. 279). While there exist many interactions, as far as medical physics and radiological dosimetry are concerned, these three photon-matter interactions are of the most importance: (1) *Photoelectric effect,* (2) *Compton scattering by "free" electron,* and (3) *Pair production*.

2.3.1 Photoelectric Effect

The photoelectric effect is an interaction between a photon and a tightly bound electron of an atom (Podgorsak, 2016, p. 335). Here, an orbital electron is ejected with kinetic energy E_K as it completely absorbs the photon's energy. Subsequently, the incident photon disappears. In Figure 2.6, we see a diagram illustrating the process.

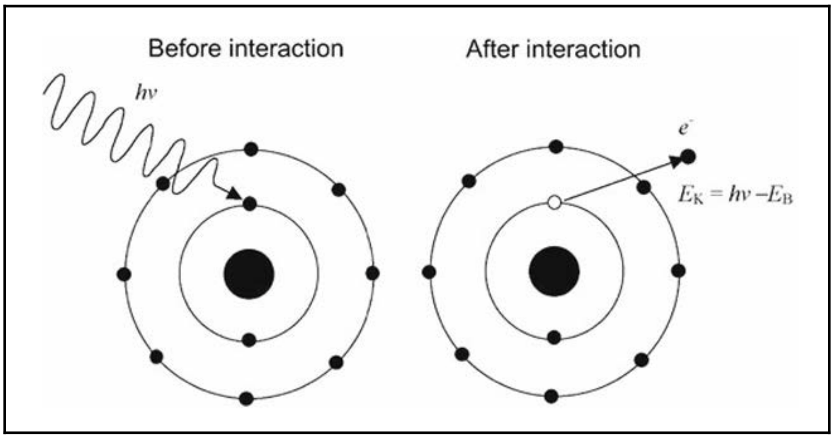

Figure 2.6: Schematic Diagram of Photoelectric Effect (Podgorsak, 2016, p. 336)

We understand the requirement for tightly bounded electrons from the conservation of total energy and momentum.

Conservation of total energy	Before: $h\nu + m_e c^2$	$h\nu = E_K$
	After: $E_K \nu + m_e c^2$	
Conservation of Momentum	Before: $p_\nu = \frac{h\nu}{c}$	$h\nu = E_K \sqrt{1 + \frac{2m_e c^2}{E_K}}$
	$After: p_e = \frac{E_K}{c}\sqrt{1 + \frac{2m_e c^2}{E_K}}$	

Clearly, momentum is not conserved between the electron and photon alone. So, this extra energy and momentum carried by a photon are transferred to another particle, the atom of that electron. This, of course, can only happen when the electron is tightly bound.

2.3.2 Compton Scattering

Shown schematically in Figure 2.7, the Compton effect, or incoherent scattering, is an interaction between a photon and a loosely bound electron (Podgorsak, 2016, p. 297). An incident photon of energy h/nu collide with an electron, resulting in a scattered photon of energy $h\nu^{'}$ and an electron, also known as a Compton electron. The scattering angle, θ is the angle between the incident photon and the scattered photon, varying from 0 to 180 degrees. The recoil angle ϕ is the angle between the incident photon and the Compton electron, ranging from 0 to 90 degrees. Due to collision and transfer of energy and momentum, the wavelength of the gamma ray photon shifts, which can be described as such:

$$\Delta\lambda = \lambda^{'} - \lambda = \lambda_C(1 - \cos\theta) \tag{2.21}$$

Where,

$\Delta\lambda$ is the change in wavelength or the difference between the scattered photon λ' and incident photon λ

λ_C is the Compton Wavelength of the electron,

$$\lambda_C = \frac{h}{m_e c} = \frac{2\pi\hbar c}{m_e c^2} = 0.0243\dot{\text{A}} \tag{2.22}$$

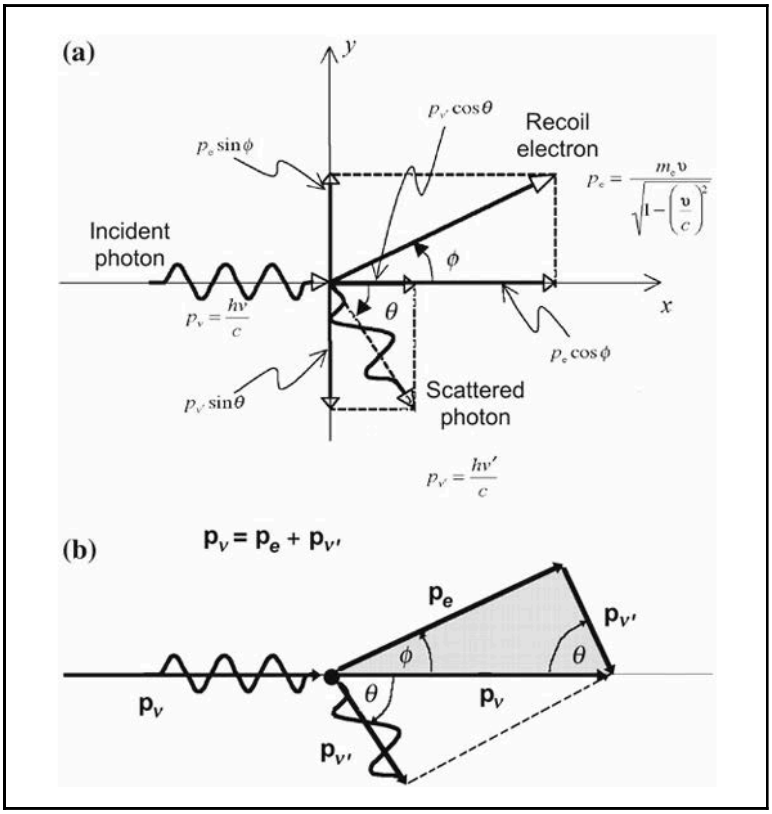

Figure 2.7: (a) A schematic diagram of Compton scattering. (b) a vector representation of Compton Scattering (Podgorsak, 2016, p. 297)

2.3.3 Pair Production

Pair production is a photon interaction that takes place when a photon's energy $h\nu$ exceeds $2m_e c^2 = 1.02\text{MeV}$, the combined rest energy of an electron and positron (Podgorsak, 2016, p. 356). During this process, the photon is fully absorbed by the atom, and an electron-positron pair is created, as shown in Figure 2.8. Three quantities—energy, electric charge, and momentum—must be conserved for the effect to occur.

In the case of $h\nu > 2m_e c^2$, linear momentum cannot be conserved for the pair production to occur in free space. This can only be achieved with a third particle, like we saw in the photoelectric effect. The photon's initial momentum $p_\nu = h\nu/c$ is larger than the total momentum after the electron-positron pair production interaction $p_{\text{pair}} = 2\gamma m_e v$ since the particle velocity v is always smaller than the speed of light c. This lack of momentum conservation, therefore, indicates the involvement of a collision partner within the absorber atom. Two collision partners are present to absorb the extra photon momentum: the atomic nucleus or an orbital electron.

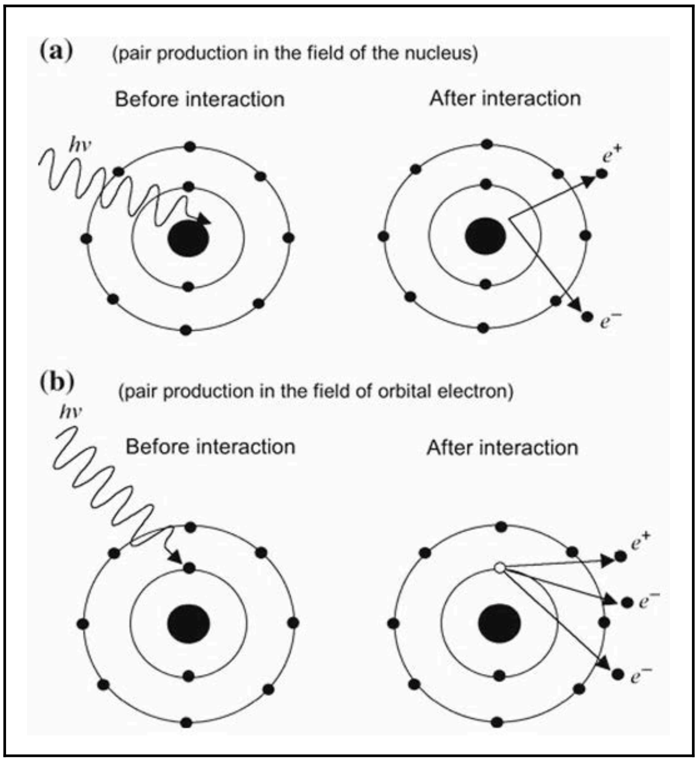

Figure 2.8: Schematic Diagram of (a) Nuclear Pair Production (b) Electron Pair Production (Podgorsak, 2016, p. 358)

In the first case, nuclear pair production occurs when the atomic nucleus absorbs the excess momentum. Due to the nucleus's large mass, the recoil energy it acquires is negligible.

Consequently, two particles—electron and positron—escape from the interaction. In the second case, triplet production occurs when an orbital electron absorbs the photon's excess momentum. The recoil energy transferred to this electron is significant, resulting in three particles escaping the interaction—two electrons and a positron.

2.3 Radioactive Equilibrium

Prince (1979) described radioactive equilibrium refers to a state in a decay chain where the number of atoms of a particular kind does not change with time. In other words, the activity of a daughter nuclide becomes constant because its production rate (from the parent's decay) equals its own decay rate, as shown in equation XX. This type of ideal was termed "Ideal equilibrium" (Podgorsak, 2016, p. 461).

$$A_p = A_d \tag{2.22}$$

$$\lambda_p N_p = \lambda_d N_d \tag{2.23}$$

However, as radioactive decay implies change, a contradiction appears. But given the case where the parent radioanuclide is significantly more long-lived than the daughter radionuclides, approximations can be reached. Two types of equilibria exist from this: transient equilibrium and secular equilibrium. For the confounds of this study, we only look at secular equilibrium.

2.5.1 Secular Equilibrium

Secular equilibrium is the common equilibrium condition where the ratio of activities of the parent and daughter radionuclides is a constant and there is no important decay of the parent nuclide during the time interval of interest (Prince, 1979). It occurs when the half-life of the parent is significantly longer than the half-life of the daughter $\lambda_p \ll \lambda_d$ (Groch, 1998,

p. 1255). Furthermore, Amols and Bardash (1993) state that secular equilibrium "occurs if and only if the half-life of the parent is at least twice that of the daughter" $\frac{t_p}{2} < t_d < t_p$. Under these conditions, we can derive an equilibrium form. From Groch (1998), we get the general equation for the activity of the daughter nuclide (p. 1255).

$$A_d = A_p \frac{\lambda_d}{\lambda_d - \lambda_p} \left(e^{-\lambda_p t} - e^{-\lambda_d t}\right) \tag{2.24}$$

$$\implies A_d \approx A_p \left(1 - e^{-\lambda_d t}\right) \tag{2.25}$$

$$\implies A_d \approx A_p \tag{2.26}$$

2.4 Gamma Spectrometry and HPGe Detector

A general description of the radionuclide detection theory is given below. This includes the principles of the gamma spectrometry system, High Purity Germanium (HPGe) detector, components used in the apparatus, and the calibration process.

2.4.1 Principles of Gamma Spectrometry

Gamma spectrometry stands as the preferred analytical method for determining both the activity levels and identity of gamma-emitting radionuclides within different sample types such as soil, water, or vegetation. In our case, it'd be fruits. The biggest advantage lies in enabling accurate multi-nuclide analysis directly on the sample, eliminating the need for complex and destructive chemical separation procedures. As this method is non-destructive, it's a lot more useful than traditional chemical methods, which are not only costly and time-consuming but also introduce additional handling risks and potential room for error. However, to get those reliable results, we need to do some crucial calibrations before analyzing the samples:

Energy Calibration

This essential step sets up how detector readings correspond to real gamma-ray energies. It requires a calibration source with multiple radionuclides emitting gamma rays across a broad energy range (from low to high). This full coverage ensures accurate energy calibration across the entire spectrum.

Efficiency Calibration

To translate measured count rates into exact activity concentrations, the system's detection efficiency must be determined. This is done by analyzing calibration standard sources with known activities. Very importantly, these standards must match the sample's physical size, composition, density, and shape. This matching reduces errors caused by factors like self-absorption. Additionally, background radiation counts must be carefully subtracted from standard source measurements to get accurate net count rates (Debertin & Helmer, 1988).

The two primary detector technologies employed in gamma analysis systems are sodium iodide (NaI) scintillation detectors and high-purity Germanium (HPGe) semiconductor detectors. While NaI detectors offer higher efficiency, HPGe detectors have become a vital tool for precise spectrometric analysis of complex radioactive samples due to their greater energy resolution. This exceptional resolution allows them to clearly differentiate between gamma rays of very similar energies, which is important for identifying specific radionuclides in mixtures like our samples.

Consequently, HPGe detectors are widely relied upon for the critical task of quantitatively determining the concentrations of specific radionuclides in challenging matrices, such as radioactive waste samples, where accurate characterization is paramount. A brief description of the HPGe detector follows in the next section.

2.4.2 High Purity Germanium (HPGe) Detector

High-purity Germanium (HPGe) detectors are now extensively used in gamma-ray spectrometry due to their exceptional performance characteristics. Using Germanium as a semiconductor for radiation detectors is due to its good charge transport properties, which allow for the usage of large-volume crystals while minimizing carrier losses from trapping or recombination. These detectors are particularly favored for resolving complex gamma-ray spectra consisting of numerous overlapping energy peaks and for identifying weak discrete-energy sources against a continuous background.

Structurally, HPGe detectors function as semiconductor diodes with a p-I-n configuration, where the intrinsic (I) region serves as the radiation-sensitive zone for X-rays and gamma photons. Under reverse bias, an electric field permeates the depleted intrinsic region. Incident photons interacting within this volume generate electron-hole pairs, which the electric field sweeps toward the p and n electrodes. A charge-sensitive preamplifier then converts this charge, proportional to the photon's deposited energy, into a measurable voltage pulse. The coaxial configuration is one in which the electric field changes inversely with the radial distance from the detector axis.

A typical coaxial HPGe detector comprises a germanium cylinder with an n-type contact on the outer surface and a p-type contact along the inner axial bore. The n contact is formed through lithium diffusion into a lapped germanium surface, while the p contact constitutes a metal-semiconductor surface barrier junction. This arrangement creates an n-p-p structure. Reverse biasing, which is applying a positive voltage to the n contact relative to the p surface, initiates a depletion region at the n boundary, extending further into the p region as the voltage increases. Due to a substantial dead layer on the n face, the p face typically functions as the photon entrance window. Ion implantation techniques may form the p contact when an ultra-thin entrance window is essential.

The HPGe detector's efficacy arises from several intrinsic properties: its high atomic number ensures efficient gamma-ray interactions; it's extremely low impurity concentration enables large depletion depths; the low energy required to create electron-hole pairs enhances energy resolution; and higher charge carrier mobility improves conductivity and fast response. Additional advantages include compact size, superior spectral resolution, and operation at room temperature.

2.4.3 System Components

The main parts of this detector, coupled with other accessories, are:

(1) Liquid nitrogen,

(2) Cryostat,

(3) Preamp

(4) Power Supply

(5) Multi-Channel Analyzer (MCA)

(6) Shielding arrangement

The block diagram of the HPGe detector system is shown in Figure.

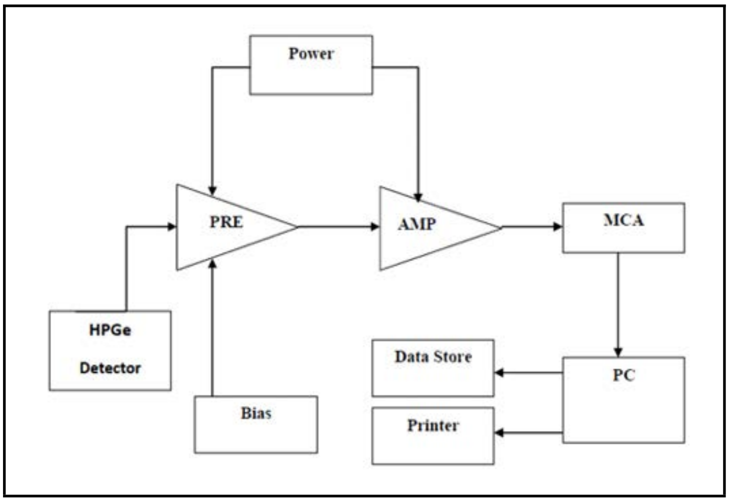

Figure 2.9: Block Diagram of HPGe Detector System (Mustakim et al., 2018)

Liquid Nitrogen Dewar

Due to Germanium's relatively low band gap, it requires cryogenic cooling for these detectors to suppress the thermal generation of charge carriers and the associated reverse leakage current to acceptable levels. Without such cooling, the resulting leakage current noise would destroy the detector's energy resolution. Liquid nitrogen LN_2, maintained at 77 degrees Kelvin, serves as the conventional cryogen. The detector is mounted in a vacuum chamber, which is attached to or kept inside a LN_2 Dawar, a double-walled vacuum-insulated vessel. With this, the sensitive detector surfaces are protected from moisture and condensable contaminants. The Dewar acts as the primary LN_2 reservoir, while the cryostat provides a path via the copper steam for heat transfer from the detector to the nitrogen reservoir.

Cryostat

A cryostat consists of a vacuum chamber that houses the detector element and a Dewar for the liquid nitrogen cryogen. Integral cryostats have a common vacuum chamber for the Dewar and detector. Here, the detector chamber and Dewar cannot be separated without breaking the vacuum, which is unlike the types of dipsticks. The cryostat is a sealed vacuum chamber, and usually the vacuum is maintained by a passive system, a molecular sieve, and placed at the bottom of the cold finger assembly. This molecular sieve absorbs any molecules that can potentially leak inside the cryostat and prevents them from depositing on the surface of the cryostat. If not the case, then an increase in surface contamination on the crystal would result in increased surface currents, which, in turn, elevate the noise and broaden the resolution.

Preamplifier

Modern gamma spectrometry systems predominantly utilize charge-sensitive preamplifiers, which generate output pulses with amplitudes proportional to the integrated charge from the detector. General-purpose versions include an RC feedback network, producing a quasi-step function output. For ultra-low-noise applications, the feedback resistor is eliminated to create a true step function output. This signal accumulates as a random staircase waveform until reset by pulsed-optical feedback circuitry. Notably, transistor reset preamplifiers (TRPs) deliver optimal performance for high-count-rate and high-resolution applications with HPGe detectors.

Germanium detector systems implement two fundamental preamplifier architectures:

1. Charge-sensitive designs using dynamic charge restoration (RC feedback).
2. Pulse charge restoration types—pulsed-optical or transistor reset—that discharge the integrator.

When photons interact with the detector, they generate very small current pulses at the preamplifier input. So, these signals require substantial amplification for later measurement. The preamplifier acts as the very first stage in the signal processing chain. Its proximity to the detector minimizes capacitive loading and reduces noise susceptibility. Additionally, the preamplifier works as an impedance transformer, presenting high input impedance to avoid detector loading while delivering low-impedance outputs to drive subsequent electronics. This configuration ensures efficient signal transfer and preserves spectral integrity throughout the processing chain.

Power Supply

A programmable dual-range, dual-polarity high-voltage (HV) supply (e.g., ORTEC 459) is used for detector biasing. The unit includes programmable voltage ranges: ±10 V to ±1300 V DC or ±1300 V to ±5000 V DC (software-limited to ≥1300 V on the 5000 V range), polarity selection, and output interface: Supplied via rear-panel SHV connector. For HPGe detector operation in this study, +3200 V was applied through the preamplifier's HV passthrough to establish the depletion field.

Multi-Channel Analyser (MCA)

Multi-Channel Analysers (MCAs) enable simultaneous pulse analysis across numerous discrete energy intervals (channels). Their core functions consist of data collection, visual spectrum monitoring, and output generation—either as final results or raw data for subsequent processing. An MCA system integrates three primary elements: an analogue-to-digital converter (ADC) for signal digitization, a digital memory buffer for data storage, and a display interface for visualization. The Wilkinson-type ADC constitutes the critical component, converting incoming analogue pulses from amplification stages into standardized digital formats. This digitization process assigns each pulse a channel number proportional to its input voltage amplitude. Identical-amplitude pulses consistently map to the same channel, ensuring spectral fidelity. Digitized counts are routed to corresponding memory addresses, where channel numbers index memory locations, incrementing respective channel counts. Consequently, the ADC's performance directly dictates key MCA characteristics.

Shielding Arrangement

Effective shielding against environmental radiation is essential for low-level activity measurements in gamma spectrometry. Due to its high density (11.4 g/cm^3) and atomic number (Z = 82), lead serves as the primary shielding material. This configuration efficiently attenuates hard gamma rays from natural backgrounds (e.g., 1.46 MeV emissions from K-40) while simultaneously mitigating cosmic ray components. However, gamma-ray interactions within lead shielding generate characteristic X-rays through photoelectric absorption. To suppress this secondary radiation, lead shielding is typically lined with steel, a material with substantially lower atomic number (Z $$\ approx$$26-28 for iron alloys) that effectively absorbs these X-rays.

2.4.4 Efficiency Metrics

This efficiency is related to a specific source-detector geometry and particular peak analysis procedure; it varies depending on the detector size and type of counting geometry, height, and weight of the standard sample (Fowler, 1965) and the environment surrounding the detector system. The counting efficiencies are measured with standard or reference samples in which the radionuclide concentrations are known. There are, however, situations where all the desired reference samples may not be known. For that, the best way would be to plot an efficiency calibration curve from the available standard sources and get an estimate from the curve. Three types of efficiencies exist that are discussed below:

Intrinsic photo-peak Efficiency

The intrinsic photo peak efficiency is defined as the fraction of gamma-rays that, upon hitting the detector, will produce counts in the corresponding photo peak. The efficiency can be obtained by using the following expression,

$$E_p = 1 - e^{-\mu t} \tag{2.27}$$

Where E_p is the photo-peak efficiency, μ is the linear attenuation coefficient of the detector at a specific energy, and t is the thickness of the detector.

Absolute Efficiency

The absolute efficiency of a counting system is the probability that a gamma ray emitted from a point source at a particular source-to-detector distance will produce a count in the corresponding photo-peak.

$$E_T = \frac{\text{Count in per second}}{\text{Gamma-ray emission per second}} \tag{2.28}$$

Relative Efficiency

Relative efficiency is the ratio of the absolute efficiency of the HPGe based on the 1.332 MeV peak of a Co-60 source positioned 25 cm from the detector to the absolute efficiency of a 3”× 3” thick NaI (Tl) crystal at the same source to detector distance (Medeiros et al., 2015). The relative photo peak efficiency:

$$E_R = \frac{R_1}{R_2} \times 100 \tag{2.29}$$

Where,

$$R_1 = \frac{\text{Count number for HPGe}}{\text{count time (s)}}$$

$$R_2 = \text{Gamma activity of the source in CPS} \times \text{Efficiency of the NaI detector}$$

2.4.5 Lower Limit Detection (LLD)

Lower Limit Detection (LLD) represents the minimum detectable activity that can be found by a measurement system under defined experimental conditions. Its value is influenced by multiple factors, including sample geometry, radiation energy, source-detector distance, detector efficiency, background radiation levels, measurement duration, and sample quantity. To determine LLD experimentally, we are to measure the gross counts N from a sample over time T, then separately determine the background count N_b over the same duration. The net sample activity is calculated as $N_\sigma = N - N_b$. Statistically, background fluctuations are characterized by the standard deviation $\sigma_b = \sqrt{N_b}$. Detection uncertainty occurs when N_σ approaches σ_b: values within this margin $N_s \leq \sigma_b$ suggest no significant activity, while exceeding $3\sigma_b$ $(N_s > 3\sqrt{N_b})$ indicates high-probability detection. This defines the detector limit as $L_D = 3\sqrt{N_b}$. For formal reporting at 95% confidence, the LLD is mathematically defined as $\text{LLD}_{95\%} = 1.645 \times 2\sqrt{2} \times \sigma_b \approx 4.65\sigma_b$, where σ_b remains the background standard deviation.

$$\text{LLD} = 1.65(2\sqrt{2})\sigma_b = 4.653 \left[\frac{N_b}{T^2}\right]^{\frac{1}{2}} \tag{2.30}$$

2.5 Biological Effects of Radiation

The interaction of ionizing radiation with biological systems leads to diverse health effects. ICRP Publication 60 (International Commission on Radiological Protection [ICRP], 1991) establishes the definitive framework for classifying ionizing radiation effects, central to modern radiological protection. Radiation interacts with living tissues primarily through ionization and excitation, depositing energy that damages critical molecules like DNA, either directly or indirectly via free radical production, as discussed in section 2.2. The effects can be categorized as either deterministic or stochastic based on their dose-response characteristics and underlying mechanisms (ICRP, 2007, p. 49).

2.5.1 Deterministic Effects (Harmful Tissue Reactions)

Deterministic or "non-stochastic" effects occur when radiation exposure exceeds a threshold dose, resulting in clinically observable damage due to substantial cell loss or functional impairment (ICRP, 2007, p. 49). The severity of these effects escalates with increasing dose above the threshold, showing the gradual deterioration of critical tissue cells. Early manifestations appear within days to weeks after exposure and include acute radiation syndromes such as hematopoietic suppression (threshold approximately 0.5 Gy), gastrointestinal damage (threshold about 6 Gy), and cutaneous erythema (threshold around 2 Gy) (ICRP, 1991, pp. 14-16). If the effects are not too severe, some may be reversible. There may be late effects which develop after months to years, and comprise of conditions like tissue fibrosis, cataract formation (thresholds ranging from 0.5-5 Gy for acute exposure), and permanent sterility (thresholds of 2.5-6 Gy for females and 3.5-6 Gy for males) (ICRP, 1991, pp. 15-16; ICRP, 2007, p. 50).

2.5.2 Stochastic Effects

Stochastic effects, conversely, lack dose thresholds, with probability of occurrence, but not severity. They represent probabilistic consequences of radiation exposure. These effects include radiation-induced malignancies resulting from somatic mutations and heritable diseases arising from germ cell mutations (ICRP, 2007, p. 50).

Risk of Cancer

As far as somatic effects are concerned, cancer risks are of the most importance. The development of radiation-associated cancers may stem from DNA damage that results in uncontrolled cell proliferation after a latency period. This latency period can range from years to decades (ICRP, 1991, p. 16). The linear-no-threshold (LNT) model, supported by the ICRP as a conservative framework for radiation protection, assumes that cancer risk increases proportionally with radiation dose at low levels, typically below 100 mSv. This model is primarily backed by epidemiological evidence from studies involving atomic bomb survivors, patients exposed to medical radiation, and radiation workers (ICRP, 2007, p. 51; National Research Council [NRC], 2006).

Modern detriment-adjusted risk coefficients account for disease severity and quality-of-life effects. For the general public, the nominal risk coefficient is currently 5.5×10^{-2} per Sv. Occupational risk estimates are marginally lower, at 4.1×10^{-2} per Sv, as worker populations typically exclude more radiation-sensitive groups (ICRP, 2007, p. 55). To address discrepancies between high- and low-dose radiation effects, a dose and dose rate effectiveness factor (DDREF) of 2 is used. This adjustment reflects the observed decrease in biological effectiveness during prolonged or low-dose exposures (ICRP, 2007, p. 53; NRC, 2006).

Risk of Hereditary Effects

Since no strong evidence of radiation-induced genetic disease in humans has been observed thus far, our understanding of heritable risks relies primarily on experimental animal studies (ICRP, 2007, p. 54; UNSCEAR, 2001). Modern risk assessments incorporate improved methodologies, resulting in a general population nominal risk coefficient of 2×10^{-3} per Sv, or about 0.2% per Gy up to the second generation.

Genetic Susceptibility to Cancer

Since ICRP 60, research has significantly improved our understanding of single-gene human genetic disorders, or high-penetrance genetic disorders that greatly increase cancer risk in carriers (ICRP, 2007, p. 56). Studies using human cell cultures and genetically modified rodents, along with limited clinical data, indicate that most rare cancer-prone genetic disorders heighten radiation sensitivity. However, due to the rarity of these high-penetrance conditions in humans, the effects on the wider population in near negligible (ICRP, 2007, p. 56). Emerging evidence also suggests that lower-penetrance gene variants, interacting with environmental and other genetic factors, may contribute to variable cancer risks after radiation exposure, but their contributions remain uncertain due to limited data.

2.6 Radiation Dose Assessment

Finally, we ought to look into a few definitions and quantities defined and improved upon by UNSCEAR (2000) that we will be using throughout the research. We begin by describing the Representative Person used to estimate the dose absorbed by the average public. Then, we define fundamental quantities like absorbed dose, equivalent dose, and effective dose—as well as annual ingestion dose and annual effective dose.

2.6.1 The Representative Person

The Representative Person, introduced in ICRP Publication 101 (ICRP, 2006), is a hypothetical construction designed to assess public radiation exposure for compliance with dose constraints. This serves as a more refined tool to represent the more highly exposed individuals in a population. The primary objective is to ensure that the dose estimated for this individual remains below the regulatory dose constraint, following the principle of optimization of protection.

Dose assessment for the Representative Person requires a detailed evaluation of all relevant exposure pathways, including atmospheric releases, liquid discharges, and direct external exposure. The analysis must ensure that no significant pathway is omitted, particularly those that may dominate overall exposure. Additionally, the spatial and temporal distribution of radionuclides must be considered, accounting for potential long-term accumulation (e.g., in river sediments) and possible future changes in land use that could alter exposure scenarios.

A critical aspect of defining the Representative Person is the selection of habit data, which includes dietary intake, residence patterns, and local resource use. These data must be reasonable (within realistic daily life changes), sustainable (maintainable over the assessment period, typically at least five years), and homogeneous (avoiding undue influence from extreme individual behaviors within the exposed subgroup). While site-specific data is preferred, the 95th percentile of national or regional consumption rates may be used as a cautious default in deterministic assessments when local data is unavailable. However, excessive conservatism, such as using extreme values in all variables, should be avoided to prevent unrealistic overestimations of dose.

For internal exposures, age-specific dose coefficients play a key role in refining dose assessments. Recognizing the practical challenges in prospective dose evaluations, ICRP recommends consolidating calculations into three broad age categories: Infant (0–5 years), using coefficients for a 1-year-old; Child (6–15 years), using a 10-year-old reference; and Adult (16–70 years), applying adult coefficients. This simplification balances precision with the inherent uncertainties in long-term exposure assessments, particularly for facilities with operational lifetimes spanning decades.

2.6.2 Absorbed Dose

Absorbed dose, D, is the fundamental dosimetric quantity used for assessments. It is averaged over a tissue or organ, with the unit of joule per kilogram, which is given the special name "gray" (Gy). The relationship of this quantity to the risk of biological effect is described by the weighted dose quantities (UNSCEAR, 2000).

2.6.3 Equivalent Dose

Equivalent dose, H_T is the averaged absorbed dose in tissue or organ T, modified by the radiation weighting factor, w_R, the values of which are given in Figure 2.10. In equation form, it is as follows:

$$H_T = \sum_R w_R D_{T,R} \tag{2.31}$$

Where $D_{T,R}$ is the mean absorbed dose in tissue or organ T due to radiation R. Its units are joules per kilogram with a special name, sievert (Sv).

Radiation weighting factors*	
Type and energy range	w_R
Photons, all energies	1
Electrons and muons, all energies	1
Neutrons, energy <10 keV	5
10 keV–100 keV	10
>100 keV–2 MeV	20
>2 MeV–20 MeV	10
>20 MeV	5
Protons, other than recoil, energy >2 MeV	5
Alpha particles, fission fragments, heavy nuclei	20

Figure 2.10: Weighing Factors (ICRP, 2012, p. 11)

2.6.4 Effective Dose

Effective dose (E) is the tissue-weighted sum of equivalent doses in all organs and tissues:

$$E = \sum_T W_T \sum_R w_R D_{T,R} \tag{2.32}$$

Similar to equivalent doses, the effective dose also has the unit of joules per kilogram, with the name sievert (Sv). The recommended values of w_T are given in Figure 2.11.

2.6.5 Dose Coefficients

Committed tissue equivalent dose per unit acute intake $h_T(\tau)$ or committed effective dose per unit acute intake $e(\tau)$, where s is the time period in years over which the dose is calculated. For each radionuclide, the ICRP 119 (ICRP, 2012) provides dose coefficients (in Sv/Bq) for the representative person of various ages.

Tissue weighting factors*		
Tissue or organ	w_T	$\sum w_T$
Gonads	0.20	0.20
Red marrow, colon, lung, stomach	0.12	0.48
Bladder, breast, liver, oesophagus, thyroid, remainder*	0.05	0.30
Skin, bone surface	0.01	0.02
	Total	1.0

Figure 2.11: Tissue Weighing Factors (ICRP, 2012, p. 12)

2.6.6 Annual Ingestion Dose and Annual Effective Dose

The annual effective dose is the total effective dose received from internal, ingestion and inhalation, and external pathways. For this study, however, we are only concerned with the ingestion of fruits. Thus, the annual effective dose through fruit ingestion, or annual ingestion dose, is the effective dose received by an individual from the ingestion of fruit each year. We determine the value by multiplying the yearly consumption of fruits per capita by the concentration activity of each radionuclide and its dose coefficients. The equation is properly shown in equation 3.4.

2.6.7 Public Exposure Limits

The ICRP (1990) confines its recommended dose limits for public exposure to doses resulting from practices—deliberate activities involving radiation sources, such as emissions from nuclear installations or waste disposal sites. Doses arising from situations requiring intervention (e.g., radon in dwellings, pre-existing environmental radioactivity) are explicitly excluded from these limits. The Commission acknowledges the challenge in defining an "unacceptable" risk level for the public but bases its recommendations on two key considerations: (1) health detriment estimates from sustained low-dose exposure (1–5 mSv/year), and (2) natural background radiation levels (typically ~1 mSv/year, but up to 2×

higher in some regions). This approach reflects a societal judgment that deliberate practices should not impose risks exceeding variations in natural exposure.

Recommended Limits for Effective Dose

An annual effective dose limit of 1 mSv is established for members of the public. To accommodate transient environmental fluctuations or operational variability, flexibility is permitted: a higher annual dose (e.g., >1 mSv) may be accepted in special circumstances, provided the average over any consecutive 5 years does not exceed 1 mSv/y. This 5-year averaging period balances lifetime risk accumulation with practical implementation. Critically, the Commission emphasizes that dose constraints applied during optimization of protection for new installations should be set below this 1 mSv/year limit to ensure compliance.

2.7 Previous Studies on Radionuclide Analysis

Mustakim et al. (2018) researched the seasonal fruits abundantly available in the local markets of Bangladesh for the presence of natural radionuclides ^{238}U, ^{232}Th, and ^{40}K. Their research goal was to estimate the radiological risks of consuming the fruits, considering the possibility of radionuclides from the soil being absorbed by the plant tissues. In total, 20 samples comprising 16 varieties of fruits were collected. These samples underwent a series of preparation steps, which included sun drying, oven drying, grinding, and sieving. Analysis was performed through high-resolution gamma-ray spectrometry using a high-purity Germanium (HPGe) detector. The analyzed results displayed activity concentration of ^{238}U from BDL to 31.13 Bq/kg and the mean value of 10.95 Bq/kg. For ^{232}Th, the value of 1.55 to 34.59 Bq/kg was measured as an average of 6.68 Bq/kg. ^{40}K was noted to have the highest concentration of radionuclide, with measurements ranging from BDL to 733.25 Bq/kg and a mean of 308.90 Bq/kg. Of importance was the observation that the ^{40}K content in bananas was higher than in comparable studies from other countries. An evaluation of the radiological risk was undertaken by estimating the internal effective dose from fruit consumption every year. Considering the average radionuclide levels and a reported fruit consumption rate of 44.7 g/day within Bangladesh, the estimated cumulative effective dose was 8.39 μSv/year. This is far below the 1 mSv/year dose limit set by the International Commission on Radiological Protection (ICRP), suggesting that the radiological risk associated with consuming these fruits is negligible. ^{238}U, ^{232}Th, and ^{40}K.

Another group of researchers, Islam et. al (2014) studied the levels of naturally occurring radionuclides, ^{228}Ra, ^{238}U, ^{232}Th, and ^{40}K, in papaya from the high-background-radiation region of Tulatoli village, Teknaf, in southeastern Bangladesh. This area is situated over a region with heavy mineral sands containing thorium-bearing monazite, which potentially results in heightened soil radioactivity, raising concerns for the population in regards to the food that they consume. The researchers collected and processed ten papaya samples using high-purity Germanium (HPGe) gamma-ray spectrometry. The average activity concentrations measured were 80.95 ± 13.61 Bq/kg for ^{228}Ra, 64.77 ± 38.47 Bq/kg for ^{238}U, 83.53 ± 20.50 Bq/kg for ^{232}Th, and 1691.45 ± 244.98 Bq/kg for, which were significantly higher than the global averages reported by UNSCEAR. Based on local consumption patterns, the estimated total annual ingestion dose of papaya was pegged at 1.10 mSv/year, which is approximately 3.8 times the benchmark of 0.29 mSv/year for exposure from terrestrial radionuclides. Out of this estimated dose, ^{228}Ra, ^{238}U, and ^{232}Th contributed 0.89 mSv/year and ^{40}K contributed 0.21 mSv/year.

Ahmed et al (2024) aimed to analyze the behavior of polonium-210 (^{210}Po) and lead-210 (^{210}Pb) accumulation in fruit from the naturally high background radiation (NHBR) region of Manavalakurichi, Tamil Nadu, India. The study area is well known for its high environmental radioactivity, especially due to the region's monazite-rich coastal sands, which makes it important to study the radiological risk of the transfer of radionuclides through the food chain. The researchers conducted a fruit and soil sample survey in eight agricultural fields and processed their samples using standardized alpha spectrometric approaches to determine the radionuclide concentrations. Soil samples yielded average activity concentrations of 64.74 Bq/kg for ^{210}Pb and 9.12 Bq/kg for ^{210}Po. The concentration of radionuclides among the fruit samples was heterogeneous. The highest concentrations were found in coconut, which contained ^{210}Po at 6.910 Bq and ^{210}Pb at 24.625 Bq. Some varieties of bananas also contained significant concentrations of the radionuclides ^{210}Po and ^{210}Pb, with ^{210}Po between 1.946 to 4.973 Bq/kg and ^{210}Pb between 19.750 to 21.500 Bq/kg. The study focused on the three age categories to evaluate the annual effective ingestion dose and Excess Lifetime Cancer Risk (ELCR) for different demographics. For adults, the effective dose was 167.9 μSv/year, for juveniles 239.9 μSv/year, and for children 352.1 μSv/year. While these figures may be exceeding some regional averages, they are still less than the international goodness of 1 mSv/year cited by ICRP and IAEA. The ELCR values for ^{210}Po doses were 8.63×10^{-6} to 4.85×10^{-4} and for ^{210}Pb were 1.17×10^{-4} to 1.47×10^{-3}. These numbers are still below the ICRP threshold of 2.5×10^{-3}, meaning there is no immediate risk of cancer from the dietary exposure, considering the region's radionuclide concentration.

Küçükönder et al. (2023) derive the radiological risk evaluation of fruits and vegetables grown in Kahramanmaraş, emphasising the accumulation of natural radionuclides ^{238}U, ^{232}Th, and ^{40}K. This study also estimates internal radiation doses and the corresponding cancer risk over a lifetime for consuming these food items for different age categories: adults, 10-year-old children, and infants. In the fruit samples, ^{238}U

concentrations varied from below detection limits to 15.29 ± 1.14 Bq/kg. The levels of ^{232}Th ranged from 0.30 ± 0.01 to 13.23 ± 1.60 Bq/kg, and ^{40}K from 5.82 ± 0.21 to 179.82 ± 1.34 Bq/kg. The weighted average activity concentrations of ^{238}U, ^{232}Th and ^{40}K in fruits were 5.31 ± 0.44 Bq/kg, 2.72 ± 0.26 Bq/kg and 56.84 ± 0.57 Bq/kg respectively. As for the vegetable samples, ^{238}U concentrations were between 0.48 ± 0.04 and 11.77 ± 0.95 Bq/kg, ^{232}Th between 0.55 ± 0.04 and 4.57 ± 0.44 Bq/kg, and ^{40}K between 9.32 ± 0.43 and 52.44 ± 0.52 Bq/kg. The average concentrations in the values from vegetables were 6.58 ± 0.65 Bq/kg for ^{238}U, 2.72 ± 0.27 Bq/kg for ^{232}Th, and 27.09 ± 0.27 Bq/kg for ^{40}K. Evaluating the potential impacts on health risks, the study calculated the effective dose for each age group based on their typical eating habits. Specifically for fruit consumption, the annual effective doses were 0.184 ± 0.001 mSv/year for adults, 0.288 ± 0.002 mSv/year for children, and 0.304 ± 0.003 mSv/year for infants. Corresponding lifetime cancer risks were $0.647 \pm 0.006 \times 10^{-4}$ for adults, $1.011 \pm 0.010 \times 10^{-4}$ for children and $1.067 \pm 0.01 \times 10^{-4}$ for infants. For vegetables, however, the annual effective doses for adults were 0.118 ± 0.001 mSv/year, for children 0.128 ± 0.001 mSv/year and infants 0.086 ± 0.001 mSv/year. The lifetime cancer risks for this were $0.416 \pm 0.004 \times 10^{-4}$ for adults, $0.449 \pm 0.004 \times 10^{-4}$ for children, and $0.304 \pm 0.003 \times 10^{-4}$ for infants.

The study by Altamemi et al. (2021) was designed to measure the activity concentration of $226^{R}a$, ^{232}Th, ^{40}K, and ^{137}Cs in some fruits as well as vegetables of Kastamonu, located in the western region of the black sea region of Turkey, using gamma ray spectrometry. In the 28 vegetable samples, the mean concentration of ^{226}Ra, ^{232}Th, and ^{40}K ranged from 0.8 ± 0.1 to 32.8 ± 1.3, 0.7 ± 0.1 to 41.3 ± 2.1, and 391.8 ± 18.3 to 4679.0 311.4 Bq/kg dry weight, respectively. In the seven samples of fruits, these radionuclide concentrations ^{226}Ra, ^{232}Th, and ^{40}K ranged from 1.3 ± 0.1 to 12.6 ± 0.4, 1.4 ± 0.1 to

15.0 ± 0.5, and 133.0 ± 8.4 to 777.0 ± 69.4 Bq/kg respectively. It is important to highlight that garlic showed the greatest concentration of ^{226}Ra and ^{232}Th, while the greater concentration of ^{40}K was found in spinach. The trace amounts of anthropogenic ^{137}Cs radionuclide were found in only four vegetables—garlic, eggplant, cucumber, and carrot—garlic containing 9.6 ± 0.3, eggplant 3.1 ± 0.1, cucumber 3.1 ± 0.1, and carrot 2.2 ± 0.1 Bq/kg. These values were validated with existing literature. The annual effective dose from ingestion for an adult was estimated as 201 µSv with 8.9×10^{-5} excess lifetime risk of cancer. The studied radionuclides, ^{40}K contributed roughly 70% towards the annual effective dose.

Abojassim et al. (2016) aimed to assess the prevalence of natural radioactivity in fruits and vegetables from Najaf Governorate, Iraq, focusing on their dietary effective dose for adults, 10-year-old children, and infants. The study determined the specific activity of ^{238}U, ^{232}Th, and ^{40}K in 31 vegetables and 9 fruits using gamma-ray spectrometry and NaI (Tl) detectors. The activity concentrations of ^{238}U, ^{232}Th and ^{40}K for the vegetables were determined to be 5.21 ± 0.47 Bq/kg, 4.76 ± 0.34 Bq/kg, and 186.15 ± 10.78 Bq/kg, respectively. In fruits, the activity concentration of ^{238}U was below detection limits, while ^{232}Th and ^{40}K averaged 2.53 Bq/kg and 211.64 Bq/kg, respectively. ^{40}K was found to be the highest in lettuce (319.21 Bq/kg), and apricot had the highest ^{40}K among the fruits (290.20 Bq/kg). Using the ICRP dose conversion factors and consumption rates from the region's dietary data, the study computed age-specific average effective doses. For adult and child vegetable consumers, the average effective dose was 0.117 ± 0.009 mSv. For infants, the dose was 0.179 ± 0.031 mSv. For fruits, the values were higher; for adults, 0.141 ± 0.008 mSv, for children, 0.295 ± 0.094 mSv, and 0.388 ± 0.101 mSv for infants. This indicates infants aged below 1 year are at heightened risk, likely due to a higher dose conversion coefficient and lower body weight. As anticipated from the radionuclide activity concentration data, all dose values calculated for the varying sample populations were below the 1 mSv/year limit recommended by the ICRP and UNSCEAR for public exposure. The research results show that there is no risk of consuming fruits and vegetables in Najaf, radiologically and health-wise, but it is essential to address Iraq's post-conflict environmental challenges, which may lead to monitoring due to the risk of soil contamination.

Podgorsak (2016) determined the levels of radionuclides, particularly ^{228}Ra, ^{232}Th, and ^{40}K, in vegetables and fruits that are widely consumed in the central region of Malaysia, as well as the radiological risk associated with the consumption of these radionuclides. The samples were procured from the local markets and were processed through HPGe gamma-ray spectrometry. The computed annual ingestion doses were calculated along with the cancer risk for three demographic categories comprising an infant (1-3 years), a toddler (7-12 years), and an adult (above 17 years), considering the dose conversion coefficient and intake rates for the respective ages. For vegetables, the activity concentrations ranged from 0.60 ± 0.57 to 5.64 ± 0.65 Bq/kg for ^{226}Ra, 0.41 ± 0.32 to 4.40 ± 0.49 Bq/kg for ^{232}Th, and 398.85 ± 6.89 to 1072.59 ± 10.25 Bq/kg for ^{40}K. The mean concentrations were 2.07 ± 0.31, 2.12 ± 0.24, and 791.51 ± 3.66 Bq/kg, respectively. For fruit samples, the mean activity concentrations were 2.44 ± 0.34 Bq/kg for ^{226}Ra, 1.54 ± 0.25 Bq/kg for ^{232}Th, and 288.63 ± 2.83 Bq/kg for ^{40}K. Annual doses for effective radiation received while consuming vegetables were 0.469 ± 0.003 mSv for infants, 0.326 ± 0.005 mSv for children, and 0.232 ± 0.003 mSv for adults. Similarly, for fruits, the doses were 0.349 ± 0.005 mSv, 0.283 ± 0.007 mSv, and 0.195 ± 0.004 mSv. Even though the global average annual dose for natural background radiation is 2.4 mSv/year, the consumption doses for infants—and in some cases, children—exceed the UNSCEAR recommended ingestion dose threshold of 0.29 mSv/year. Regardless, all values fall under the limits of accepted safety thresholds. The estimation of the cancer risk for adults consuming vegetables and fruits was 8.13×10^{-3} and 6.83×10^{-4}, respectively, both of which are significantly lower than the background radiation exposure cancer risk $8.4 \times 10^{-3]}$. Following the Cohen and Lee risk model, the life-shortening effect of consuming these radionuclides was negligible, 2.13 days for vegetables and 1.57 days for fruits.

The scope of the research conducted by Sowole & Olaniyi (2018) was to analyze the naturally occurring radionuclides ^{238}U, ^{232}Th and ^{40}K in fruits collected from three major markets in Ijebu-Ode, Ogun State, Nigeria, and calculate the annual committed effective dose (ACED) for consumers. This study describes the pathways for radionuclide contamination of food, predominantly through soil and water, and demonstrates the potential public health risk of prolonged exposure to food in the presence of high natural background radiation. Gamma-ray spectrometry was used to analyze twelve types of fruit—orange, pineapple, banana, and mango—over the specified study period. The complex analysis showed that the maximum concentrations obtained of ^{40}K, ^{238}U and ^{232}Th were recorded in pineapple (102.36 ± 10.81Bq/kg), orange (12.18 ± 4.36Bq/kg) and mango (8.01 ± 3.25Bq/kg), respectively. Average concentrations, in all samples, were 78.51±8.66Bq/kg for ^{40}K, 9.24 ± 3.40 Bq/kg for ^{238}U and 6.34 ± 2.29Bq/kg for ^{232}Th. None of the samples contained radionuclides from anthropogenic sources. The fruits' consumption led to the annual committed effective doses, which were calculated with the use of predetermined dose conversion factors. For ^{40}K, the highest ACEDs were 0.091 mSv/year, 0.079 mSv/year for ^{238}U and 0.265 mSv/year for ^{232}Th with an average of 0.070, 0.060 and 0.197 mSv/year, respectively. The cumulative average dose was 0.11 mSv/year, which still remains far below the international safety dose limit of 0.3 mSv/year for the consumption of natural radionuclides (UNSCEAR, 2000).

Lastly, Shanthi et al. (2010) focused on the radiological health hazards stemming from the consumption of food crops grown in the high natural background radiation areas (HLNRA) of southwest India in the coastal region of Midalam and the adjacent villages of Kanyakumari district, Tamil Nadu. These locations have an enriched concentration of monazite-bearing sands, which are a considerable source of thorium and uranium, resulting in high soil radioactivity. To estimate the internal exposure through diet, the researchers conducted a complete dietary survey and measured the activity concentration of ^{226}Ra, ^{228}Ra, ^{228}Th, and ^{40}K in rice, blackgram, milk, fish, fruits, some vegetables, and tubers that are part of the South Indian dietary pattern. The researchers conducted a complete dietary survey and collected samples, which were then analyzed using gamma-ray spectrometry. Radionuclide concentrations were also computed on a fresh-weight basis. Based on local dietary habits, the intake of these radionuclides was calculated. Additionally, of the food groups examined, the greatest concentrations and greatest intake were noted for ^{40}K which were mostly in rice and banana. Overall dietary intakes were measured at 3.05 Bq/day for ^{226}Ra, 2.26 Bq/day for ^{228}Ra, 18.07 Bq/day for ^{228}Th, and 121.88 Bq/day for ^{40}K. The annual internal doses for each isotope were measured at 0.201 mSv for ^{226}Ra, 0.659 mSv for ^{228}Ra, 0.475 mSv for ^{228}Th, and 0.460 mSv for ^{40}K, summing up to 1.80 mSv/year. This is, of course, excessively greater than the ICRP's public recommended dose of 1 mSv/year. These people residing in HLNRA are primarily influenced by dietary habits in terms of internal radiation exposure. The major culprits are ^{228}Ra and ^{228}Th, with potassium contributing too. Although ^{40}K is a radioactive isotope and is biologically regulated and obligatory for human metabolism, the high consumption of thorium and radium series nuclides is worrying in terms of prospective chronic illnesses. Regions rich in radioactive minerals require constant monitoring, and radiation protection policies at the national level need to account for dietary radiation exposure.

2.8.1 Limitations

Analyzing the existing body of literature, a few distinct observations can be made. First, despite the wide array of studies pertaining to fruit and vegetable radionuclide concentrations, they were mostly from outside Bangladesh. Only two published articles—Mustakim et al. (2018) and Islam et al. (2014)—were found that coincide with our topic. Additionally, most radioactivity surveys in Bangladesh have focused on soils, water, or select foodstuffs. For instance, Kakolee et al. (2021) measured U-238, Th-232, and K-40 in soils of the Chandpur district, and Sarker et al. (2021) measured these radionuclides in powdered milk from Dhaka markets. However, there is a lack of literature specifically concerning fruits.

Second, very few have focused specifically on the highly consumed fruits in specific regions of Bangladesh. Only Mustakim et al. (2018) investigated NORM activity and annual internal dose in seasonal fruits, but their samples came from Rajshahi and Natore districts in northern Bangladesh. Region-specific estimations remain scarce; no published study has yet surveyed naturally occurring radionuclides in fruits, particularly in the context of local markets like Dhaka, limiting the ability to make localized public health assessments.

Third, existing literature rarely accounts for age-dependent annual dosage, leaving a significant gap in understanding how ingestion risks vary across different population groups such as infants, children, and adults. Only a few have made attempts to make this distinction such as Küçükönder et al. (2023), Priharti & Samat (2016) and Abojassim et al. (2016). As we understand, internal dosages and dose coefficients can vary for different age groups. Mustakim et. al (2018), however, used the dose coefficient for adults to measure the average annual dose, which may not be methodologically sound considering the average consumption rate are established to vary for age groups.

Fourth, a further limitation lies in the absence of accurate (or close to accurate) fruit consumption rate data based on age within the studies. Studies such as Küçükönder et al., (2023), while have considered age-dependency, they failed to include accurate regional consumption rates. Abojassim et al., (2016), for example included data collected from UNSCEAR (2000), and Mustakim et. al (2018) had collected theirs from WHO (1988)—which may not reflect the fruit consumption trends.

This study was designed to address these shortcomings by estimating fruit intake based on population demographics and providing age-dependent annual ingestion dose calculations based on available secondary data, thereby contributing new insights to the existing body of research.

Chapter 3: Methodology

In this chapter, we outline and discuss the methodology employed in conducting our study. We start by discussing the sample collection process, then discussing the sample processing method before we take readings, the process of taking readings using a High-purity Germanium detector, and how we calculated the annual effective dose for the consumption of fruits in Dhaka City.

3.1 Sample Collection

3.1.1 Rationale for Sampling Dhaka Markets

The present study focuses on fruits that have been collected from local markets in Dhaka, the capital city of Bangladesh. There are several reasons for this choice. First, Dhaka is the most populous city in Bangladesh and a major hub for trade and distribution. Fruits sold in Dhaka markets come from various regions of the country and are distributed in the city. So sampling here provides a cross-section of what consumers eat. Second, market fruits directly represent the public's exposure, since people typically buy and consume these produce items locally. Thus, it would be reasonable to consider Dhaka markets as sampling sites.

The fruit samples were bought from the local markets of Shadarghat, the port of Dhaka. As stated previously, Dhaka is the hub for distribution. And within, Sadarghat port is where the majority of the fresh produce arrives from different regions and is then distributed among the various local sellers in the city. The fruits were collected over the months of June to December, 2024. This gave us enough time to efficiently gather most of the fruits from all seasons. The fruits, shown in Table 3.1, were chosen according to the following criteria:

- Season
- Availability
- Nationwide production level

Fruits that are regularly consumed during each season. For each season—Summer (*Grisma ritu*), Rainy (*Barsa ritu*), Autumn (*Sarat ritu*), Late Autumn (*Hemanta ritu*), Winter (*Shitt ritu*) and Spring (*Basant ritu*)—one to two fruits were collected. Furthermore, two types of banana fruits that are available and grown throughout all seasons, *Bangla* and *Chompa kola*. Each of these fruits is of high production locally. In total, 13 samples were collected—11 of which are seasonal and 2 all-season—with mass ranging from 4 to 6 kilograms. They were then transported to our BRAC University Laboratory, where the samples were processed for the next steps.

3.2 Sample Processing

For the radionuclide concentration process, the fruit samples need to be finely powdered first. The fruits were first peeled, and the edible parts were separated from any seeds. This is because we are concerned with the fruit bits that are regularly consumed by humans. They were then weighed using a weighing machine and recorded as shown in Table 3.1. Following the recommendations of the International Atomic Energy Agency [IAEA] (1989)'s Technical Report Series no. 295, the fruits were cut into thin slices, as shown in Figure 3.1, roughly with a thickness of 0.5 inches and length dependent on the convenience of handling and drying.

Figure 3.1: Example of fruit slices. Dragon fruits (Left) and Orange (right).

They were then arranged and dried in the convection oven at 100 degrees Celsius until mostly dried; later dried at between 110 to 120 degrees to remove any remaining moisture and put in a zip-lock bag to measure the sample weight and store. The result looked like the following Figure 3.2. The dried samples were once again weighed and then finely powdered using a grinder. The grinder was cleaned thoroughly after each sample was powdered to avoid cross-contamination. The powder was later weighed and stored in air-tight plastic containers as shown in Figure 3.3. The powder samples were then kept in a dry environment for a minimum of 30 days for them to reach secular equilibrium between radionuclides and their daughter products.

Figure 3.2: Dried fruit slices stored in zip-lock bag and measured in weighing machine.

Figure 3.3: Final dried fruit powder samples put in air-tight plastic containers, labeled, and stored for at least 30 days

Table 3.1: Fruit sample data								
Fruit Name	Original Mass (g)	Mass Used (g)	Edible Mass After Preparation (g)	Mass Used for Drying (g)	Dried Mass (g)	Powered Mass (g)	dry-to-wet mass ratio	Powdering Date
Banana (Champa Kola)	4000	4000	2630	2030	546	539	0.27	08/12/24
Banana (Bangla Kola)	4000	4000	2253	1553	385	380	0.25	28/11/24
Ber (Boroi)	4000	4000	3414	2195	350	344	0.16	14/12/24
Dragon fruit	4000	4000	2385	2385	302	292	0.13	30/11/24
Guava (Peyara)	4000	3300	2305	2305	334	332	0.14	03/12/24
Hog plum (Amra)	6000	5500	3523	1947	282	278	0.14	14/12/24
Olive (Jolpai)	6000	6000	4131	3723	361	358	0.10	08/12/24
Orange (Malta)	4000	3608	2850	2850	365	362	0.13	05/12/24
Mango (Himsagor)	4000	3210	1620	1620	323	319	0.20	05/12/24
Tangarine (Komola)	4000	3770	2157	2157	241	239	0.11	03/12/24
Papaya (Pepe)	4000	4000	2806	2806	272	270	0.10	14/12/24
Pineapple (Anaros)	5500	5000	3416	3107	315	312	0.10	08/12/24
Starfruit (Kamranga)	4000	3872	3872	3272	253	248	0.08	03/12/24

3.2.1 Dry-to-wet mass ratio

From Table 2, we also see the dry-to-wet mass ratio of fruits. This is calculated using the following formula:

$$\text{Dry-to-Wet Mass Ratio} = \frac{\text{Dried Mass}}{\text{Mass Used For Drying}} \tag{3.1}$$

Note that we did not include the peels and seeds of the fruits in our calculations.

3.3 Gamma Spectrometry with HPGe Detector

Previously in section 2.4, we discussed the theoretical background of gamma spectrometry and High Purity Germanium (HPGe) detector. We will now discuss the procedure followed for determining the radionuclide concentration. The processed dried fruit powder were taken to the Bangladesh Atomic Energy Comission (BAEC), Dhaka for the activity measurements.

3.3.1 Instrumentation

Radionuclide activity concentrations in fruit samples were quantified using a low-background, high-resolution gamma-ray spectrometry system. The system incorporated a p-type coaxial High Purity Germanium (HPGe) detector with a relative efficiency of 19.6% and energy resolution of 2.3 keV at the 1.332 MeV photopeak. This detector was coupled to a Mestro32 Multichannel Analyzer (MCA) and supporting microprocessors. Continuous cooling was maintained via a liquid nitrogen cryostat to minimize thermal leakage current. To mitigate environmental interference, the detector was housed within a cylindrical lead shield, featuring an inner copper layer to attenuate Pb X-ray fluorescence. The assembly was capped with a movable steel cover and lead plate to further isolate the detector from laboratory radiation sources.

Energy calibration was performed using certified point sources (^{22}Na, ^{57}Co, ^{60}Co, ^{133}Ba, and ^{137}Cs) traceable to national standards. Efficiency calibration employed mixed gamma standards (122–1408 keV) supplied by the Health Physics Division (Atomic Energy Centre, Dhaka), following established protocols. Standard sources with known activities were prepared in geometries identical to fruit samples to ensure matrix-matched measurements. The resultant efficiency curve covered energies from 60 to 2000 keV and was applied to quantify radionuclides of interest across this range. Background spectra were acquired using an empty sealed beaker counted under identical geometric conditions as samples. These spectra enabled correction of net peak areas for measured isotopes by subtracting ambient radiation contributions. The full efficiency calibration profile is illustrated in Figure 3.4.

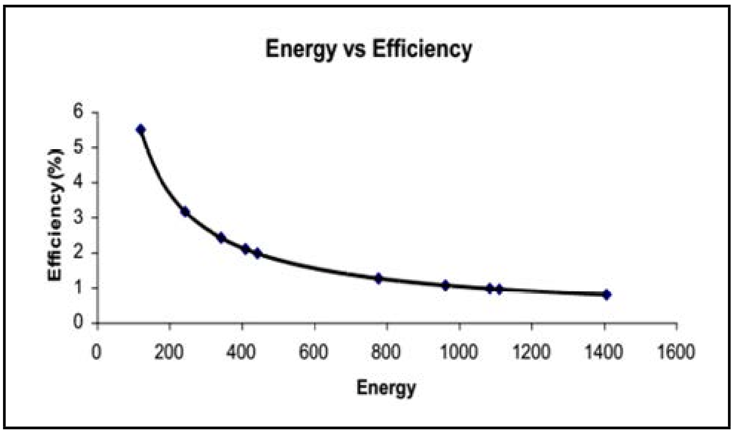

Figure 3.4: Energy vs Effiency curve (Mustakim et al., 2018)

3.3.2 Radioactivity Measurement

We were to identify the radionuclides and find their activity concentrations in prepared fruit samples. Measurements were conducted for a standardized duration of 15,000 seconds using an ORTEC high-purity Germanium (HPGe) detector system. To ensure statistical accuracy in net count determinations, background radiation measurements were performed for identical counting times as sample analyses, thereby minimizing uncertainty. Following data acquisition, each sample spectrum underwent detailed analysis through energy calibration and efficiency calculation. The identification of radionuclides had been achieved by matching observed peak centroid energies against reference gamma-ray energy data from established literature. This allowed us to detect and quantify the presence of U-238, Th-232, and K-40. Both U-238 and Th-232 activities were determined indirectly within their decay chains under the assumption of secular equilibrium, using gamma emissions from their daughter radionuclides. Activity concentrations of U-238 were derived from the weighted average of four gamma transitions: Pb-214 at 295.2 keV, Pb-214 at 351.9 keV, Bi-214 at 609.3 keV, and Bi-214 at 1120.2 keV. Similarly, Th-232 concentrations were calculated using emissions from its daughter nuclides: Pb-212 at 238.6 keV, Tl-208 at 583.1 keV, Ac-228 at 911.2 keV, and Ac-228 at 968.9 keV. In contrast, K-40 activity was measured directly through its characteristic 1460.8 keV gamma transition.

Reference gamma peaks were selected based on the following criteria: adequate discriminability in the spectrum to avoid peak overlaps and sufficient intensity of emission for proper analysis. Following this, activity concentrations were calculated by integrating net peak areas after background subtraction. Each recorded spectrum underwent background correction to isolate sample-specific radiation signatures. The integrated areas of photopeaks corresponding to the specified gamma energies were converted to activity values using detector efficiency calibrations established at these precise energies. Figure 3.5 shows a typical gamma spectrometry system for a fruit sample.

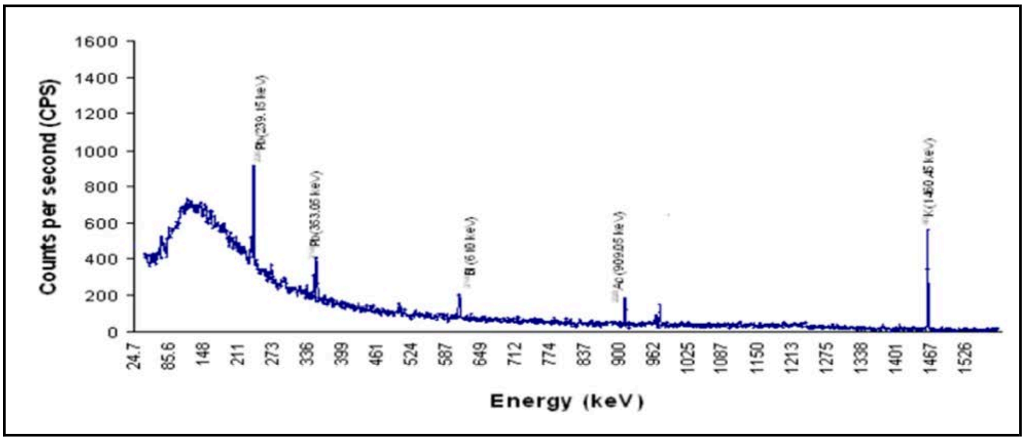

Figure 3.5: Typical gamma spectrometry system for fruit samples (Mustakim et al., 2018)

Activity Concentration Calculation

The specific activity of each fruit sample is given as follows:

$$A = \frac{N \times 100 \times 1000}{P_{\gamma} \times \varepsilon \times W} \tag{3.2}$$

Where,

N is the net count per second (CPS). The net count rate associated with the activity measurement is the difference between the gross count rate of the sample (N_s) and the background count rate (N_b): $N = N_s - N_b$.

P_{γ} is the transition probability of gamma-ray

ε is the efficiency in per cent

W is the fresh weight of the fruit samples in grams.

It should be noted that each count rate has a standard deviation (σ) associated with it. The standard deviation of the distribution is the square root of the mean value for a particular sampling interval. This can be expressed as,

$$\sigma = \pm \left[\frac{A_s}{T_s} + \frac{A_b}{T_b} \right]^{\frac{1}{2}} \tag{3.3}$$

Where,

A_s is the sample count rate,

A_b is the background count rate,

T_s is the sample count time, and

T_b is the background count time.

3.4 Tools for Statistical Analysis: Google Sheets and SPSS

To ensure a comprehensive and systematic analysis of the data obtained from the Bangladesh Atomic Energy Commission (BAEC), two powerful tools were employed: Google Sheets for data organization and visualization, and SPSS (Statistical Package for the Social Sciences) for advanced statistical computations.

Data Processing and Visualization with Google Sheets

The initial phase of data analysis was conducted using Google Sheets, a versatile and accessible spreadsheet tool. The activity concentration measurements provided by BAEC were systematically entered, cleaned, and formatted to ensure accuracy. It was used to create dynamic charts and graphs, giving us clearer visual representations of trends, distributions, and comparisons across the samples from the other studies.

Statistical Analysis with SPSS

While SPSS is traditionally used in social sciences, its robust statistical capabilities made it an ideal choice for this study. Combined with the structured dataset prepared in Google Sheets, SPSS was utilized to perform descriptive statistical analyses, including mean, standard deviation, skewness, etc.. This software ensured precise calculations and reliable outputs. The integration of both tools—Google Sheets for data preparation and SPSS for statistical evaluation—streamlined the analytical workflow, enhancing both efficiency and accuracy.

3.5 Annual Dose Calculation

The formula for calculating the annual effective dose (AED) from fruit ingestion is as follows (Küçükönder et al., 2023; Mustakim 2018 et al., 2018):

$$D_E = \sum (C_r A_{rw}) \cdot R_f \tag{3.4}$$

Where,

D_E (Sv/y) is the Annual Effective Dose for fruit ingestion,

C_r (Sv/Bq) is the Dose Coefficient of a specific radionuclide that we are calculating for, A_{rw} (Bq/kg) is the activity concentration for the specific radionuclide measured for fresh fruits, and

R_f (kg/y) is the annual consumption rate of fruits.

As per the International Commission of Radiological Protection [ICRP] 101 (2006) recommendations, there are three categories of age that we can find: infants (1 year), children (10 years), and adults (16 - 70 years). While they recognize a total of six categories, for practical implications, these three are sufficient. The corresponding dose coefficients are as follows (ICRP, 2006):

Table 3.2: Age-dependent Dose Coefficients of U-238, Th-232, and K-40					
Radionuclide	**Half-life (year)**	**f (>1 years)**	**Infant (1 year)**	**Children (10 years)**	**Adult**
^{238}U	4.47E+09	0.02	1.20E-07	6.80E-08	4.50E-08
^{232}Th	1.41E+01	0.0005	4.50E-07	2.90E-07	2.30E-07
^{40}K	1.28E+09	1	4.20E-08	1.30E-08	6.20E-09

The numerical values of age-dependent annual average fruit consumption are tricky to determine as no data is available for Bangladesh, let alone Dhaka city. However, within reasonable estimations, we might be able to calculate the values. According to the BBS (2023) the average national fruit consumption is 95.6g (p. 49). However, this average includes both the urban and rural regions, as well as being the average of the whole nation. Given that our samples were collected from Dhaka city, these samples will likely be consumed primarily in urban areas, and as such, the results should be considered for urban area consumption. Also, the average not only includes fresh fruits, but also processed/preserved products, seeds, and nuts—which we do not include in our sample list. As such, we chose the average consumption of fresh and frozen fruits at 101.13g (BBS, 2023, p. 50).

In addition, the average consumption does not specify age groups, whereas we wish to find the annual effective dose for different categories. At the same time, we understand that different age groups have differing consumption levels. Therefore, we have to look for a method that could give us a close estimation of the age-dependent consumption rate. For this, we can consider a weight distribution based on population in the urban areas of the Dhaka division. The equation looks as follows:

$$P_I \cdot F_I + P_C \cdot F_C + P_A \cdot F_A = 101.13g \tag{3.5}$$

Here, P_I, P_C, and P_A are the percentages of the population of the three groups—infants, children, and adults, respectively—from urban Dhaka division areas. F_I, F_C, and F_A are the fresh/frozen fruit yearly consumption amounts in grams. From the Population and Housing Census 2022 report of BBS (2023), we find the population sizes for divisional and urban Dhaka regions, shown in Table 3.3. However, since no city-level data is available, we used the urban population size to estimate Dhaka city's population. This should be reasonable considering that, in terms of weight distribution, the majority of Dhaka division's urban population is the Dhaka city population—coming at roughly 49%.

Additionally, while there is no exact age-dependent fruit consumption rate for Bangladesh, a report published in the Commission of the European Communities (1991) have found the ratios to be 0.33 and 0.69 times that of the adult consumption of fruits for infants and children, respectively (p. 99). Thus, we'll be using those ratios in our weighted average equation moving forward.

Table 3.3: Population sizes

Single Age	Bangladesh Population Size	Urban Dhaka Population Size
0	2170243	198029
1	3501359	382335
2	3301546	355977
3	3240132	350233
4	3367602	354951
5	3173549	341258
Total (0 - 5)	**18754431**	**1982783**
6	2932804	313810
7	3282761	348411
8	3226019	348513
9	2713731	299642
10	3378858	369094
11	2941861	327145
12	3812403	418281
13	2894055	320962
14	3305514	368942
15	3313650	367679
Total (6 - 15)	**31801656**	**5465262**
Total (16+)	**114594405**	**13310677**

To determine the population percentages, we sum the total number of single-age population sizes and divide the number by the total population. The equations look as follows:

$$P_I = \frac{\text{Population size of age 0 to 5}}{\text{Total Population}} \times 100\% \tag{3.6}$$

$$P_C = \frac{\text{Population size of age 6 to 15}}{\text{Total Population}} \times 100\% \tag{3.7}$$

$$P_A = \frac{\text{Population size of age 16+}}{\text{Total Population}} \times 100\% \tag{3.8}$$

Thus, in Table 3.4 and Table 3.5, we see the age category percentages required to determine the annual effective dose from fruit ingestion. As mentioned previously, the ICRP 101a publication report category of *Infants* has the age range of 0 to 5, *Children* has the age range of 6 to 15, and *Adults* has the range of 16 to 70. We took the percentages of the population of the three categories. For the sake of simplicity and further ease of calculation, for the *Adult* category, we include the population of people 70+. It should be noted that, from 71 to 100+ age, the population percentage is slightly over 1%, which is within reasonable limits of uncertainty.

Table 3.4: Population of Urban Dhaka categorised by age range

Category	**Age Range**	**Population size**	**Percent (%)**	**Total Dhaka Urban Population**
Infant (1 year)	0 - 5	1982783	9.54	20758722
Children (10 years)	6 - 15	3482479	16.78	
Adult (16 - 70 years)	16 +	15293460	73.68	

Table 3.5: Population of Bangladesh categorised by age range

Category	**Age Range**	**Population size**	**Percent (%)**	**Total Bangladesh Population**
Infant (1 year)	0 - 5	18754431	11.35	165150492
Children (10 years)	6 - 15	31801656	19.26	
Adult (16 - 70 years)	16 +	114594405	69.39	

Once we have the required values, in the results section, we will see all of these come together to give us the annual effective dosage for each age group.

Chapter 4: Results

In this chapter, we will be looking into the results obtained from the previous procedures. This will be divided into several parts: one describing the results from the radionuclide concentration and annual dosage analysis,

4.1 Activity Concentrations

In the first section, we present the results obtained from the seasonal fruits and their activity concentrations and compare them with previous similar studies from different sources. We then calculate the annual effective—or internal—dose.

As mentioned in the previous chapter on methodology, we use equation 3.2 to find the activity concentrations for the individual fruits and radionuclides, ^{238}U, ^{232}Th, and ^{40}K. In Table 4.1, we see all the activity concentrations of the seasonal fruits obtained from the Bangladesh Atomic Energy Commission (BAEC). The determined activities of ^{238}U, ^{232}Th, and ^{40}K ranged from 1.23 ± 0.63 Bq/kg to 8.28 ± 0.65 Bq/kg, BDL to 6.01 ± 0.66 Bq/kg, and 30.62 ± 1.88 Bq/kg to 227.7 ± 11.14 Bq/kg respectively. The mean value of the fruit concentrations was calculated to be 3.62 ± 0.67 Bq/kg, 2.33 ± 0.48 Bq/kg, and 80.98 ± 18.26 Bq/kg for ^{238}U, ^{232}Th, and ^{40}K respectively. On the other hand, the concentrations of ^{238}U, ^{232}Th, and ^{40}K for the carrot sample came out to be 2.06 ± 0.11, 3.37 ± 0.2, and 60.68 ± 3.86, respectively. Generally, we find that K-40 is is much greater in concentrations than U-238 or Th-232, about 22.37 and 34.76 times greater, respectively.

Table 4.1: Activity Concentrations in Bq/kg			
Sample Name	^{238}U	^{232}Th	^{40}K
Banana (Champa Kola)	8.28 ± 0.65	5.81 ± 0.79	227.7 ± 11.14
Banana (Bangla Kola)	7.97 ± 0.63	6.01 ± 0.66	217.80 ± 12.01
Ber (Boroi)	3.16 ± 0.26	1.91 ± 0.14	71.71 ± 3.47
Dragon fruit	3.14 ± 0.19	1.92 ± 0.13	77.30 ± 4.75
Guava (Peyara)	3.25 ± 0.23	2.12 ± 0.15	80.86 ± 5.56
Hog plum (Amra)	2.96 ± 0.27	1.89 ± 0.13	49.71 ± 3.38
Olive (Jolpai)	1.35 ± 0.02	1.91 ± 0.06	39.78 ± 2.26
Orange (Malta)	2.60 ± 0.01	1.34 ± 0.13	46.01 ± 2.25
Mango (Himsagor)	6.65 ± 0.13	2.98 ± 0.25	92.2 ± 7.08
Tangarine (Komola)	1.63 ± 0.11	1.35 ± 0.85	39.71 ± 3.03
Papaya (Pepe)	2.52 ± 0.11	1.26 ± 0.16	40.61 ± 2.39
Pineapple (Anaros)	2.26 ± 0.10	1.73 ± 0.01	38.71 ± 3.07
Starfruit (Kamranga)	1.23 ± 0.63	BDL	30.62 ± 1.88
Mean ± SE	**3.62 ± 0.67**	**2.33 ± 0.48**	**80.98 ± 18.26**

Table 4.2 shows us some of the descriptives we found using SPSS. The standard deviation of the results comes up to be 2.41 Bq/kg, 1.73 Bq/kg, and 68.84 Bq/kg, respectively. Skewness, the measure of the asymmetry of a distribution, is determined to be 1.22, 1.47, and 1.81, respectively; kurtosis, the tailedness of a distribution, is 0.146, 1.75, and 2.19.

Table 4.2: Some Descriptive Statistics of the Results

	^{238}U	^{232}Th	^{40}K
Mean	3.62	2.39	80.98
Std. Error	0.67	0.48	18.26
Std. Deviation	2.41	1.73	68.84
Minimum	1.23	BDL	30.62
Maximum	8.28	5.81	227.7
Range	7.05	6.01	197.08
Skewness	1.22	1.47	1.81
Kurtosis	0.146	1.75	2.19

In Figures 4.1 and 4.2, we see a chart of the activity distributions of our results. While most concentrations were comparable, the two banana samples and mango samples had above-average concentrations. *Chompa kola* and *Bangla kola* had the U-238 levels of 8.28 ± 0.65 Bq/kg and 7.97 ± 0.63 Bq/kg, respectively; mango had the concentration of 6.65 ± 0.13 bq/kg. This difference from the average is approximately 128.7%, 120.2%, and 83.7% for *Chompa, Bangla,* and *Himsagor* mango, respectively. Similarly, for K-40, *Chompa kola, Bangla kola,* and mango samples were about 181.2%, 169.0%, and 13.9% greater than the average, respectively.

Out of the lowest observed, starfruit and olive samples had the lowest U-238 of 1.23 ± 0.63 Bq/kg and 1.35 ± 0.02 Bq/kg, respectively. The lowest ones in Th-232 were starfruit, Below Detection Level (BDL), and Orange, 1.34 ± 0.13 Bq/kg.

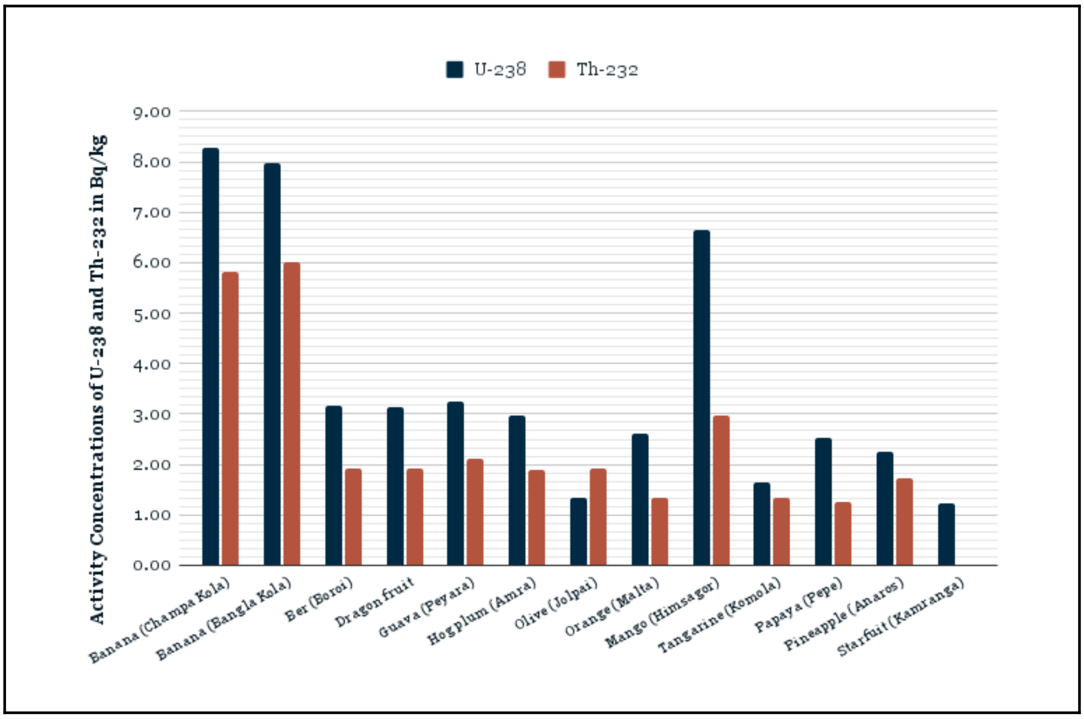

Figure 4.1: Mean U-238 and Th-232 concentrations of the present study

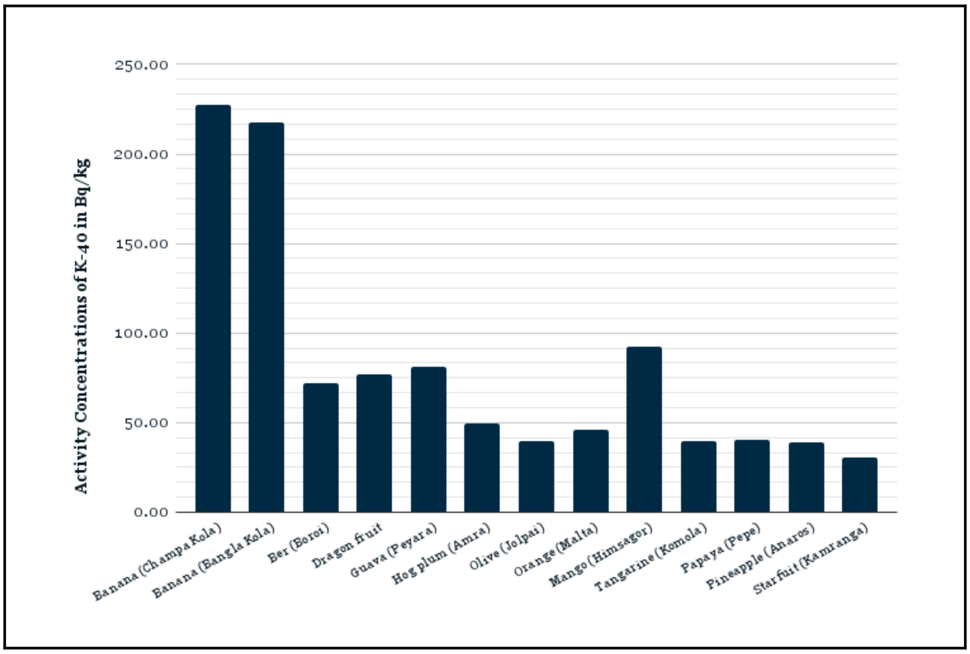

Figure 4.2: Mean K-40 concentrations of the present study

4.1.1 Comparison with previous studies

Given our results, we can compare them with the previous studies and in the later section discuss their significance. In Table 4.4, we see the collected radioactivity levels in different regions. From the eight studies besides this one, two are from Bangladesh.

Table 4.4: Mean activity concentrations of the studies in Bq/kg

Location/Region	^{238}U	^{232}Th	^{40}K	Citation
Dhaka, Bangladesh	3.62 ± 0.67	2.39 ± 0.48	80.98 ± 18.26	Present Study
Rajshahi and Natore, Bangladesh	10.95	6.68	308.9	(Mustakim et al., 2018)
Tulatoli, Bangladesh	64.77 ± 38.47	83.53 ± 20.50	1691.45 ± 244.98	(Islam et al., 2014)
Ogun State, Nigeria	9.24 ± 3.40	6.34 ± 2.29	78.51 ± 8.66	(Sowole & Olaniyi, 2018)
Najaf Governorate, Iraq	BDL	2.53 ± 0.106	211.64 ± 17.96	(Abojassim et al., 2016)
Kahramanmaraş, Turkey	5.31 ± 0.44	2.72 ± 0.26	56.84 ± 0.57	(Küçükönder et al., 2023)
Central Zone, Malaysia	-	1.54 ± 0.25	288.63 ± 2.83	(Priharti & Samat, 2016)
W. Black Sea, Turkey	-	6	464.5	(Altamemi et al., 2021)
South India	-	-	67.59 ± 17.78	(Shanthi et al., 2010)

Figures 4.3 and 4.4 show a visual illustration of the result comparison with previous studies. Küçükönder et al. (2023), Abojassim et al., 2016, and Sowole & Olaniyi, 2018 seem to be the most comparable to this study. Compared to the values found in Mustakim et al. (2018) and Islam et al. (2014) were considerably higher than our results. U-238, Th-232, and K-40 in former study were 10.95 bq/kg, 6.68 bq/kg, and 308.9 bq/kg, respectively. The

results was 2.025, 1.867, and 2.815 times greater. The later study shows even more significant differences.

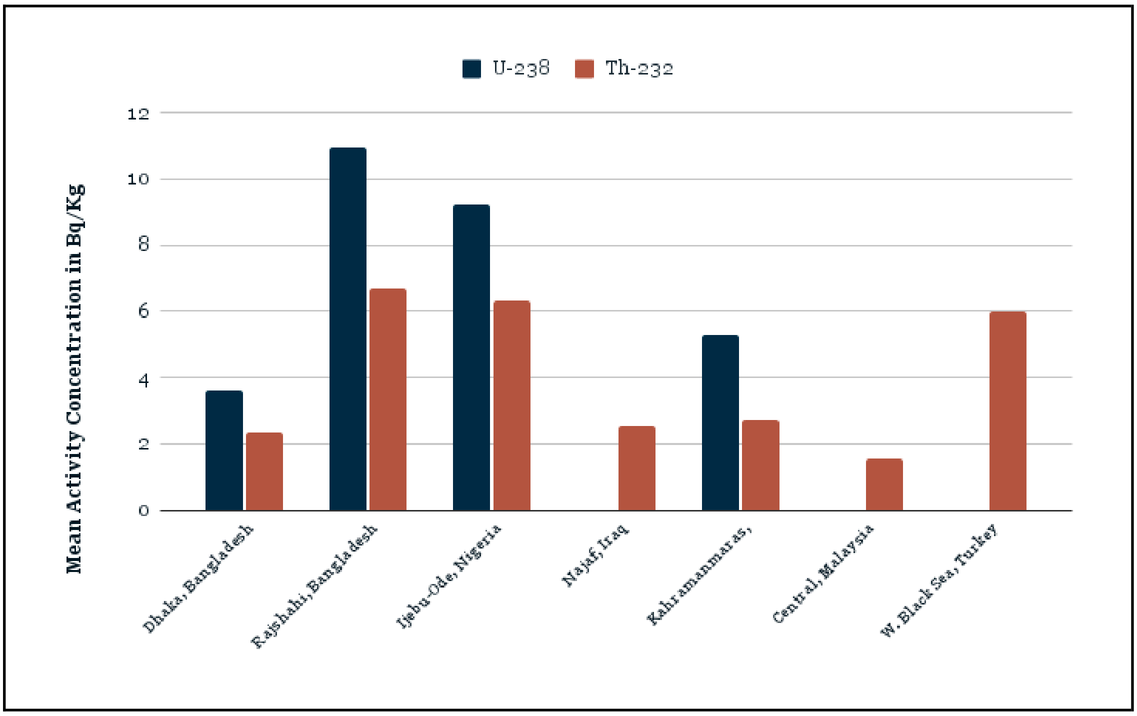

Figure 4.3: Mean U-238 and Th-232 concentrations of selected studies

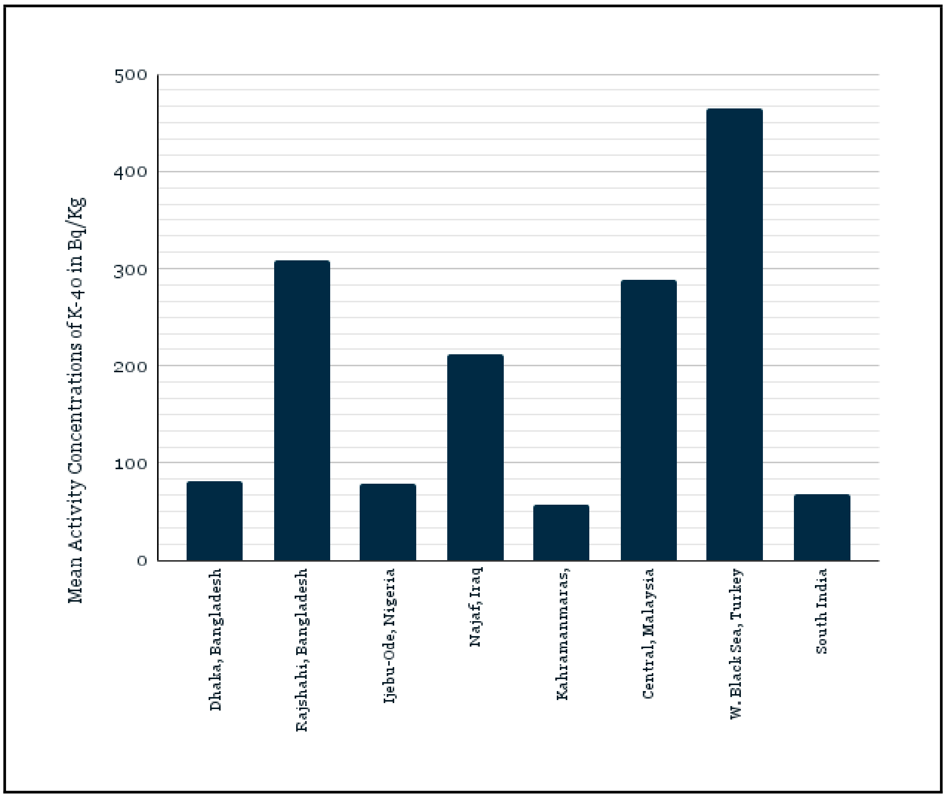

Figure 4.4: Mean K-40 concentrations of selected studies

Bananas

Table 4.5 shows the table of the activity concentrations of bananas of this study in comparison with other studies from different regions. Figure 4.5 further visually illustrates the difference in activity concentrations of bananas between different regions for U-238 and Th-232, and Figure 4.6 shows the same for K-40. We see that our banana samples were generally higher in terms of U-238 and Th-232 concentrations. Only the *Champa* Banana sample of Mustakim et al. (2018) was significantly higher than the rest, being 197.5% greater than the *Champa* bananas of our study. Their banana-4 sample showed the least U-238 concentration of 1.53 ± 1.07, and banana-3 was the least in terms of Th-232, 1.55 ± 0.73. Besides Sowole and Olaniyi (2018), all other banana sample K-40 concentrations were comparable.

Table 4.5: Concentrations of Bananas

Fruit Sample	Location	U-238	Th-232	K-40
Banana (Champa Kola) (Present Study)	Dhaka, Bangladesh	8.28 ± 0.65	5.81 ± 0.79	227.7 ± 11.14
Banana (Bangla Kola) (Present Study)	Dhaka, Bangladesh	7.97 ± 0.63	6.01 ± 0.66	217.80 ± 12.01
Banana-1 (Sobri kola) (Mustakim et al., 2018)	Rajshahi, Bangladesh	2.47 ± 1.67	3.82 ± 0.75	287.16 ± 48.64
Banana-2 (Sagor kola) (Mustakim et al., 2018)	Rajshahi, Bangladesh	4.09 ± 2.77	1.55 ± 0.73	443.92 ± 56.63
Banana-3 (Champa kola) (Mustakim et al., 2018)	Rajshahi, Bangladesh	24.63 ± 8.62	5.43 ± 0.86	322.81 ± 53.40
Banana-4 (Bichi kola) (Mustakim et al., 2018)	Rajshahi, Bangladesh	1.53 ± 1.07	4.55 ± 0.97	362.46 ± 64.51
Banana (Sowole & Olaniyi, 2018)	Ogun State, Nigeria	9.6	6.49	76.98
Banana (Abojassim et al., 2016)	Najaf Governorate, Iraq	BDL	2.92 ± 0.05	154.26 ± 0.94
Banana (Priharti & Samat, 2016)	Malaysia (Central)	-	-	401.59 ± 5.85
Banana (Shanthi et al., 2010)	South India	-	-	136.2 ± 8.3

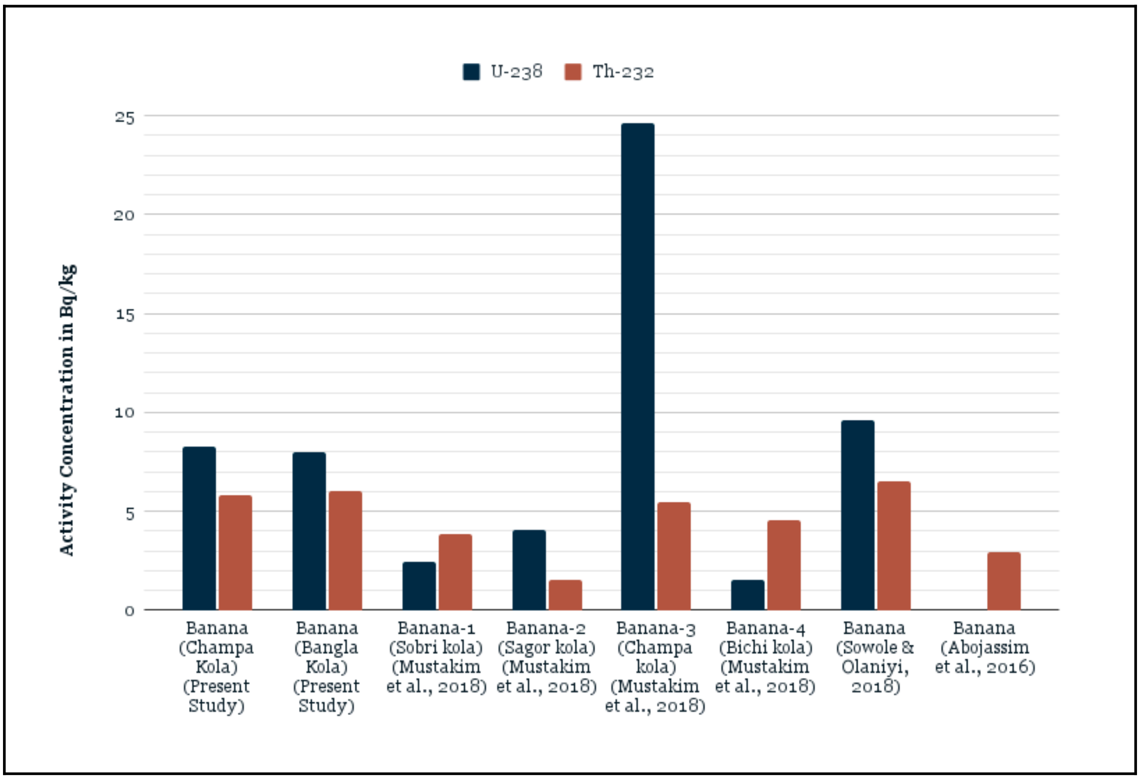

Figure 4.5: Banana activity concentrations for U-238 and Th-232

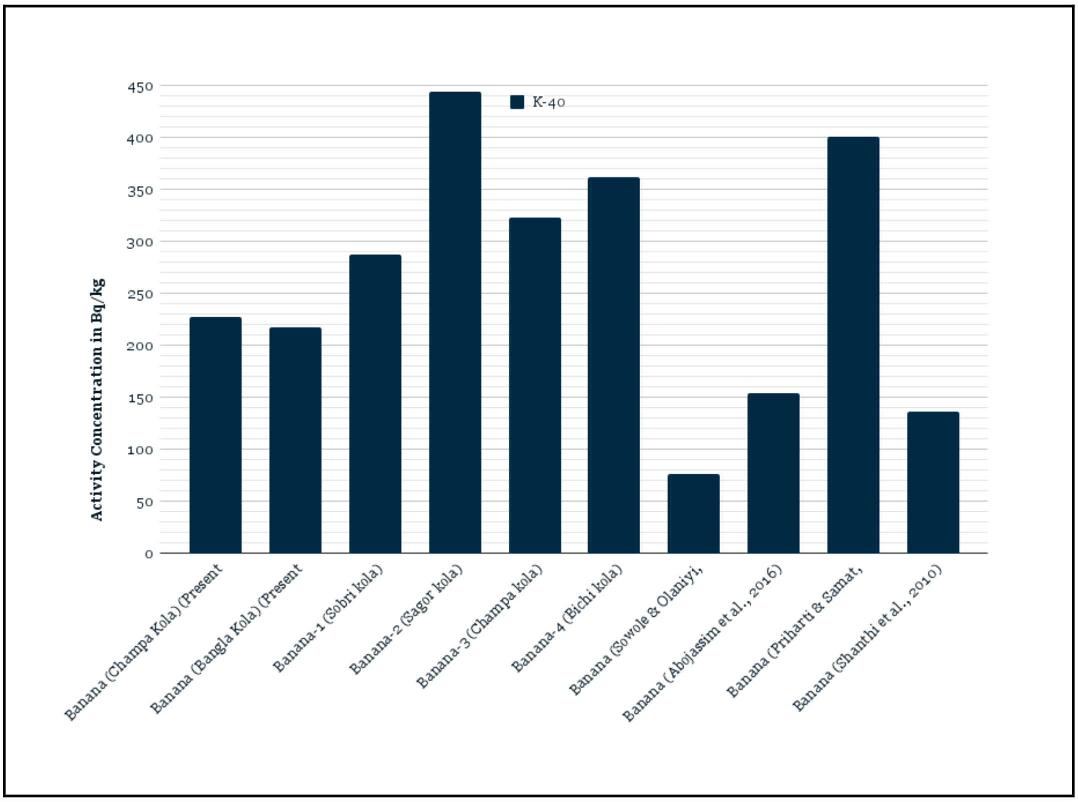

Figure 4.6: Banana activity concentrations for K-40

Mangoes

Table 4.6 shows the table of the activity concentrations of mango of this study in comparison with other studies from different regions. Figure 4.7 further visually illustrates the difference in activity concentrations of mangoes between different regions for U-238 and Th-232, and Figure 4.8 shows the same for K-40. We see that, for U-238 and Th-232, other than mango-2 sample of Mutakim et al. (2018) and Sowole and Olaniya's (2018) Th-232 mango sample, everything is similar. As for K-40, our data is close to the average.

Table 4.6: Concentrations of Mango

Mango (Himsagor) (Present Study)	Dhaka, Bangladesh	6.65 ± 0.13	2.98 ± 0.25	92.2 ± 7.08
Mango-1 (Fazliaam) (Mustakim et al., 2018)	Rajshahi, Bangladesh	7.39 ± 1.37	2.78 ± 0.67	123.66 ± 43.75
Mango-2 (Atiaam) (Mustakim et al., 2018)	Rajshahi, Bangladesh	1.95 ± 1.33	7.92 ± 7.10	182.84 ± 85.95
Mango (Sowole & Olaniyi, 2018)	Ogun State, Nigeria	8.11	6.52	77.09
Mango (Shanthi et al., 2010)	South India	-	-	50.44 ± 4.4

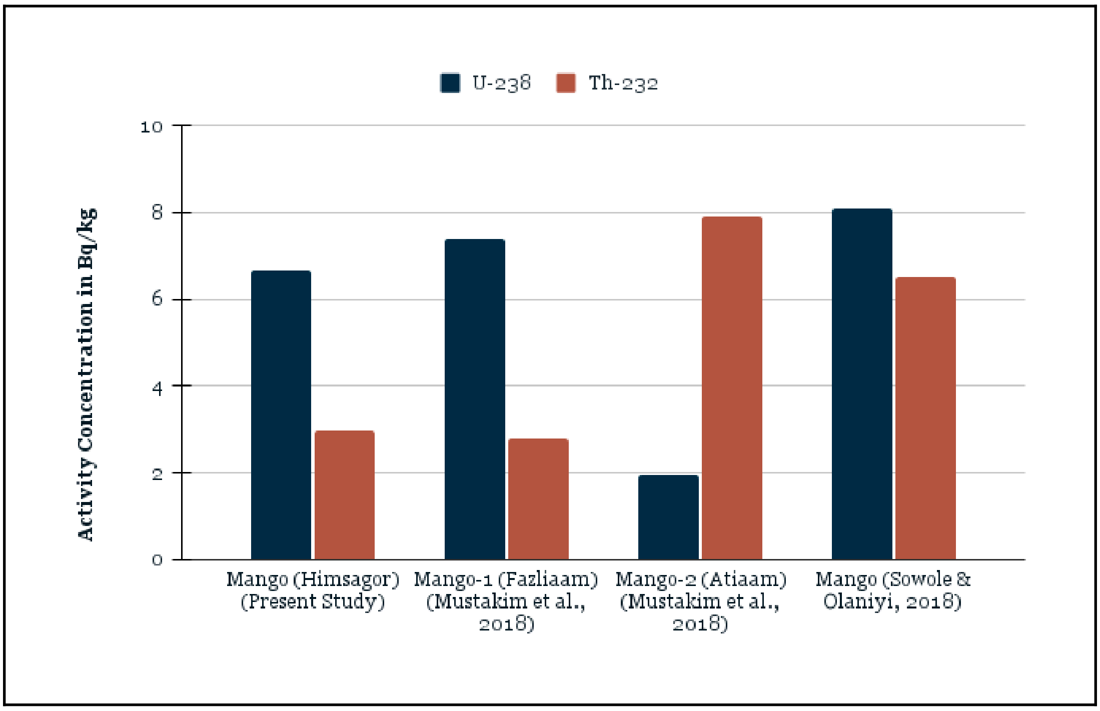

Figure 4.7: Mango activity concentrations for U-238 and Th-232

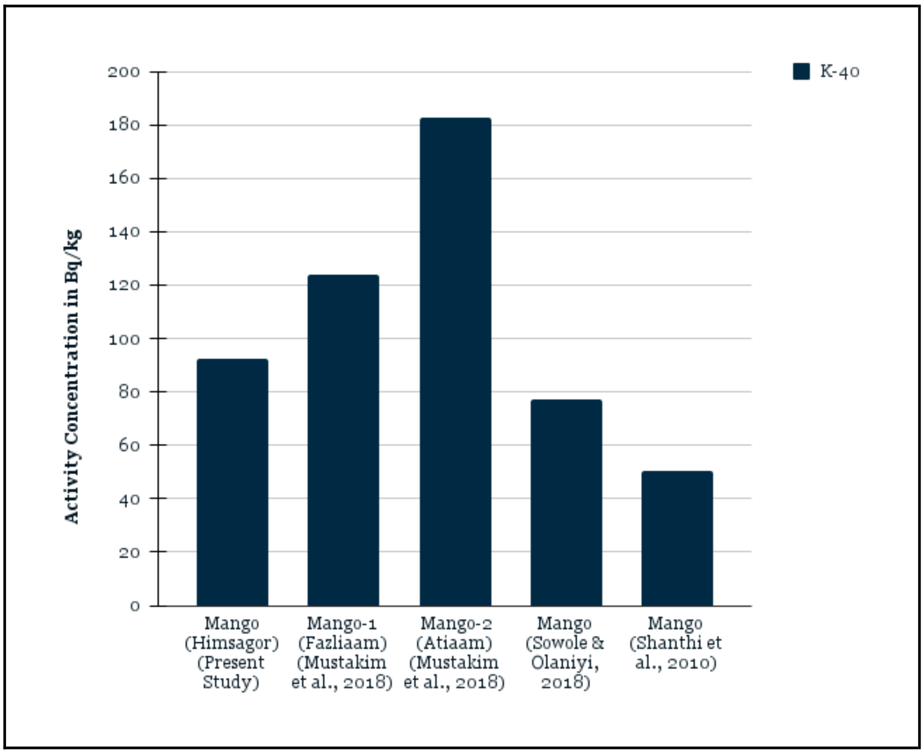

Figure 4.8: Mango activity concentrations for K-40

Pineapples

Table 4.7 shows the table of the pineapple activity concentrations of this study in comparison with other studies from different regions. Figure 4.9 further visually illustrates the difference in activity concentrations of pineapples between different regions for U-238 and Th-232, and Figure 4.10 shows the same for K-40. We see that our results were significantly lower than the others, besides the U-238 orange sample of Mustakim et al. (2018), which came out as Below Detection Level (BDL).

Table 4.7: Concentrations of Pineapple

Pineapple (Present Study)	Dhaka, Bangladesh	2.26 ± 0.10	1.73 ± 0.01	38.71 ± 3.07
Pineapple (Mustakim et al., 2018)	Rajshahi, Bangladesh	BDL	5.28 ± 0.87	247.18 ± 53.39
Pineapple (Sowole & Olaniyi, 2018)	Ogun State, Nigeria	9.77	6.99	88.76

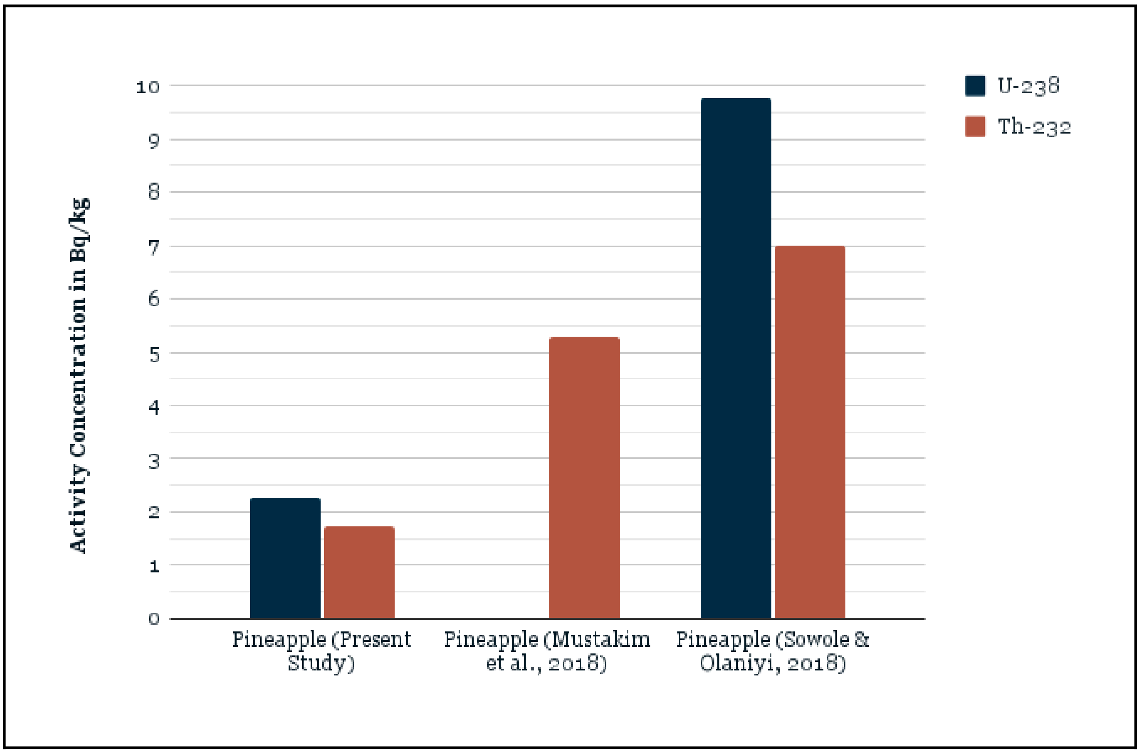

Figure 4.9: Pineapples activity concentrations for U-238 and Th-232

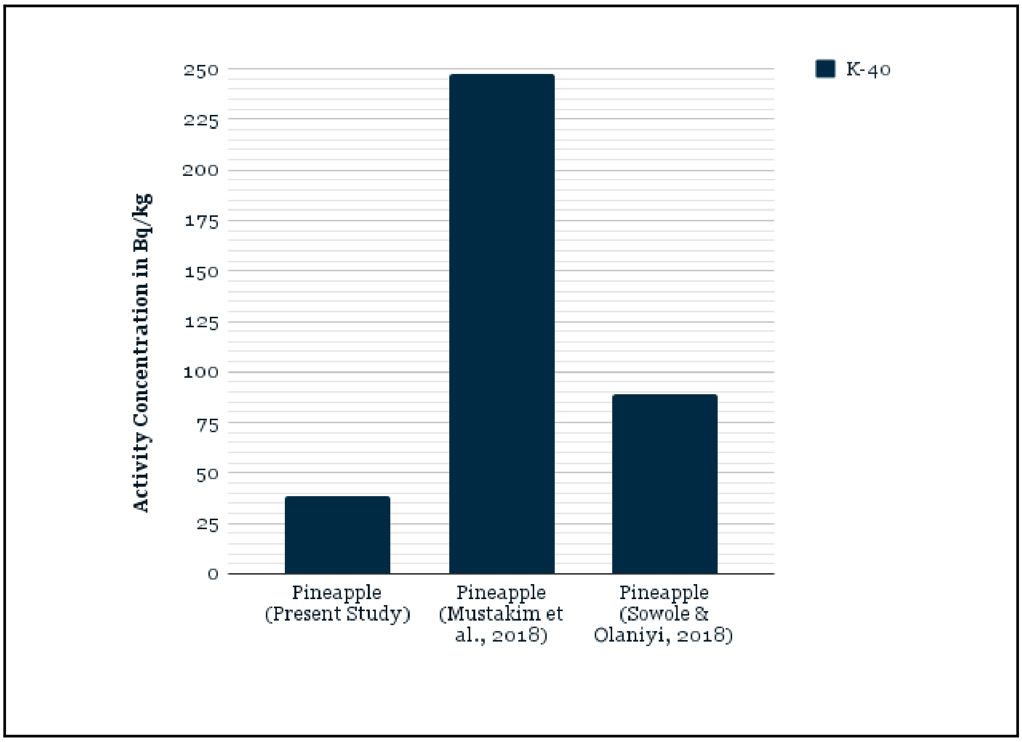

Figure 4.10: Pineapple activity concentrations for K-40

Oranges

Table 4.8 shows the table of the orange activity concentrations of this study in comparison with other studies from different regions. Figure 4.11 further visually illustrates the difference in activity concentrations of oranges between different regions for U-238 and Th-232, and Figure 4.12 shows the same for K-40. We see that, excluding Abojassim et all. (2016), all results of oranges were much higher than ours. Sowole and Olaniyi (2018) were the closest.

Table 4.8: Concentrations of Orange

Orange (Present Study)	Dhaka, Bangladesh	2.60 ± 0.01	1.34 ± 0.13	46.01 ± 2.25
Orange (Sowole & Olaniyi, 2018)	Ogun State, Nigeria	9.49	5.41	72.21
Orange (Abojassim et al., 2016)	Iraq	BDL	2.58 ± 0.06	195.50 ± 1.46
Orange (Priharti & Samat, 2016)	Malaysia (Central)	-	BDL	279.74 ± 7.70

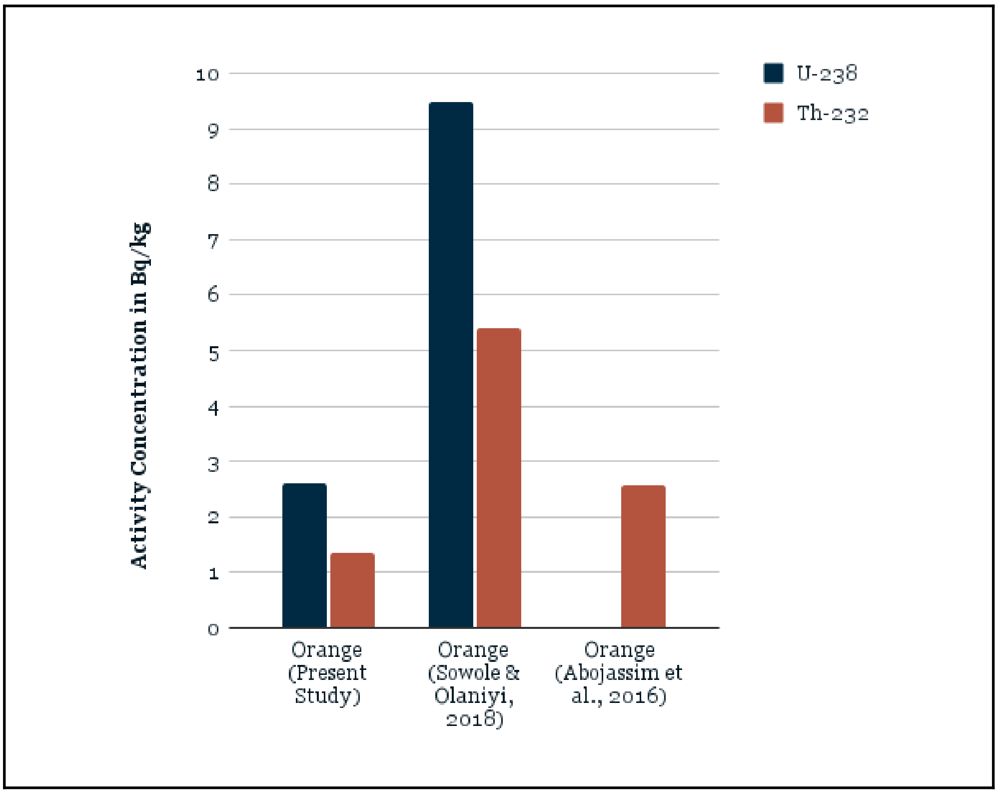

Figure 4.11: Orange activity concentrations for U-238 and Th-232

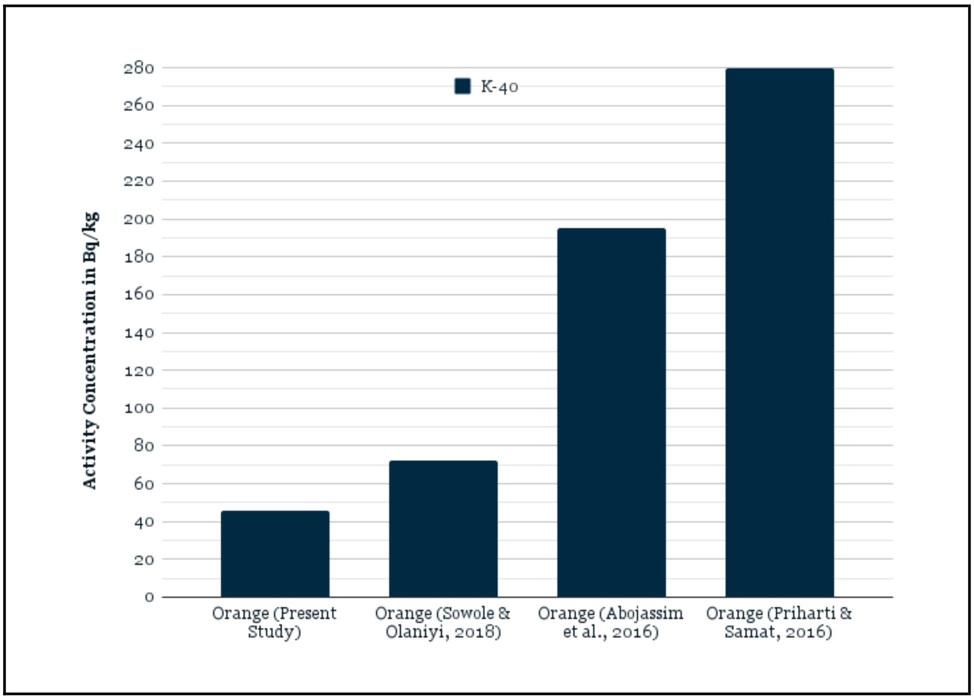

Figure 4.12: Orange activity concentrations for K-40

Guava

Table 4.9 shows the table of the activity concentrations of guava in this study in comparison with other studies from different regions. Figure 4.13 further visually illustrates the difference in activity concentrations of guavas between different regions for U-238 and Th-232, and Figure 4.14 shows the same for K-40. We see that our results were significantly lower than those of Mustakim et al. (2018). Guava K-40 of Shanthi et al. (2010), however, showed less.

Table 4.9: Concentrations of Guava

Guava (Present Study)	Dhaka, Bangladesh	3.25 ± 0.23	2.12 ± 0.15	80.86 ± 5.56
Guava (Mustakim et al., 2018)	Rajshahi, Bangladesh	24.48 ± 7.85	10.67 ± 5.09	347.93 ± 80.71
Guava (Shanthi et al., 2010)	South India	-	-	33.4 ± 4.5

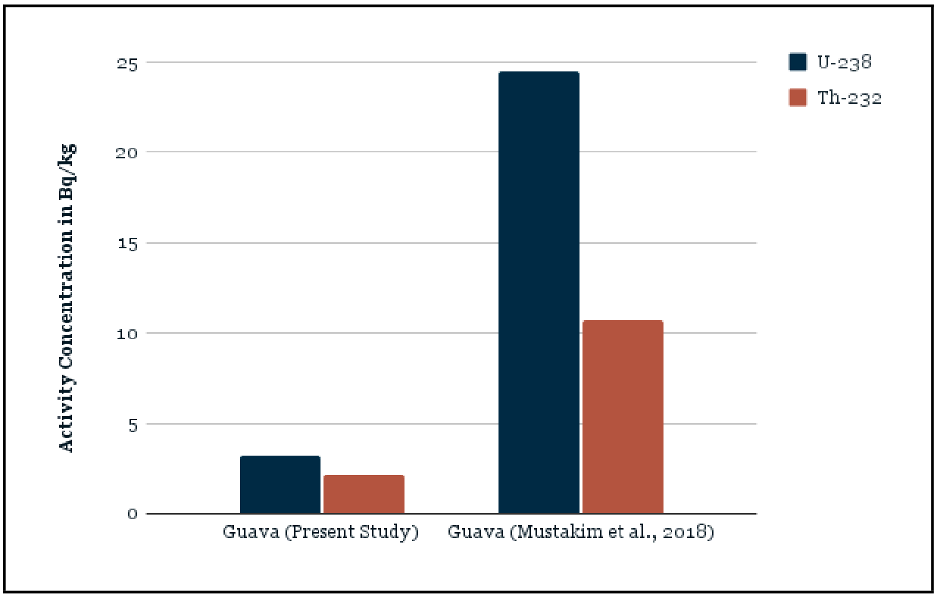

Figure 4.13: Guava activity concentrations for U-238 and Th-232

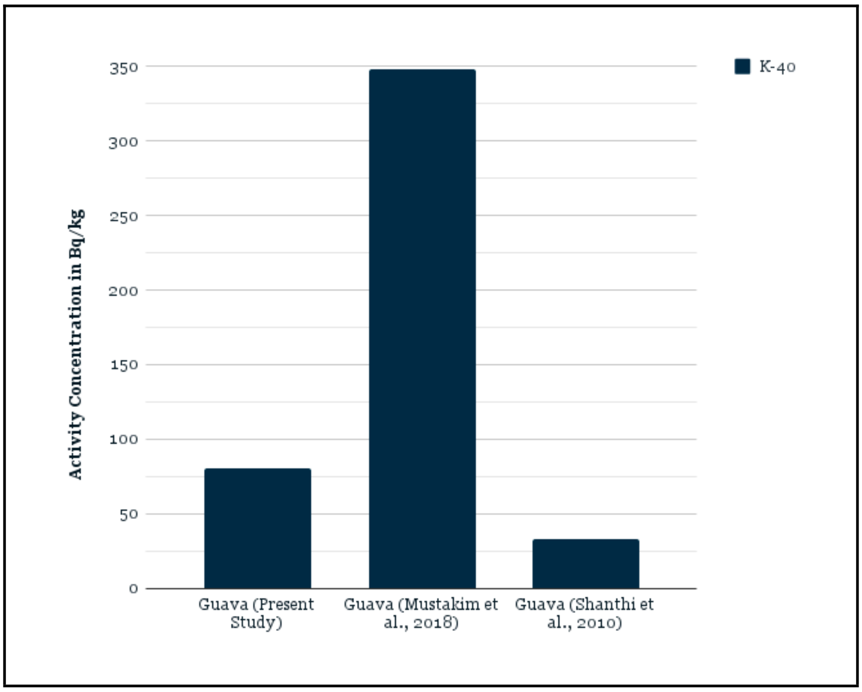

Figure 4.14: Guava activity concentrations for K-40

Jujube

Table 4.10 shows the table of the activity concentrations of jujube of this study in comparison with other studies from different regions. Figure 4.15 further visually illustrates difference in activity concentrations of jujubes between different regions for U-238 and Th-232, and Figure 4.16 shows the same for K-40. We see that both Ber and Jujube samples from Muktaskim et al. (2018) showed similar concentrations for U-238 with out study. However, for both Th-232 and K-40, those two concentrations were significantly higher.

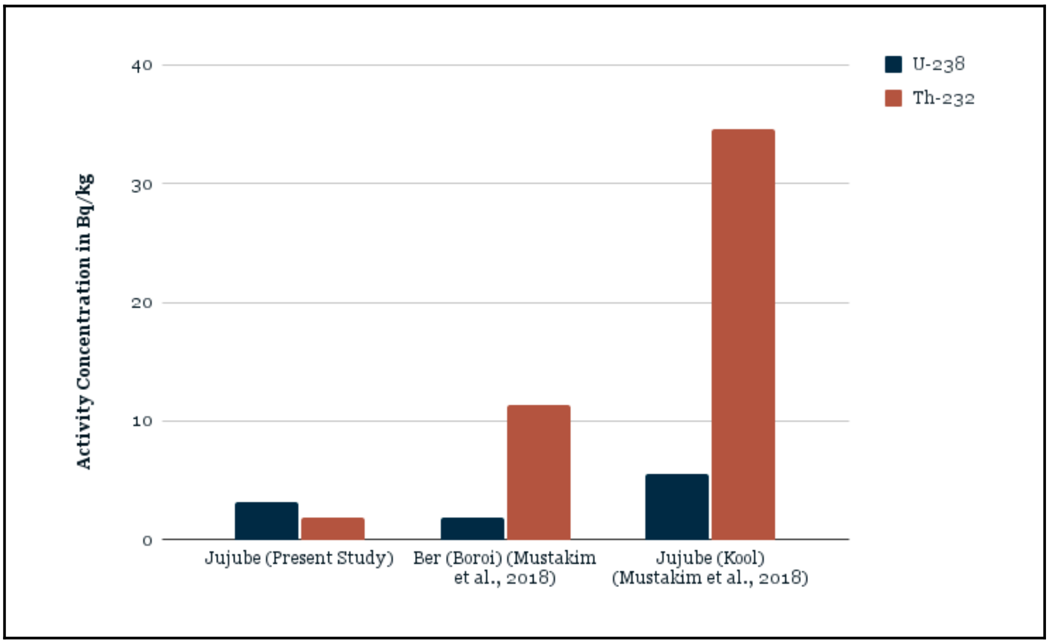

Figure 4.15: Jujube activity concentrations for U-238 and Th-232

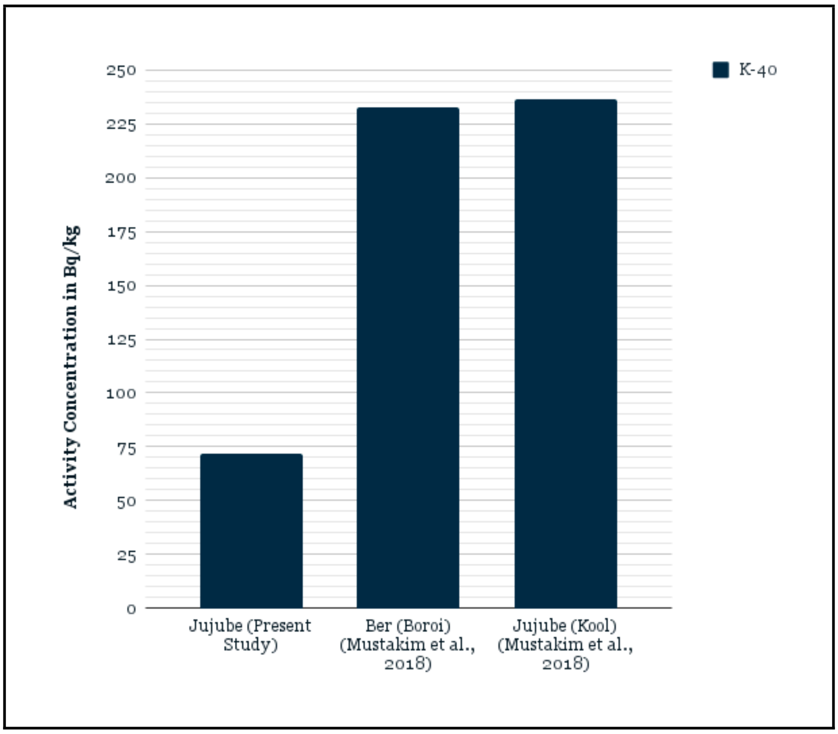

Figure 4.16: Jujube activity concentrations for K-40

Table 4.10: Concentrations of Jujube				
Jujube (Present Study)	Dhaka, Bangladesh	3.16 ± 0.26	1.91 ± 0.14	71.71 ± 3.47
Ber (Boroi) (Mustakim et al., 2018)	Rajshahi, Bangladesh	1.89 ± 1.39	11.33 ± 3.25	232.79 ± 51.09
Jujube (Kool) (Mustakim et al., 2018)	Rajshahi, Bangladesh	5.59 ± 2.25	34.59 ± 7.43	236.17 ± 79.24

Starfruit

Table 4.11 shows the table of the activity concentrations of starfruit of this study in comparison with other studies from different regions. Figure 4.17 further visually illustrates difference in activity concentrations of jujubes between different regions for U-238 and Th-232, and Figure 4.18 shows the same for K-40. While U-238 and Th-232 were smaller, K-40 results show a huge difference of 19.49 times.

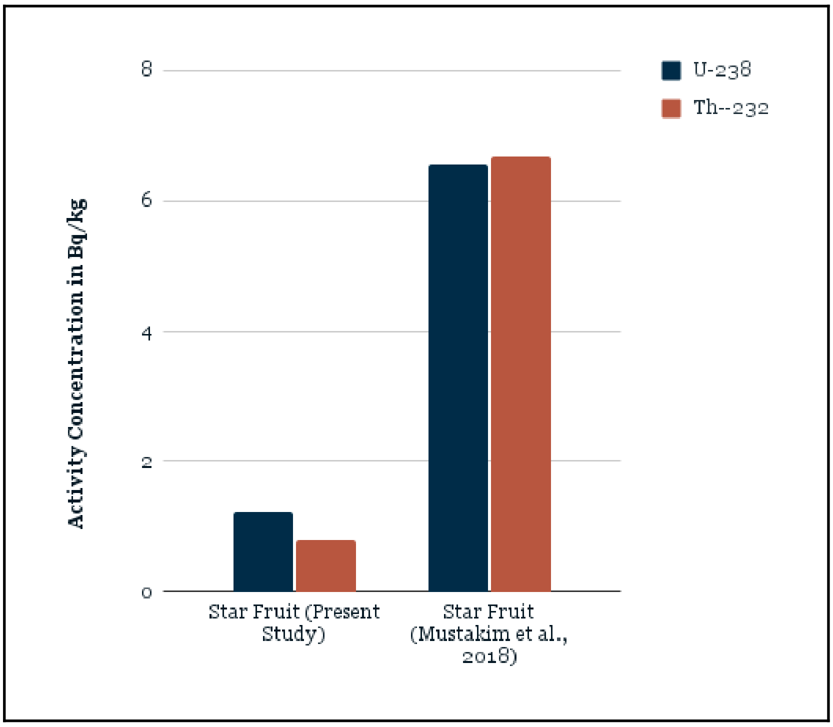

Figure 4.17: Starfruit activity concentrations for U-238 and Th-232

Table 4.11: Concentrations of Star fruit				
Star Fruit (Present Study)	Dhaka, Bangladesh	1.23 ± 0.63	BDL	30.62 ± 1.88
Star Fruit (Mustakim et al., 2018)	Rajshahi, Bangladesh	6.55 ± 9.82	6.68 ± 1.08	596.78 ± 69.62

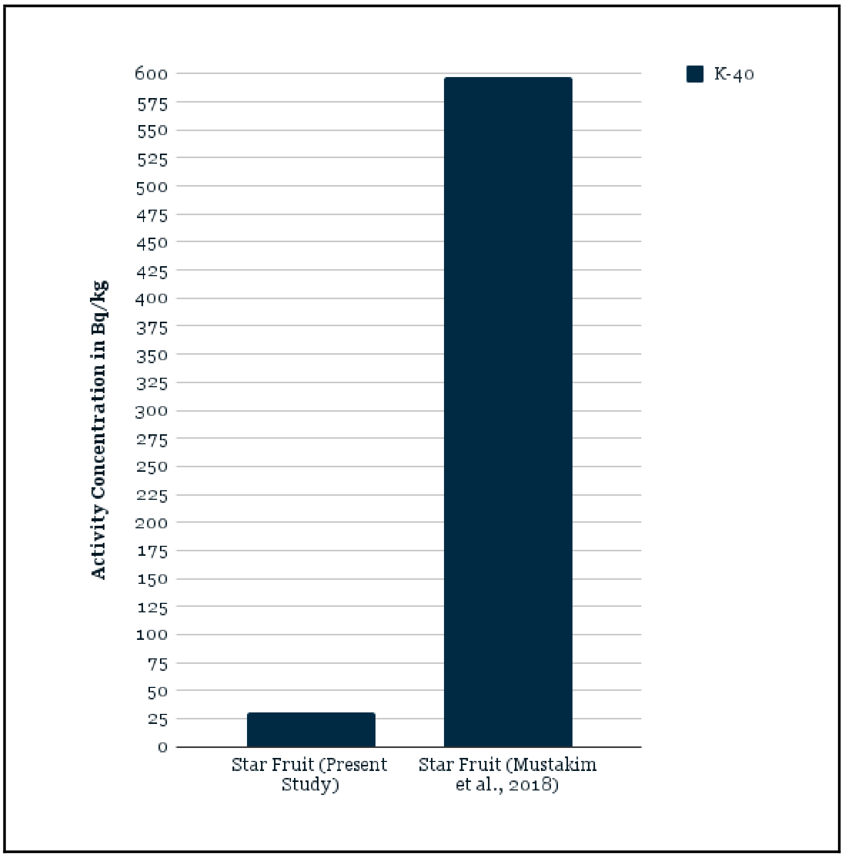

Figure 4.18: Starfruit activity concentrations for K-40

Papaya

Table 4.12 shows the table of the activity concentrations of papayas of this study in comparison with other studies from different regions. Figure 4.19 further visually illustrates difference in activity concentrations of jujubes between different regions for U-238 and Th-232, and Figure 4.20 shows the same for K-40. Our data for U-238 and Th-232 are somewhat comparable to Mutakim et al. (2018), and Priharti and Samat (2016). for K-40, besides Priharti and Samat (2016), every other study showed a significant difference.

Table 4.12: Concentrations of Papaya

Papaya (Present Study)	Dhaka, Bangladesh	2.52 ± 0.11	1.26 ± 0.16	40.61 ± 2.39
Papaya (Mustakim et al., 2018)	Rajshahi, Bangladesh	BDL	2.90 ± 0.80	733.25 ± 61.17
Papaya (Islam et al., 2014)	SE Bangladesh	64.77 ± 38.47	83.53 ± 20.50	1691 ± 245
Papaya (Priharti & Samat, 2016)	Malaysia (Central)	-	0.56 ± 0.48	651.64 ± 9.75
Papaya (Shanthi et al., 2010)	South India	-	-	59.5 ± 6.3

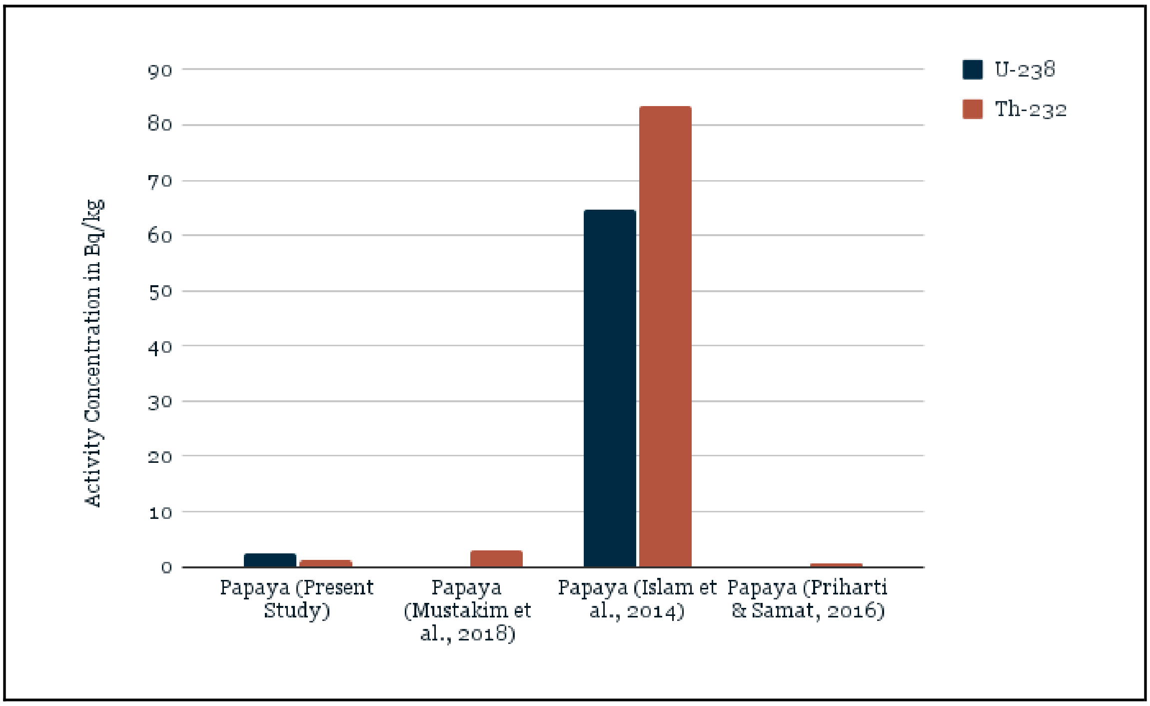

Figure 4.19: Papaya activity concentrations for U-238 and Th-232

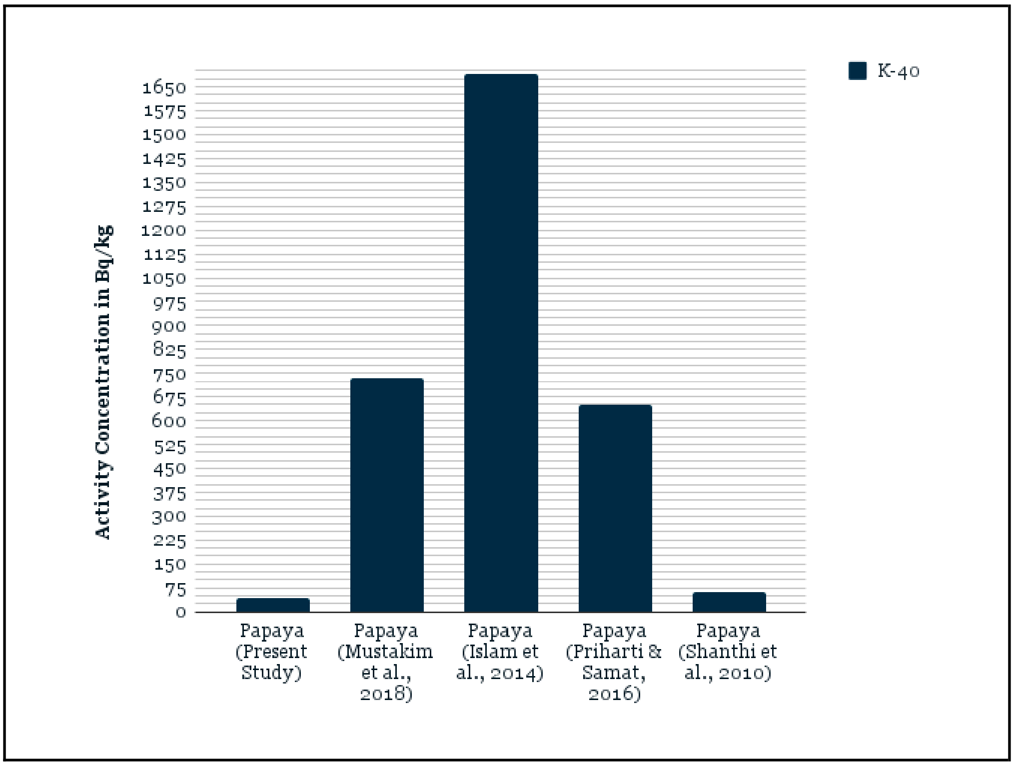

Figure 4.20: Papaya activity concentrations for K-40

4.2 Estimated Age-dependent Fruit Consumption Rate

From the previous section, we observed a lack of data on age-dependent fruit consumption rates. As such, we had to utilise existing data on the national average daily fruit consumption rate and the population sizes in urban regions to find an estimated result. The calculation goes as follows:

$$P_I \cdot F_I + P_C \cdot F_C + P_A \cdot F_A = 101.13\text{g} \tag{4.1}$$

$$\implies \frac{9.54}{100} \cdot 0.33F_A + \frac{16.78}{100} \cdot 0.69F_A + \frac{73.68}{100} \cdot F_A = 101.13 \tag{4.2}$$

$$\implies 0.8841F_A = 101.13 \tag{4.3}$$

$$\implies F_A = 114.4g \tag{4.4}$$

Since we have established that the daily average fruit consumption for adults is 114.4g, following the ratios, we can say

$$F_I = 0.33F_A = 37.75g \tag{4.5}$$

$$F_C = 0.69F_A = 78.93g \tag{4.6}$$

Thus, in Table 4.3 shown below, we present the estimated fruit consumption rates for urban areas.

Table 4.13: Age-dependent Fruit Consumption Rates (Dhaka City)

Category	Age Range	Fruit Consumption per day per capita (g/day)	Fruit Consumption per year per capita (kg/y)
Infant (1 year)	0 - 5	37.75	13.78
Children (10 years)	6 - 15	78.93	28.81
Adult (16 - 70)	16 +	114.4	41.76

Repeating the same procedure used here on the the national population sizes from Table 3.5, we find the daily fruits consumption per capita to be 34.82g/day, 72.78 g/day, and 105.5g/day for infants, children, and adults, respectively. Table 4.14 shows the estimated age-dependent fruit consumption of Bangladesh:

Table 4.14: Age-dependent Fruit Consumption Rates (Bangladesh)

Category	Age Range	Fruit Consumption per day per capita (g/day)	Fruit Consumption per year per capita (kg/y)
Infant (1 year)	0 - 5	34.82	12.71
Children (10 years)	6 - 15	72.78	26.56
Adult (16 - 70)	16 +	105.5	38.51

4.3 Annual Effective Dose (AED)

After determining the required values, we are now prepared to calculate the result for age-dependent Annual Effective Dose (AED) from fruit ingestion. From equation 3.4:

$$D_E = \sum (C_r A_{rw}) \cdot R_f$$

Calculating AED for an adult, D_{EA}:

$$D_{EA} = \left[\left(4.5 \times 10^{-8}\right)(3.62) + \left(2.3 \times 10^{-7}\right)(2.33) + \left(6.2 \times 10^{-9}\right)(80.98)\right] \cdot (41.76)$$

$$D_{EA} = 5.015 \times 10^{-5} \text{ Sv/Y} \approx 0.0502 \text{ mSv/Y} \tag{4.7}$$

We repeat the process for children, D_{EC} and infants D_{EI}:

$$D_{EC} = \left[\left(6.8 \times 10^{-8}\right)(3.62) + \left(2.9 \times 10^{-7}\right)(2.33) + \left(1.3 \times 10^{-8}\right)(80.98)\right] \cdot (28.81)$$

$$D_{EC} = 5.689 \times 10^{-5} \text{ Sv/Y} \approx 0.0569 \text{ mSv/Y} \tag{4.8}$$

$$D_{EI} = \left[\left(1.2 \times 10^{-7}\right)(3.62) + \left(4.5 \times 10^{-7}\right)(2.33) + \left(4.2 \times 10^{-8}\right)(80.98)\right] \cdot (13.78)$$

$$D_{EI} = 6.73 \times 10^{-5} \text{ Sv/Y} \approx 0.0673 \text{ mSv/Y} \tag{4.9}$$

Thus, we get our results of age-dependent AED in Dhaka City to be 0.0673 mSv/y, 0.0569 mSv/y, and 0.0502 mSv/y for infants, children, and adults, respectively. The data is neatly shown in the Table 4.15 below:

Table 4.15: Age-dependent Annual Effective Dose from Fruit Ingestion in Dhaka City

Category	Age Range	AED from ^{238}U (mSv/y)	AED from ^{232}Th (mSv/y)	AED from ^{40}K (mSv/y)	Total Annual Effective Dose from Fruit Ingestion (mSv/y)
Infant (1 year)	0 - 5	0.00599	0.0144	0.0469	0.0673
Children (10 years)	6 - 15	0.00709	0.0195	0.0303	0.0569
Adult (16 - 70)	16 +	0.00680	0.0224	0.0210	0.0502

Repeating the same process for Bangladesh, we get:

$$D_{EA} = \left[\left(4.5 \times 10^{-8}\right)(3.62) + \left(2.3 \times 10^{-7}\right)(2.33) + \left(6.2 \times 10^{-9}\right)(80.98)\right](38.51)$$

$$D_{EA} = 4.624 \times 10^{-5} \text{Sv/y} \approx 0.0462 \text{mSv/y}$$

$$D_{EC} = \left[\left(6.8 \times 10^{-8}\right)(3.62) + \left(2.9 \times 10^{-7}\right)(2.33) + \left(1.3 \times 10^{-9}\right)(80.98)\right](26.56)$$

$$D_{EC} = 5.245 \times 10^{-5}\text{Sv/y} \approx 0.0525\text{mSv/y}$$

$$D_{EI} = \left[\left(1.2 \times 10^{-7}\right)(3.62) + \left(4.5 \times 10^{-7}\right)(2.33) + \left(4.2 \times 10^{-8}\right)(80.98)\right](12.71)$$

$$D_{EI} = 6.201 \times 10^{-5}\text{Sv/y} \approx 0.0621\text{mSv/y}$$

Thus, we get our results of age-dependent AED in Bangladesh to be 0.0621 mSv/y, 0.0525 mSv/y, and 0.0462 mSv/y for infants, children, and adults, respectively. The data is neatly shown in Table 4.16.

Table 4.16: Age-dependent Annual Effective Dose from Fruit Ingestion in Bangladesh

Category	**Age Range**	**AED from ^{238}U (mSv/y)**	**AED from ^{232}Th (mSv/y)**	**AED from ^{40}K (mSv/y)**	**Total Annual Effective Dose from Fruit Ingestion (mSv/y)**
Infant (1 year)	0 - 5	0.0055	0.0133	0.0432	0.0621
Children (10 years)	6 - 15	0.00650	0.0180	0.0280	0.0525
Adult (16 - 70)	16 +	0.00628	0.0206	0.0193	0.0462

4.3.1 AED comparison with other studies

The results we estimated differed from the previous studies. Table 4.17 shows the results from others studies. Additionally, notes are given to give context for the results. Other than Altamemi et al., (2021), the rest of the study results differed with ours by several a few order of magnitudes. Mustakim et al. (2018), for example, was lower than an order of magnitude, whereas Islam et al. (2024) and Shanthi et al. (2010) were 2 orders higher of magnitude.

Table 4.17: Annual Ingestion Dose from Studies

Location	Annual Dose (mSv/y)	Note:
Rajshahi & Natore, Bangladesh (Mustakim et al., 2018)	0.00839 [Adult]	The average fruit consumption rate was used, along with the Dose Coefficients for adults.
Tutolia, Bangladesh (Islam et al., 2014)	1.1 [Adult]	
Ijebu-Ode, Nigeria (Sowole & Olaniyi, 2018)	0.11 [Not specified]	If annual doses of U-238, Th-232, and K-40 were added, then it would've been 0.327 mSv y^{-1}. Consumption rate and dose coefficient not specified.
Najaf, Iraq (Abojassim et al., 2016)	0.388 ± 0.101 [Infants] 0.295 ± 0.094 [Children (10 years)] 0.141 ± 0.008 [Adults]	Data is sourced from UK (Scottish Environment Protection Agency [SEPA], 2011). Consumption rate is at 97.5th percentile, above average.
Kahramanmaraş, Turkey (Küçükönder et al., 2023)	0.304 ± 0.003 [Infants] 0.288 ± 0.002 [Children (10 years)] 0.184 ± 0.001 [Adults]	Consumption rate same as Abojassim et al. (2016)
Central Malaysia (Priharti & Samat, 2016)	0.349 ± 0.005 [Infants 1-3 years] 0.283 ± 0.007 [Children 7-12 years] 0.195 ± 0.004 [Adults >17 years]	Followed local data
South India (Shanthi et al., 2010)	1.795 [Adults]	Both fruits and vegetables were measured.
W. Black Sea, Turkey (Altamemi et al., 2021)	0.0766 [Adults]	Intake data not specified
Dhaka City, Bangladesh (Present Study)	0.0673 [Infants (1 year)] 0.0569 [Children (10 years)] 0.0502 [Adults (16 - 70 years)]	

4.3.2 Threshold for Fruit Consumption

We know that the recommended total exposure limit is 1 mSv/y. Using this information, we can find the amount of fruit one would have to consume to exceed this limit. For an adult, we find the threshold R_{fa}:

$$\left[\left(4.5 \times 10^{-8}\right)(3.62) + \left(2.3 \times 10^{-7}\right)(2.33) + \left(6.2 \times 10^{-9}\right)(80.98)\right] R_{fa} = 1{\times}10^{-3}$$

$$R_{fa} = 832.7 \text{ Kg/Y} \approx 2.281 \text{ Kg/day} \tag{4.10}$$

For children:

$$\left[\left(6.8 \times 10^{-8}\right)(3.62) + \left(2.9 \times 10^{-7}\right)(2.33) + \left(1.8 \times 10^{-8}\right)(80.98)\right] R_{fc} = 1{\times}10^{-3}$$

$$R_{fc} = 506.4 \text{ Kg/Y} \approx 1.387 \text{ Kg/day} \tag{4.11}$$

For infants:

$$\left[\left(1.7 \times 10^{-7}\right)(3.62) + \left(4.5 \times 10^{-7}\right)(2.33) + \left(4.2 \times 10^{-8}\right)(80.98)\right] R_{fi} = 1{\times}10^{-3}$$

$$R_{fi} = 204.7 \text{ Kg/Y} \approx 0.561 \text{ Kg/day} \tag{4.12}$$

The data is presented in the following table:

Table 4.18: Age-dependent Fruit Consumption Rates Threshold in Dhaka City

Category	**Age Range**	**Fruit Consumption rate Threshold in Urban Regions (kg/day)**	**Fruit Consumption rate Threshold in Urban Regions (kg/y)**
Infant (1 year)	0 - 5	0.5610	204.7
Children (10 years)	6 - 15	1.387	506.4
Adult (16 - 70 years)	16 +	2.281	832.7

Chapter 5: Discussions

In this chapter, we discuss the measured and calculated results shown in the previous chapter and highlight their differences, similarities, and significance.

5.1 Differences and Similarities Within the Study

We first begin with the differences in concentration levels. Within the study, as mentioned in the previous section, differences in concentration and annual effective dose have been observed.

5.1.1 Activity concentrations

First, the two banana samples in the study showed above-average radionuclide concentration for all three radionuclides, followed by the mango samples. Bananas are especially rich in potassium and accumulate K-40 accordingly. They take in radionuclides via root uptake in high amounts. Mango trees tend to have large, deep‑rooted fruit trees, its fruit also showed elevated radionuclides, likely due to uptake of soil minerals and any local fertilizer residues. Also, at the time of buying, they were very ripe, which could lead to a longer period of accumulation. Higher values in these fruits could also arise from local soil composition and common use of N–P–K fertilizers (adding K, U, Th) in orchards.

We found that starfruits had the lowest U-238, Th-232, and K-40 concentrations. This can be explained by their plant structure. Starfruit trees typically have shallower roots, often needing low-depth soils, and receiving little fertilization. As such, uptake of soil radionuclides becomes very small. Additionally, referring back to our Table 3.1, our starfruit pulp is ~92% water, leaving only 8% of dry mass. Due to this, radionuclides are highly diluted. Thus, even if the dry matter contained U-238 and Th-232 at a similar specific activity as other fruits, the fresh‑fruit measurement appears very low.

Fruits like dragon fruit, guava, papaya, ber (jujube), and hog plum showed comparable levels of U-328 and Th-232. The later three have similar tree structure and similar dry-to-wet ratio. Although we are not aware of the origin of the fruits, we could assume their soil had similar concentrations. Thus, other than K-40 of hog plum sample, it makes sense for them to have similar levels of radionuclides. However, the dragon fruit, having a different plant structure, we could assume that the accumulation and soil content were such that their levels were similar.

5.1.2 Age-dependent Annual Effective Dose

As we have calculated, we see that infants and young children tend to receive higher dosages than adults. Considering the fruit consumption rates, infants receive 34.1% more dosage than adults annually. Despite this, the results are far below the recommended limits put forward by ICRP. The simple reason is that the dose coefficients for infants are higher than those of adults. The dose coefficients are estimated based on the biokinetics of the references. Infants, children, and adults all have structures with differing mass, size, etc., affecting the dose conversion factor calculation (ICRP, 2002). Having a small frame, underdeveloped tissues, and organs leads to higher absorption per unit time. Due to this, the risk of internal absorption is much higher and gradually decreases as the person reaches adulthood.

The differences in the national and urban Dhaka doses are hardly surprising. Due to the age group proportions being different, the fruit consumption for each group had also changed, and thus, the observed change in the effective dose. Indeed, the national fruit consumption rate is lower than that of urban households, which generally have a high-income level and are more likely to buy fruits. The total population, including rural households, is expected to have lower fruit consumption and thus, lower effective dose from fruit ingestion.

5.2 Differences and Similarities with Previous Studies

We also noticed differences with other studies, which we will try to explain in the upcoming sections. It should be noted, however, that since we lack the knowledge of the origin of the fruits, our explanatory powers are rather limited.

5.2.1 Activity Concentrations

It is observed that there is an overall higher level of K-40 in all the studies. This may be likely due to the tendency of fruits to uptake potassium via roots and have higher levels of potassium. So, as a consequence, they are to have higher K-40. It could also be that those soils, at least at the depth where plant roots may be, have higher levels of potassium.

Compared to Mustakim et al. (2018), this study had very low levels of radionuclides. Given that the sample collection locations were different but constrained within, a few considerations can be made. First, the area where their fruit sample had grown was richer overall. In other words, those areas had higher concentrations of U-238, Th-232, and K-40. And thus, higher uptake. If we consider that the fruits are coming from different regions, the overall radionuclide concentration has gone down since 2016, when Mustakim et al. (2018) collected their samples. Second, it could also be the case that due to intensive cultivation with high‑yield crops, all the radionuclide reserves had depleted. Such potassium‑poor soils may offer less for root uptake, so the plants and their fruits accumulate less K-40. Without knowing the exact locations from which the fruits had be grown, we will lack proper explanations.

When comparing the banana samples with Mustakim et al. (2018), we find that only the K-40 concentration was lower, whereas U-232 and Th-232 were similar. This indicates that while the soil had similar, if not higher, concentrations of uranium and thorium, the potassium levels are lacking something. On the other hand, the average K-40 activities we measured are comparable to those reported for Nigeria (Sowole & Olaniyi, 2018), which would imply that the potassium content and/or root uptake rate are similar to those here. However, given that their U-238 and Th-232 amounts are more than two to three times, assuming similar root uptake their soil or atmospheric deposition may be significantly higher.

5.2.2 Annual Effective Dose

The data on the annual effective dose is, no doubt, mixed (Table 4.17). In terms of results, Altamemi et al. (2021) were the closest to ours. While we see that the activity concentrations of our study are comparable to those of studies like Abojassim et al. (2016), Küçükönder et al., (2023), and Priharti and Samat (2016) their AEDs are higher than this study. Upon closer inspection, it becomes trivially true that the reason behind this difference is due to the differing consumption rates of fruits. Abojassim et al., (2016) used the data from SEPA (20011), which may not be reflective of the Iraq's true fruit consumption rate. Küçükönder et al., (2023), too, used the same data and found similarly high result. Priharti and Samat (2016) were the only study that included their local data. Additionally, Abojassim et al., (2016) had used the proper averages provided by SEPA (2011), their results would have been similar to ours. For example, the AED of adults was 0.141 mSv/y, where the consumption rate was held to be 75kg. Using 20kg, the average, instead, would give 0.0376 mSv/y—which is in the same order of magnitude as ours. Thus, while the concentrations were similar, the discrepancy in the annual doses had been caused by differing fruit intake rate being used.

The study done by Mustakim et al. (2018) is more closely tied to this one. Their annual ingestion dose is significantly smaller, coming at 8µSv/y. This seems somewhat absurd, however, given that their mean activity concentrations were far greater. A few details can be considered in explaining this difference. Their choice of fruit consumption rate was 44g/day or 16.32 kg/y. Excluding the fact that the data can be considered outdated in light of newer data, doing the calculation accordingly should give them

$$D_{EA} = \left[\left(4.5 \times 10^{-8}\right)(10.95) + \left(2.3 \times 10^{-7}\right)(6.68) + \left(6.2 \times 10^{-9}\right)(308.9)\right](16.32)$$

$$D_{EA} = 6.435 \times 10^{-5} \approx 0.0644 mSv/y \tag{5.1}$$

This result, too, is in the same order of magnitude as ours and the other papers mentioned. Given this result, their actual annual dose seems like an error.

5.3 Implications

From a health standpoint, these radionuclide levels pose negligible risk. Compared to other studies, the activities measured were much lower, implying low contamination of soils, especially for potassium. We found our annual doses to be 0.0673 mSv/y, 0.0569 mSv/y, and 0.0502 mSv/y for infants, children, and adults, respectively. By contrast, international bodies consider up to 1 mSv/y as a safe level. Unless an adult consumes upwards of 2.821 kg/day (section 4.3.2), neglecting all other exposures, there is little chance of risk. In practical terms, eating these fruits adds only a tiny fraction of the normal background exposure. Because all measured values in Bangladeshi fruits are below global averages and the resultant dose is orders of magnitude below the 1 mSv guideline, no special health action is needed.

5.4 Study Limitations

This study has several limitations that must be acknowledged. First, while the fruits were collected from local markets, their origins are unknown. As such, it is not possible to explain with certainty why certain fruits have more or less radionuclide concentrations than others. Second, the sample set encompassed only a limited range of fruits, restricting intra-fruit variability and potentially underrepresenting broader dietary patterns. Third, reliable data on actual fruit consumption rates—specifically segregated by age groups and individual fruit types—were unavailable at the district or city level. We, therefore, had to rely on divisional-level estimates and national surveys, which may not accurately wholly reflect Urban Dhaka's specific consumption habits. Fourth, our analysis was confined to the three primary naturally occurring radionuclides U-238, Th-232, and K-40. Other potentially relevant radionuclides (e.g., Ra-226, Pb-210) were not measured such as that in [cite the indian paper], precluding calculation of the total internal dose. Fifth, age-dependent ingestion rates were approximated from general demographic proportions rather than measured dietary surveys, introducing uncertainty into annual effective dose estimates for infants, children, and adults. Lastly, the lack of fruit-specific consumption rates further limits the precision of dose calculations, as varying dietary preferences among age groups could not be accounted for.

5.5 Future Study Possibilities and Recommendations

Building on the present work, future research should broaden the scope of radionuclide analysis and geographic coverage to capture a more complete picture of dietary radiation exposure in Bangladesh. Studies must measure a wider suite of naturally occurring radionuclides—including Ra-226, Pb-210, and relevant progeny—to quantify total internal exposure and calculate cumulative ingestion doses. Parallel sampling campaigns in rural markets and production areas are also essential, as they will reveal regional variations in soil geochemistry, agricultural practices, and resulting NORM uptake in fruits. Additionally, district-level or division-specific dose assessments should be conducted to provide localized annual effective dose estimates and identify areas where targeted monitoring or mitigation may be necessary.

To support these future investigations, national and regional authorities should commission up-to-date, comprehensive surveys of food ingestion rates—including fruit-specific consumption disaggregated by age group and locality—and secure detailed, city- and district-level demographic data. Such data will underpin more accurate, age-stratified dose calculations for representative populations. Moreover, expanding the variety of sampled fruits (including off-season and imported produce) and adopting enhanced analytical protocols will refine transfer factor estimates and hazard indices. Together, these measures will strengthen the evidence base for regulatory standards, inform public health guidelines, and ensure that radiological risk assessments reflect the true exposure experienced by both urban and rural consumers.

Chapter 6: Conclusions

This study set out to assess the presence of naturally occurring radioactive materials—specifically U-238, Th-232, and K-40—in seasonal fruits collected from local markets in Dhaka City and to estimate the age-dependent annual effective dose (AED) received by urban consumers of Dhaka Division through fruit ingestion. The results showed measurable levels of these radionuclides across all fruit types, with K-40 generally exhibiting the highest activity concentrations, consistent with its natural abundance in potassium-rich produce. Although some variation was observed among fruit types, all estimated AEDs for infants, children, and adults remained below the internationally accepted public exposure limit of 1 mSv/year, suggesting that consumption of these fruits poses no significant radiological health risk under current conditions. The study contributes to the limited body of research on dietary NORM exposure in Bangladesh by offering localized data from Dhaka City, incorporating age-specific dose assessments, and applying a more rigorous and transparent methodology than prior works. However, limitations such as a narrow sample range, absence of city-specific fruit consumption data, and the exclusion of other radionuclides beyond U-238, Th-232, and K-40 must be acknowledged. Despite these constraints, the findings provide a useful baseline for urban exposure estimates and underscore the need for continued monitoring. Future studies should expand to rural regions, include a broader spectrum of radionuclides, and integrate detailed dietary and demographic data to better inform food safety standards and public health policy.

Bibliography

Abojassim, A. A., Hady, H. N., & Mohammed, Z. B. (2016, September 30). Natural radioactivity levels in some vegetables and fruits commonly used in Najaf Governorate, Iraq. *Journal of Bioenergy and Food Science*, *3*(3), 113-123. http://dx.doi.org/10.18067/jbfs.v3i3.108

Ahmed, M. S., Priyadharshini, M., Santhanabharathi, B., Pradhoshini, K. P., Parveen, M. H. S., War, M. U. D., Muthukumaravel, K., Duong, V.-H., & Musthafa, M. S. (2024). Health risk assessment of radionuclides in edible fruits cultivated around natural high background radiation areas of Manavalakurichi, Tamil Nadu, India. *International Journal of Environmental Analytical Chemistry*, 1-14. https://doi.org/10.1080/03067319.2024.2362827

Altamemi, R. A. A., Turhan, Ş., & Kurnaz, A. (2021, October 28). Natural and anthropogenic radioactivity in some vegetables and fruits commonly consumed in the Western Black Sea region of Turkey. *Radiochimica Acta*, *109*(12), 935-942. https://doi.org/10.1515/ract-2021-1100

Amols, H. L., & Bardash, M. (1993, November). The definition of transient and secular radioactive equilibrium. *Medical Physics*, *20*(6), 1751-1752. https://doi.org/10.1118/1.596963

Bangladesh Bureau of Statistics. (2023, November). *Population and Housing Census 2022*. Ministry of Planning. https://bbs.portal.gov.bd/sites/default/files/files/bbs.portal.gov.bd/page/b343a8b4_956b_45ca_872f_4cf9b2f1a6e0/2024-01-31-15-51-b53c55dd692233ae401ba013060b9cbb.pdf

Bangladesh Bureau of Statistics (BBS). (2023, Decemeber). *HOUSEHOLD INCOME AND EXPENDITURE SURVEY 2022 - FINAL REPORT*. Ministry of Planning, Government of the People's Repiblic of Bangladesh. https://bbs.portal.gov.bd/sites/default/files/files/bbs.portal.gov.bd/page/b343a8b4_956b_45ca_872f_4cf9b2f1a6e0/2023-12-28-14-40-ac2b3d298f569f155a80871a49b7dd9e.pdf

Bangladesh Bureau of Statistics (BBS). (2025, June). *Yearbook of Agricultural Statistics - 2024*. Ministry of Planning, Government of the People's Repubic of Bangladesh. https://bbs.portal.gov.bd/sites/default/files/files/bbs.portal.gov.bd/page/1b1eb817_9325_4354_a756_3d18412203e2/2025-06-09-12-39-7f8d0b17c93237117fdd6567de090928.pdf

Burton, R. E., & Kebler, R. W. (1960, January). The “half-life” of some scientific and technical literatures. *Journal of the Association for Information Science and Technology*, *11*(1), 18-22. https://doi.org/10.1002/asi.5090110105

Cowart, J. B., & Burnett, W. C. (1994, July 1). The Distribution of Uranium and Thorium Decay-Series Radionuclides in the Environment—A Review. *Journal of Environmental Quality*, *23*(4), 651-662. https://doi.org/10.2134/jeq1994.00472425002300040005x

Debertin, K., & Helmer, R. G. (1988). *Gamma- and X-ray Spectrometry with Semiconductor Detectors*. North-Holland. https://inis.iaea.org/records/dr0ev-nv541

Egidi, P. (1997, August 1). *Introduction to naturally occurring radioactive material*. https://www.osti.gov/servlets/purl/560732

European Commission, Sinnaeve, J., & Gerber, G. (1991). *Underlying data for derived emergency reference levels : Post-Chernobyl action*. Publications Office. https://op.europa.eu/s/z78o

Fowler, E. B. (1965). *Radioactive fallout, soils, plants, food, man*. Elsevier.

Groch, M. W. (1998, September 1). Radioactive Decay. *RadioGraphics*, *18*(5), 1247-1256. https://doi.org/10.1148/radiographics.18.5.9747617

Guagliardi, I., Rovella, N., Apollaro, C., Bloise, A., Rosa, R. D., Scarciglia, F., & Buttafuoco, G. (2016, December). Modelling seasonal variations of natural radioactivity in soils: A case study in southern Italy. *Journal of Earth System Science*, *125*, 1569–1578. https://doi.org/10.1007/s12040-016-0758-y

International Atomic Energy Agency. (n.d.). *Radiation in Everyday Life | IAEA*. International Atomic Energy Agency. Retrieved August 4, 2025, from https://www.iaea.org/Publications/Factsheets/English/radlife

International Atomic Energy Agency. (1989). *Measurement of Radionuclides in Food and the Environment*. Vienna. https://www-pub.iaea.org/MTCD/Publications/PDF/trs295_web.pdf

International Atomic Energy Agency. (2005). *Environmental and Source Monitoring for Purposes of Radiation Protection*. https://www.iaea.org/publications/7176/environmental-and-source-monitoring-for-purposes-of-radiation-protection

International Commission of Radiological Protection. (2006). Assessing Dose of the Representative Person for the Purpose of the Radiation Protection of the Public. ICRP Publication 101a. *Annals of the ICRP*, *36*(3). https://www.icrp.org/publication.asp?id=ICRP%20Publication%20101a

International Commission on Radiological Protection. (1991). 1990 Recommendations of the International Commission on Radiological Protection. ICRP Publication 60. *Annals of ICRP*, *21*. https://www.icrp.org/publication.asp?id=ICRP%20Publication%2060

International Commission on Radiological Protection. (2006). Assessing Dose of the Representative Person for the Purpose of the Radiation Protection of the Public. ICRP Publication 101a. *Annals of ICRP*, *36*(3). https://www.icrp.org/publication.asp?id=ICRP%20Publication%20101a

International Commission on Radiological Protection. (2007). The 2007 Recommendations of the International Commission on Radiological Protection. ICRP Publication 103. *Annals of ICRP*, *37*. https://www.icrp.org/publication.asp?id=ICRP%20Publication%20103

International Commission on Radiological Protection. (2012). Compendium of Dose Coefficients based on ICRP Publication 60. ICRP Publication 119. *Annals of ICRP*, *41*. https://www.icrp.org/publication.asp?id=ICRP%20Publication%20119

Islam, A., Begum, A., Yeasmin, S., & Sultana, M. S. (2014, July). Assessment of dose due to natural radio-nuclides in vegetables of high background radiation area in south-eastern part of Bangladesh. *International Journal of Radiation Research*, *12*(3), 271-275. https://ijrr.com/article-1-1286-en.html

Kakolee, K. F., Pervin, S., Shahabuddin, M., Siraz, M. M. M., & Yeasmin, S. (2021, December). Measurement of Natural Radioactivity due to 226Ra, 232Th and 40K in Soil at Chandpur District, Bangladesh. *Jagannath University Journal of Science*, *8*(1), 59-65. https://www.jnu.ac.bd/journal/assets/pdf/8_1_406.pdf

Küçükönder, E., Gümbür, S., Söğüt, Ö., & Doğru, M. (2023, March 17). Radioactivity amounts, annual effective dose rate, and lifetime cancer risk estimation of some vegetable and fruit samples cultivated in Kahramanmaraş, Turkey. *Environmental Monitoring and Assessment*, *195*. https://doi.org/10.1007/s10661-023-11098-9

Leutz, H., Schulz, G., & Wenninger, H. (1965, April). The decay of potassium-40. *Zeitschrift für Physik*, *187*, 151-164. https://doi.org/10.1007/BF01387190

Medeiros, M. P.C., Rebello, W. F., Lopes, J. M., Silva, A. X., & Associacao Brasileira de Energia Nuclear (ABEN), Rio de Janeiro, RJ (Brazil). (2015). *Relative efficiency calculation of a HPGe detector using MCNPX code*. international nuclear atlantic conference. Brazilian nuclear program. State policy for a sustainable world; 12. ENAN: meeting on nuclear applications (INAC 2015), Sao Paulo, SP (Brazil).

Mustakim, R., Ferdous, J., Begum, A., & Islam, A. (2018, November 8). Natural Radionuclides Concentrations and Annual Effective Dose in Seasonal Fruits of Bangladesh. *Nuclear Science*, *3*(3), 28-35. https://doi.org/10.11648/j.ns.20180303.11

National Research Council. (2006). *Health Risks from Exposure to Low Levels of Ionizing Radiation: BEIR VII Phase 2*. Washington, DC: The National Academies Press. https://doi.org/10.17226/11340

Nursapina, N.A., Shynybek, B.A., Matveyeva, I.V., Nazarkulova, S.N., Štrok, M., Benedik, L., & Ponomarenko, O.I. (2022). Effect of mineral fertilisers application on the transfer of natural radionuclides from soil to radish (Raphanus sativus L.). *Journal of Environmental Radioactivity*, *247*. https://doi.org/10.1016/j.jenvrad.2022.106863

Podgorsak, E. B. (2016). *Radiation Physics for Medical Physicists* (3rd ed.). Springer International Publishing. https://link.springer.com/book/10.1007/978-3-319-25382-4

Priharti, W., & Samat, S. B. (2016). RADIOLOGICAL RISK ASSESSMENT FROM THE INTAKE OF VEGETABLES AND FRUITS IN MALAYSIA. *Malaysian Journal of Analytical Sciences*, *20*(6), 1247-1253. http://dx.doi.org/10.17576/mjas-2016-2006-03

Sarker, M. S. D., Rahman, R., Siraz, M. M. M., Khandaker, M. U., & Yeasmin, S. (2021, November). The presence of primordial radionuclides in powdered milk and estimation of the concomitant ingestion dose. *Radiation Physics and Chemistry*, 188. https://doi.org/10.1016/j.radphyschem.2021.109597

Scottish Environment Protection Agency. (2012, October). *Radioactivity in Food and the Environment, 2011. Appendix 1*. https://www.sepa.org.uk/media/104099/rife_17_appendix.pdf

Shanthi, G., Kumaran, J. T. T., Gnana Raj, G. A., & Maniyan, C. G. (2010, July). Natural radionuclides in the South Indian foods and their annual dose. *Nuclear Instruments and Methods in Physics Research Section A: Accelerators, Spectrometers, Detectors and Associated Equipment*, *619*(1-3), 436-440. https://doi.org/10.1016/j.nima.2009.10.068

Sowole, O., & Olaniyi, O.E. (2018, February 8). Assessment of radioactivity concentrations and effective of radionuclides in selected fruits from major markets at Ijebu – Ode in Ogun State, southwest of Nigeria. *Journal of Applied Sciences and Environmental Management*, *22*(1), 95-98. https://doi.org/10.4314/jasem.v22i1.17

Spieler, H. (2005). *Semiconductor Detector Systems*. Clearedon Press.

United Nations Scientific Committee on the Effects of Atomic Radiation. (2000). *UNSCEAR 2000 Report Volume I*. UNSCEAR. https://www.unscear.org/unscear/en/publications/2000_1.html

Vearrier, D., Curtis, J. A., & Greenberg, M. I. (2009, June 3). Technologically enhanced naturally occurring radioactive materials. *Clinical Toxicology*, *47*(5), 393-406. https://doi.org/10.1080/15563650902997849